On the Enrichment of Magnetic Heavy Minerals in a Coastal Environment

Exploration, Examination, Explanation

Dissertation

zur Erlangung des

Doktorgrades der Naturwissenschaften

am Fachbereich Geowissenschaften

der Universität Bremen

vorgelegt von

Tobias Kulgemeyer

1. Gutachter:	Prof. Dr. Tilo von Dobeneck
2. Gutachter:	Prof. Dr. Karin Bryan

BREMEN, 23. AUGUST 2016

Declaration

Name: Tobias Kulgemeyer

Address: Spittaler Str. 50, 28359 Bremen

Herewith I declare that

I. This document and the accompanying data have been composed by myself and describes my own work.

II. Material from the published or unpublished work of others, which is referred to in this dissertation, is credited to the author in the text.

III. This work has not been submitted for any other degree.

Bremen, 23. August 2016

Signature

Contents

Zusammenfassung

In dieser Arbeit wird ein neuer methodischer Ansatz zur detaillierten Erfassung von Anreicherungen magnetischer Schwerminerale im Küstenraum durch integrierte geophysikalische and sedimentologische Daten vorgestellt, die beobachteten Anreicherungsmuster interpretiert und ihre Formationsmechanismen diskutiert. Zu den verwendeten Methoden zählen die elektromagnetische Vermessung des Untergrunds entlang von Profillinien, die Fotografie des Meeresboden in Nahaufnahmen, verschiedene Labormethoden zur Analyse der generellen and spezifisch der magnetischen Korngröße und Mineralogie sowie numerische Modellierung von bi-fraktionalem Sedimenttransport. Als bespielhaftes Studiengebiet wurde ein Areal in der westlichen Bay of Plenty (Neuseeland) mit Ausmaßen von 60 km $\times$ 7 km und Wassertiefen von 2-35 m ausgewählt.

Als hauptsächliches Instrument wurde ein benthischer Profilierschlitten genutzt, welcher mit einem Induktionsspulensensor zur Messung der magnetischen Suszeptibilität und elektrischen Leitfähigkeit entlang von 33 küstenparallelen Profilen ausgerüstet war. Die Parameter stehen mit der Konzentration magnetischer Minerale und der Porosität des Sediments in Verbindung. Weitere Instrumente umfassen eine CTD mit Trübesensor and eine bugmontierte, hochauflösende Kamera mit LED-Blitzlichtern. Hiermit wurden ca. 800.000 fortlaufende, überlappende Fotografien von 40 $\times$ 40 cm großen Bereichen des Meeresbodens gemacht.

Diese Daten wurden zusammen mit der korrespondierenden akustischen Rückstreuung eines Sidescan Sonars genutzt, um den generellen sedimentologischen Rahmen zu erfassen. Die visuelle Erscheinung des Sediments auf Fotografien wird für eine grundsätzliche Klassifizierung genutzt, welche später mit granulometrischen und mineralogischen Ergebnissen verfeinert wird. Die sich daraus ergebende Lithofazies wird zwischen den Profilen auskartiert, wobei hierzu wenn möglich die charakteristische akustische Rückstreuung genutzt wird. Hauptsächliche Lithofazies ist ein holozäner Feinsand, welcher eine transgres-

siv überarbeitete Serie von ursprünglich pleistozänen Mittel- bis Grobsanden überlagert. Die Rückstreuung wird auch genutzt um großskalige Strukturen des Meeresbodens zu klassifizieren, insbesondere Dünen und Sorted Bedforms. Deren Verbreitung und Orientierung lässt auf einen wetterbedingt bidirektionalen Sedimenttransport schließen, der während Schönwetterperioden von Nordosten nach Südwesten und während Sturmereignissen entgegengesetzt orientiert ist. Anreicherungen magnetischer Minerale treten in küstenparallelen Strukturen im spätholozänen Feinsand zwischen 5-15 m auf, sowie as großräumige Strukturen in einigen Grobsanden. Während erstere typischerweise eine niedrige Porosität aufweisen, können letztere in hoch- und niedrigporöse Bereiche unterteilt werden. Gesteinsmagnetische Untersuchungen weisen auf Magnetit und zwei verschiedene Titanomagnetite (TM40, TM60) als hauptsächliche Träger der Suszeptibilität hin. Weitere eisenhaltige Phasen umfassen Hämatit und Ilmenit. Die beobachteten Anreicherungen werden basierend auf den gegenwärtigen und vergangenen Umweltbedingungen, die mit der jeweiligen Lithofazies verbunden sind, sowie der Kombination aus Mineralkonzentration und Porosität interpretiert. Die küstenparallelen Strukturen stellen einen aktiven Prozess dar, während die Anreicherungen in älteren Sedimenten als Relikte aufgefasst werden. Hohe Porosität wird als Indikator für sich ändernde energetische Bedingungen während der holozänen Transgression verstanden.

Der Mechanismus für die aktive Anreicherung im Feinsand wird mit einem numerischen Modell weiter untersucht. Dieses zeigt wie die Position solcher Strukturen von der selektiven Entnahme gröberer, nicht-magnetischer Partikel aus dem Bett gegenüber kleinerer magnetischer Schwermineralpartikel, in Abhängigkeit von den lokalen Scherkräften. Der Grad der Anreicherung wird weitestgehend von differenziellen Transport dieser Phasen bestimmt.

Insgesamt demonstrieren die Ergebnisse dieser Arbeit eine effektive neuartige Vorgehensweise zur Kartierung eines Gebietes, der detaillierte Ergebnisse und schlüssige Interpretationen in relativ kurzer Zeit ermöglicht. Sie zeigen die Bedingungen, unter denen sich natürliche Sortierungsmuster basierend auf Korngröße und Dichte entlang der Küste ausbilden. Die grundsätzlichen

Mechanismen lassen sich ähnlich beschaffene Gebiete und eine breite Auswahl verschiedener Schwerminerale übertragen. Dies beinhaltet auch die Detektion stark angereicherter Seifen von wirtschaftlicher Bedeutung. Die Ergebisse lassen sich im Küstenmanagement nutzen, um Transportwege des Sediments nachzuvollziehen und Gebiete die identifizieren, welche durch den Abtransport leichter Mineralien stärker von Erosion betroffen sind, aber auch solche, in denen der zurückgebliebene angereicherte Sand durch Abschirmungseffekte eine höhere Stabilität des Meeresbodens bewirkt.

Abstract

In this thesis, an approach for the detailed assessment of magnetic heavy mineral enrichments in a coastal environment using integrated geophysical and sedimentological data is developed, the observed enrichment patterns are interpreted, and their formation mechanisms discussed. Used methods are electromagnetic profiling of the subsurface, close-up seafloor photography, various laboratory techniques to analyze bulk and magnetic grain sizes and mineralogy, and numerical modelling of bi-fractional sediment transport. The studies take place in an exemplary study area in the western Bay of Plenty (New Zealand) with dimensions of 60 km $\times$ 7 km in water depths from 2-35 m.

Primary instrument was a benthic profiling sled equipped with an induction coil sensor for measurements of the apparent magnetic susceptibility and electric conductivity of the uppermost 0.5-1 m of the seafloor along 33 cross-shore profiles. These parameters translate to the concentration of magnetic minerals and sediment porosity. Further instruments include a CTD with turbidity sensor and a bow-mounted high-resolution camera with LED flashlights. With this camera, ca. 800,000 continuous, overlapping photographs of 40 $\times$ 40 cm sections of the seafloor were taken.

This data was used along with the corresponding acoustic backscatter of a sidescan sonar survey in the area to establish the general sedimentological framework. The visual appearance of sediments on the photographs is used to establish a basic classification, later refined by granulometric and mineralogical considerations. The combined lithofacies is mapped out between profiles using their characteristic acoustic backscatter. The main lithofacies are a late Holocene fine sand overlaying a transgressionally reworked series of medium to coarse grained, originally Pleistocene, deposits. Backscatter is also used for classification of large-scale bedforms, specifically subaquatic dunes and sorted bedforms. Their occurrence and orientation indicate a bi-directional net transport going from north-west to south-east during fair weather and in the opposite direction during

stormy periods.

Magnetic mineral enrichments occur in coast-parallel structures in the late Holocene fine sands between 5-15 m water depth, and as wide-spread structures in some coarse sands. While the former typically have a low porosity, the latter can be further divided in structures with low or very high porosity. Rock magnetic analysis indicates magnetite and titanomagnetite as the main carriers of susceptibility. Further iron-bearing phases include hematite and ilmenite. The enrichments are interpreted based on past and present environmental conditions associated with their lithofacies, and the combination of magnetic mineral concentration and porosity. The coast-parallel structures are seen as an active feature, while the ones in older facies appear to be relics. High porosity is seen as an indicator for changing energetic conditions during the Holocene transgression, allowing the entrainment of a wide range of grain sizes.

The formation mechanism for the active enrichments in fine sand is investigated with a numerical model. This shows how the position of these structures is determined by the selective entrainment of coarser, non-magnetic particles over smaller magnetic heavy minerals depending on the local bed shear stress. The degree of enrichment is largely influenced by differential transport of these phases.

Overall, the findings of this thesis demonstrate an innovative, effective way to approach an unmapped area and reach detailed results with conclusive interpretations in a relatively short time. It shows the conditions under which natural sorting patterns due to size and density develop along the coast. The basic formation mechanisms are applicable to other areas in similar coastal settings and for a diverse range of heavy minerals. This includes the detection of high-grade enrichments of economic value. The results can be used for coastal management, as they can help to identify sediment pathways and areas of increased erosion due to the removal of light minerals, but also potentially increased stability due to the armoring effect of the remaining lag.

Chapter 1

Introduction

This thesis presents novel methods to assess and analyze the distribution of magnetic minerals in context with the general lithofacies and sediment dynamics of the littoral realm. The included studies cover an area located on the shoreface of the Bay of Plenty, New Zealand (Fig. 1.1). This area provides excellent conditions for the used methods by its volcanoclastic sediments that contain a mostly diagenetically unaltered suite of magnetic minerals, relatively simple boundary conditions for sediment transport with long, straight shorelines and gentle slopes, but also because of the logistical support provided by the international graduate school INTERCOAST, a cooperation between the University of Bremen and the University of Waikato. The utilized geophysical and sedimentological exploration in an integrated multi-proxy approach of combined electromagnetic, optical, acoustic and sample-based methods constitute a very powerful approach to map, describe and analyze dynamic coastal sediment systems from observation. *In situ* and laboratory data are examined and put in context in a GIS environment. This allows to identify the distribution patterns of magnetic minerals and to explain the distribution and formation process by numerical modelling.
Natural magnetic minerals [1] are iron oxides (e.g. magnetite, hematite), hydroxides (e.g. goethite) and sulphides (e.g. pyrite, pyrrhotite) that commonly occur in as accessory minerals in rocks and sediments. Petrologically, they belong to the loosely-defined group of heavy minerals. These are characterized by

[1] In this thesis, the term "magnetic minerals" refers to those minerals that can carry a remanent magnetization, whether it results from ferro-, ferri- or canted antiferromagnetism.

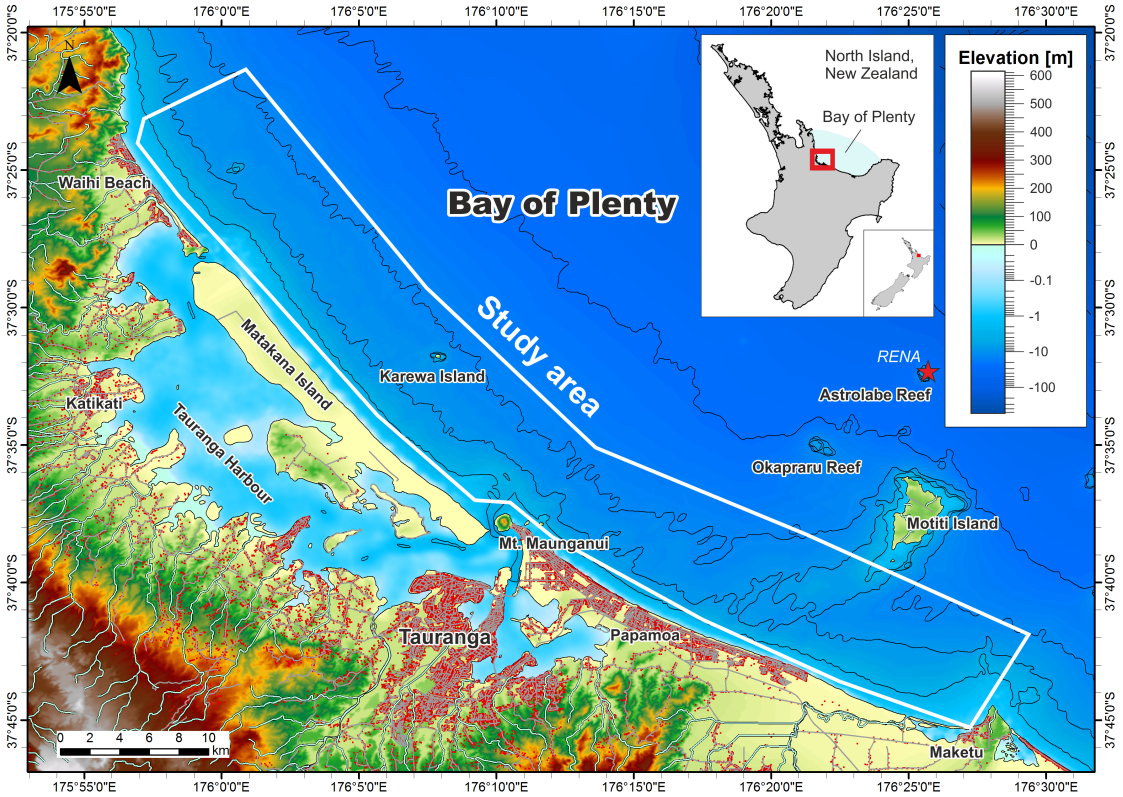

Figure 1.1: Location of the study area in the Bay of Plenty, New Zealand. Geographic data from Land Information New Zealand (LINZ).

their density, which is relatively high when compared to quartz (2650 kg/m^3), the most common mineral on the surface of Earth. Heavy minerals, among other applications, are often critical components to fully characterize a rock or determine the provenance of a sediment, but are often difficult to acquire from bulk material and need to be extracted by fractionation with high density liquids. Rock magnetic analyzes can be done with bulk sediment and provide a wide range of information about the magnetic target minerals. The presence and concentration of magnetic minerals can even be detected *in situ* by measuring the magnetic susceptibility of a rock or sediment.

Apart from their density, accessory heavy minerals are further characterized by their usually smaller grain size. The individual particles therefore differ in in their hydrodynamic behavior from the bulk of light minerals, which is reflected in their respective spatial distribution among an area with variable energetic conditions. Where the concentration of these minerals is relatively high compared to the typical sediment composition of the respective lithofacies, the are said to be

enriched, and the corresponding areas are called enrichments. If a sediment is sufficiently enriched to be of economic interest, it is called a placer.
Placers provide valuable metallic and non-metallic resources. Examples include magnetite, ilmenite, zircon, chromite, wolframite, gold, diamonds and many more. New Zealand is the world's leading producer of magnetite from mineral placers (Elsner, 2010); these mining operations take place on the west coast, whereas the enrichments in the Bay of Plenty investigated in this study are all low-grade (in the range of 1 %) and without economic value. However, the scientific reasons to study heavy mineral enrichments are numerous.

1.1 Motivation and Objectives

The distribution of the heavy mineral fraction within a sediment results from various sorting processes during entrainment, transport, settling and burial (Komar & Wang, 1984; Slingerland & Smith, 1986). It reflects the hydrodynamic conditions in an area of deposition and is constrained by the geological framework such as source rock petrology, regional topography or bathymetry, climate and sealevel. This makes them an interesting source of data to research sediment provenance (Oldfield et al., 1979; Li et al., 2015; Razik et al., 2015; Krippner et al., 2016) and investigate transport paths and mechanisms (May, 1973; Gallaway et al., 2012; Razik et al., 2013). High concentrations of heavy minerals can be indicative of an erosive environment (Frihy, 1994; Frihy et al., 1995; Zhang et al., 2010), but the remaining lag of silt-sized particles has the potential to re-stabilize the seafloor (Bartzke et al., 2013; Bartzke & Huhn, 2015). Iron oxides and sulphides provide insight into diagenetic processes, often linked to environmental and climatic changes (Maher, 1986; Wilson & Roberts, 1999; Razik et al., 2013; Just et al., 2014). Magnetite has recently been shown to act as a bioavailable battery, providing electron sources and sinks for oxidizing and reducing microorganisms (Byrne et al., 2015).
In many ways, heavy minerals are a key component to understand long-term sediment dynamics. Enrichments form in various different environments (Slinger-

land & Smith, 1986), e.g. in rivers (Duk-Rodkin et al., 2001; Burton & Fralick, 2003) and deltas (Frihy & Komar, 1993; Corbett & Burrell, 2001), or in marine environments between on beaches (Komar & Wang, 1984; Bryan et al., 2007; Gallaway et al., 2012) and the inner shelf (Elsner, 1992; Hamilton & Collins, 1998). As most of the world's population centers are located in coastal regions, the processes in these often highly dynamic environments are of great interest for science and society.

While a general research interest in heavy mineral enrichments is evident, three factors were instrumental in the planning of this thesis. The first was the development of the benthic electromagnetic (EM) profiler *NERIDIS* (Neritic Discoverer) at the MARUM Center for Environmental Research of the University of Bremen by Müller et al. (2012). This, so far unique, instrument is capable of measuring the magnetic susceptibility and electric conductivity of near-surface sediments on the seafloor with high precision and spatial resolution. The ability to house further equipment – a CTD with turbidity meter and a camera for close-up seafloor photography – make this instrument a powerful tool to collect a wealth of interpretable data along hundreds of kilometers of profiles during a single survey.

A second factor was the existing scientific cooperation between the University of Waikato in New Zealand with the University of Bremen in Germany through the INTERCOAST (IC) program. One of these collaborative projects (Badesab et al., 2012) was the first to describe elevated concentrations of titanomagnetite in certain cost-parallel areas in the Bay of Plenty.

The third factor was an incident on 5 October 2011, when the the container vessel MV *RENA* ran aground in the Bay of Plenty on Astrolabe Reef. For an evaluation by the "*RENA* Long Term Environmental Recovery Monitoring Program" a quick assessment of the state of the seafloor by various bio- and geoscientific studies was desirable (Battershill et al., 2013). Through the connection to IC, it was decided to co-finance a *NERIDIS* survey in the area adjacent to the site of the incident. This would provide scientific data for the next IC project, and help the recovery program by assessing the state of the seafloor and looking out for oil spills and metal debris on photographs and EM data. The survey took place in

November 2012. Fortunately, only a minimal contamination was detected.
The scientific results of this survey and two following sampling campaigns in 2013 and 2015 are presented in three publications that form the main body of this thesis. The collective aims of these studies are:

- To establish a strategy for the integrated use of electromagnetic, photographic, hydroacoustic, and sample based sedimentological and geophysical datasets for the assessment of sediments in a coastal system
- To investigate magnetic mineral enrichments in this system in context with the general lithofacies and past and present sediment dynamics
- To develop a model for the formation of the observed enrichments that is applicable to other areas in a similar geological setting

1.2 Structure

The structure of this cumulative thesis can be described in a thematic and a functional way. The thematic structure is given by the subtitle of this thesis, and overlaps between the chapters. As such, chapters 1 and 2 are describe the exploration and examination of sediments in general, respectively the specific magnetic phase. A hypothesis for the explanation of structures observed in the distribution of magnetic minerals is developed and tested in chapters 2 and 3. Chapters are organized following the functional structure:

- **Chapter 2:** *Lithofacies distribution and sediment dynamics on a storm-dominated shelf from combined photographic, acoustic and sedimentological methods (Bay of Plenty, New Zealand) by Tobias Kulgemeyer, Tilo von Dobeneck, Hendrik Müller, Karin Bryan, Willem de Lange and Christopher Battershill, published in Marine Geology, Vol. 376, pp. 158-174.* This chapter deals with the determination of the sedimentological background of the study area. An approach for the classification of sediments using close-up seafloor photography combined with textural and mineralogical data obtained from reference samples is presented. Where possible, this is

expanded using the characteristic acoustic backscatter of a lithofacies from side scan sonography to map out their distribution. This in turn is combined with evidence from the type and orientation of bedforms as well as bottom turbidity to establish general sediment dynamics.

- **Chapter 3:** *Magnetic mineral and sediment porosity distribution on a storm-dominated shelf investigated by benthic electromagnetic profiling (Bay of Plenty, New Zealand) by Tobias Kulgemeyer, Tilo von Dobeneck, Hendrik Müller, Karin Bryan, Willem de Lange and Christopher Battershill, submitted to Marine Geology on 30 May 2016* This study is concerned with the investigation of the distribution of magnetic heavy minerals by electromagnetic benthic profiling. Using the electric conductivity and the magnetic susceptibility of the seafloor, the porosity and the concentration of magnetic minerals are mapped out and enrichments identified. Magnetic minerals are classified by rock magnetic laboratory analysis and linked to the established general lithofacies. The (depth-integrated) electromagnetic data is also compared to surficial samples and sediment cores to investigate vertical distribution of magnetic minerals. Distribution and type of magnetic minerals, seafloor porosity, general lithofacies and sediment dynamics are used to classify different types of enrichments and develop a conceptual model for their formation.

- **Chapter 4:** *Formation process of coast-parallel heavy mineral enrichments investigated by exploratory numerical modelling by Tobias Kulgemeyer and Karin Bryan, under preparation* The conceptual model is tested by numerical modelling. Selective entrainment and differential transport of a bi-fractional sediment consisting of a major quartz and a minor magnetite phase is simulated and the resulting cross-shore concentrations compared to the distribution of magnetic minerals observed in the electromagnetic data. The effects of changing hydrodynamic and geological conditions are investigated and the strengths and limitations of the model are discussed.

All laboratory analyses were performed by the author of this thesis. All interpretations were developed and formulated by the author, and discussed with the co-authors of the respective publications. Text, graphics and tables are the work of the author, with refinements made after discussion with the co-authors of the respective publications. The *NERIDIS* survey in the Bay of Plenty was conducted before the start of this project without participation of the author by Hendrik Müller, Tilo von Dobeneck, Christian Hilgenfeldt and Benjamin Baasch. Likewise, the conversion of raw EM and acoustic data to SI units was performed by Hendrik Müller and Konstantin Reeck prior to this thesis. Initial data processing (interpolation of electromagnetic data and photographic sediment classification) was done by the author during six months in a preceding M.Sc. thesis (Kulgemeyer, 2013). The the acoustic data used in this thesis was gathered in a sidescan sonar survey by Seaworks Ltd. The numerical model is based on an existing model by Murray & Thieler (2004) and Coco et al. (2007).

1.3 Physical background

In this section, the most important physical aspects featured in this work shall be briefly explained. These are the principles of sediment transport as the central process in the included studies, and the magnetic susceptibility as the most important indicative parameter used. As a multi-proxy study, numerous other parameters are utilized in various measurement techniques, explaining all of these fundamentals in detail would go beyond the scope of a Ph.D. thesis.

1.3.1 Principles of sediment transport

Forces acting on a grain

Water in motion over a sediment bed – be it from the flow of a current or the orbital motion imposed by waves – applies a frictional force to the seafloor which deforms the bed in the direction of motion; the force per unit area is the called bed shear stress τ_b.

The balance of forces acting on a resting grain shall be illustrated with an example (Fig. 1.2). A grain with diameter d and density ρ is protruding out of the horizontal plane of homogeneous, cohesionless bed B by a distance s. Acting on the grain is the specific gravity F_G, applied to the center of gravity C_1. Between the bed plane and the line connecting C_1 to the center of gravity of the downflow grain C_2 is the pivot point P. The grain has to rotate around this point at an angle α to be set in motion. Now a laminar current applies a fluid force F_F, consisting of the horizontal drag force F_D and the vertical lift force F_L (this includes buoyancy and upward turbulence due to eddies forming around the grain), with the angle ξ between F_F and the horizontal plane. It is applied on a point along the extended line between C_1 and C_2, the normal to the pivot line p. As the current velocity is decreasing towards the bed and only the protruding part of the grain can be affected, the application point A does not have to be in the center of gravity; the exact point depends on the structure of current as well as the shape of the grain and has to be determined experimentally (Slingerland & Smith, 1986). The critical condition for the initiation of motion is fulfilled if

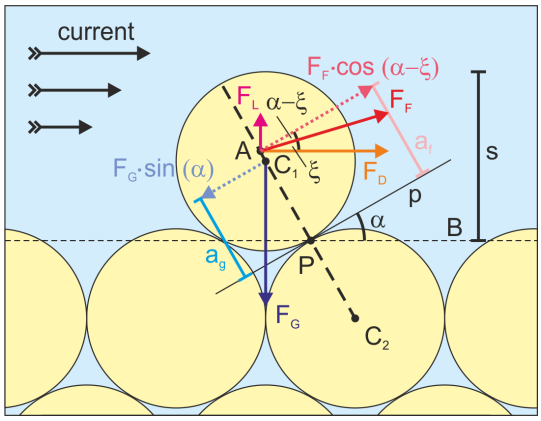

Figure 1.2: Forces acting on resting grain with related definitions, after Slingerland & Smith (1986)

$$F_F > F_G \frac{a_g sin(\alpha)}{a_f cos(\xi - \alpha)} \tag{1.1}$$

Entrainment from a sediment bed

Moving on from an individual grain to a sediment bed, the fluid forces act as the bed shear stress τ_b, and the resisting forces are collectively termed the critical shear stress τ_{cr}. In a natural sediment, it depends on size and density of the grains, their shape, the packing of the material and cohesion. As any problem involving a great number of particles, this is extremely complex and a

solid theoretical foundation does not exist yet. A widely used empirical reference curve (Fig. 1.3) for the critical shear stress was experimentally derived by Shields (1936). Here, a dimensionless shear stress $\theta = \frac{\tau_b}{gd(\rho-\rho_w)}$ was used to determine the point of erosion for a bed with dimensionless grain size $D = d(\frac{g((\rho/\rho_w)-1)}{\nu^2})^{1/3}$, where ρ_w is the density of water, ν its viscosity and g gravity.

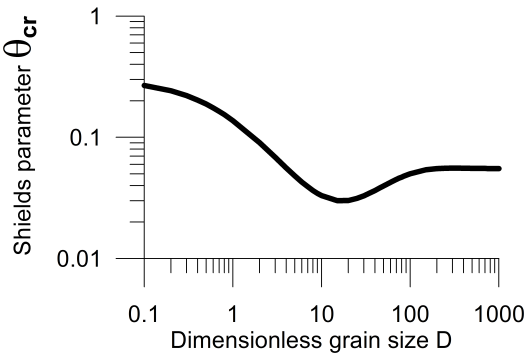

Figure 1.3: Dimensionless critical shear stress θ_{cr} for a homogeneous, non-cohesive bed of dimensionless grain size D according to Shields (1936), using a mathematical approximation of Soulsby & Whitehouse (1997)

Another reference diagram was developed by Hjulström (1935, 1939), which instead of shear stress makes uses of the flow velocity U. This diagram includes a second curve, below which previously entrained sediment is deposited, thus dividing the diagram in areas that indicate erosion, transport and deposition. While the Hjulström diagram is more detailed, the use of the flow velocity is physically problematic and the Shields curve has become the standard reference for most applications. In the following decades, researches made numerous additions, modifications and improvements on the original curve to compensate for its shortcomings, e.g. an inaccuracy for fine grain sizes, a theoretical foundation for this empirical curve, and the fact that it is only applicable to a homogeneous bed, where all grains have the same size and are made from the same material (van Rijn, 1993; Soulsby & Whitehouse, 1997; vanRijn, 2007a; Miedema, 2010). One important addition is the modification of the critical bed shear stress for fractions of different-sized particles in a mixed (graded) bed. Widely used is the hiding factor of Egiazaroff (1965), which relates the critical shear stress of a fraction to that of the median grain size (van Rijn, 2007c). This factor takes into account that smaller grains a shielded within the pore space of surrounding larger grains and are therefore less exposed to the flow than they are in a homogeneous bed. Likewise, larger grain protrude more

out of the bed than in a homogeneous bed, and are therefore more exposed. Consequently, fine grains in a mixed bed are harder (and coarse grains easier) to entrain than predicted by the Shields curve. In some cases, the hiding factor can even become large enough to enable the preferential entrainment of coarse over fine grains in a mixed sediment. This is an important sorting mechanism called selective entrainment.

Shear sorting of a mixed bed

If shear stresses are not sufficient to entrain sediment, they can still have an effect on the vertical distribution of grain size fractions in a mixed bed by shear sorting. In a sheared surface, a force perpendicular to the plane of shearing is present called dispersive pressure. This acts more on large grains, which will move upwards in the sediment (Bagnold, 1954, 1956).

Transport mechanisms

Once entrained, sediment can be transported either as bedload by rolling, sliding and saltation, or as suspended load in the water column. The sheer volume of the latter easily makes it the dominant mode of transport, especially for finer grain sizes (vanRijn, 2007b). Bedload transport on the other hand is strongly related to the development of bedforms like ripples and dunes (vanRijn, 2007a). The vertical velocity profile of the transporting current is approximately constant for most of the water depth, and decreases to zero in a boundary layer in proximity to the bed (Fig. 1.4). Depending on the magnitude of the current, it can be well-stratified (laminar flow, for low velocities) or well-mixed (turbulent flow, for high velocities). Natural water currents are almost always turbulent. An exception is an area very close to the bottom, rarely more than a few millimeter thick, where the current velocity is rapidly approaching zero. Here, linearly decreasing laminar flows prevail and hence it is called the laminar, or viscous, sublayer (Wright et al., 1999). This can only develop on relatively smooth beds, on rough beds with sufficiently large particles, grains protrude into the turbulent flow and thus break down the sublayer. Evidently, bedload and suspended load are transported at

different rates in the water column. Furthermore, different grain size fractions of suspended load are carried higher up in the water column by diffusion and are consequently transported at different rates (Slingerland & Smith, 1986).

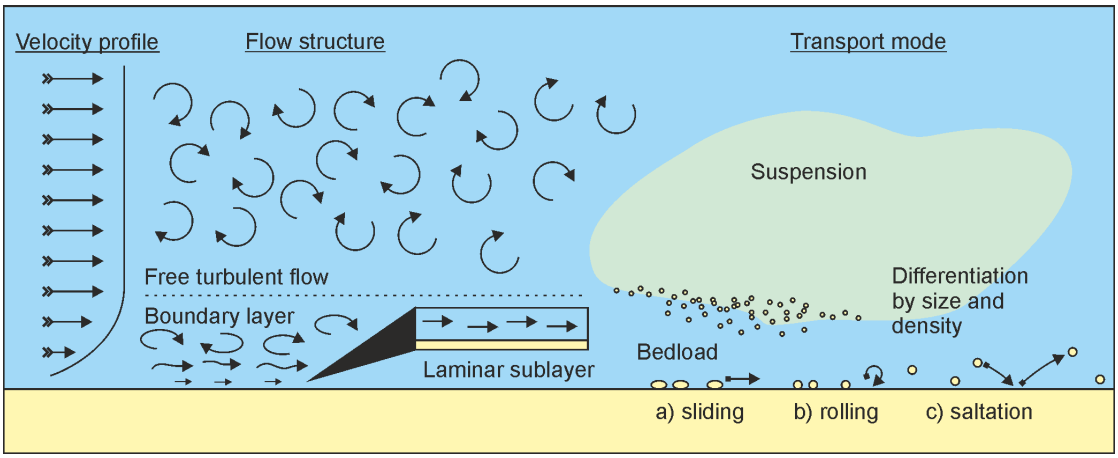

Figure 1.4: Flow velocity, structure and modes of sediment transport throughout the water column

Settling and deposition

Where current velocities throughout the water column decrease below a grain size specific velocity, sediment will settle down again. As larger grains settle at higher velocities, they can be deposited while smaller grains are still transported. Temporarily varying wave and current conditions lead to the burial of interchanging layers of coarse and finer grains in a deposit. Particles frequently settle down and are re-entrained during transport, and the closer the particle is transported to the bottom, the more this stop-and-go motion is influencing the transport rate. Selective entrainment, shear sorting, differential transport, settling and burial are interacting sorting mechanisms that can all contribute to the development of heavy mineral enrichments in varying degrees (Slingerland & Smith, 1986).

1.3.2 Basic concepts of mineral magnetism

Types of magnetism

Magnetic susceptibility is a property of matter that describes how it reacts to an external magnetic field. All atoms have magnetic properties, which arise from

the magnetic moment resulting from electron spin and orbital motion. Atoms therefore acts as elemental magnets. In atoms with filled electron shells (paired electrons) the individual spins cancel each other out. If an external magnetic field is applied to such an atom, a sideways Lorentz force causes precession of electrons orbiting the nucleus, which produces a magnetic moment directed opposite to the direction of the field. This effect is the ubiquitous diamagnetism (Evans & Heller, 2003).

If the electrons shells are not completely filled and unpaired electrons are present, the electrons spins are no longer balanced and the atom has a net magnetic moment. Usually, the magnetic moments of atoms in a mineral crystal are randomly oriented, resulting again in a zero net magnetic moment of the crystal. In an external magnetic field, they become increasingly aligned parallel to the field. If the external field is removed, the magnetic moments will quickly randomize again due to thermal interference. This effect is called paramagnetism (Evans & Heller, 2003).

In crystals where the orbitals of unpaired electrons in adjacent atoms closely overlap, another effect called ferromagnetism is observed. If the distance between atoms is too small, there is a high probability that two unpaired electrons of the same shell are occupying the same space. Following Pauli's exclusion principle, their spins must be oriented opposite to each other, thus canceling their magnetic moments out. However, there is also an electrostatic Coulomb interaction taking place between the electrons, which requires potential energy in the system. For slightly greater distances between the atoms, this energy can be minimized if the spins are aligned parallel. The electrons still move freely from one atom to another, but can no longer occupy the same space at the same time. If the system does not receive sufficient energy (e.g. by heating), the alignment of magnetic moments is permanent and holds after the external field is removed. This direct exchange is only happening in a pure substance, like elemental iron, which does not exist in nature. In natural iron oxides, two Fe^{2+} or Fe^{3+} ions are instead coupled to an intermediate O^{2-}, which leads to an indirect or superexchange between the Fe ions (Dunlop & Özdemir, 1997).

The crystal structure often favors exchange coupling of electrons along certain axes, which causes magnetic anisotropy. Further energy is required to assemble groups of elemental magnets by magnetostatic interaction. For grains above a certain size range, magnetostatic energy can be minimized by subdividing the crystal in regions called magnetic domains where all magnetic moments are aligned parallel (Halgedahl, 2007). In an unmagnetized ferromagnetic sample, the domains are randomly oriented. Magnetization by an external field creates domains that are oriented close to the direction of the field to grow until the particles is completely magnetized, or saturated, in this direction (Fig1.5).
Depending on the crystal structure of magnetized particles it can again be energetically favorable to orient atomic moments in different lattices anti-parallel to each each other. If they cancel each other out completely, the crystal is antiferromagnetic (Fig1.5). If the sublattices are occupied by atoms with an unequal number of magnetons[2], a net magnetic moment remains; this is called ferrimagnetism and is the type of magnetism most often encountered in natural magnetic minerals, e.g. in magnetite. But even if the number of magnetons in both sublattices is equal, the crystal structure can prevent a perfectly anti-parallel orientation and the particle will posses a small net magnetic moment. This is known an spin-canted antiferromagnetism, the prime example being hematite (Dunlop & Özdemir, 1997).

[2]The Bohr magneton describes the elemental magnetic moment of an electron caused by spin and orbital momentum

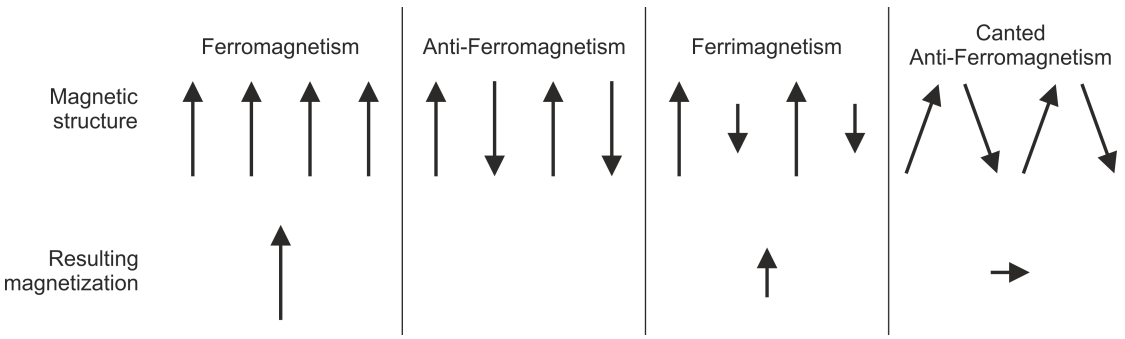

Figure 1.5: Magnetic structures and the resulting net magnetization, after Dunlop & Özdemir (1997)

Magnetic susceptibility

Susceptibility is a parameters that describes how a material reacts to an applied magnetic field. Whether it is caused by dia-, para- or ferromagnetism, due to the alignment of magnetic moments the crystal will develop its own magnetic field. This is called induced magnetization M; and the susceptibility κ is a measure of induced magnetization change per unit volume of a substance and external field change. κ links the induced magnetization of a crystal to an external field H as

$$M = \kappa H \tag{1.2}$$

κ is a property of a volume of the respective material. As H and M have the same unit [3], κ is dimensionless. As the *in-situ* volume of unconsolidated samples if often unknown, measurements are often expressed as mass-specific susceptibility χ. It is related to the (volumetric) susceptibility by the density ρ and has a unit of m^3/kg.

$$\chi = \frac{\kappa}{\rho} \tag{1.3}$$

Susceptibility can further depend on the frequency of the external field; this effect is dependent on grain size and although it is significant for very small (so-called superparamagnetic) crystals it can be neglected for micron-sized grains (Petrovsky, 2007). The linear relation of M and H is strictly speaking only valid for dia- and paramagnetic materials (Petrovsky, 2007). In undersaturated materials the increase in magnetization is hysteretic, and only approximately linear for low fields (initial or low-field susceptibility). A more general definition of susceptibility is

$$\kappa = \frac{\Delta M}{\Delta H} \tag{1.4}$$

Magnetic hysteresis (see Fig. 1.6) has several key points, that are important parameters for the characterization of ferromagnetic materials. Starting with an unmagnetized sample, if the external field is increased from 0, the initial slope

[3] The field strength H is measured in A/m, fields are also often characterized by the flux density B measured in T. H and B are related by the magnetic permeability of free space $\mu_0 = 4\pi \cdot 10^{-7}$ H/m; the unit H (Henry) has an value of $1\ \mathrm{kg \cdot m^2/s^2 \cdot A^2}$

very close to the origin is described by κ.

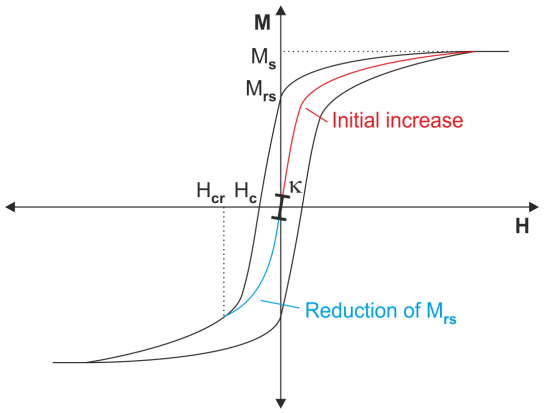

Figure 1.6: Schematic magnetic hysteresis with key points, after Evans & Heller (2003)

The slope declines in higher fields until it converges to the saturation magnetization M_s. In natural samples, higher fields will only increase the magnetization beyond this points due to paramagnetic components. If the external field is reduced back to zero, a remanent magnetization M_{rs} will remain. If now an opposite field is applied, it has to reach a certain field strength H_c, called the coercive force or coercivity, to reduce the total magnetization to zero. This is achieved by canceling out the induced and remanent magnetization along a certain axis with the opposite field, thus reducing the flux density in the material. However, if this field would be removed now, a remanent magnetization would still remain in the sample. To permanently erase M_{rs}, the coercivity of remanence H_{cr} needs to be applied. Increasing and decreasing H in both directions between the respective saturation fields creates a major hysteresis loop (Evans & Heller, 2003).

1.4 Principal methods

1.4.1 Electromagnetic benthic profiling

Electromagnetic methods have been used in marine geophysics since the early twentieth century (Constable & Srnka, 2007), first as passive magnetotelluric measurements that image the electric conductivity (or resistivity) of the subsurface according to naturally induced currents (e.g. by geomagnetic field variations). The low frequency of these sources allows to target deep crustal structures, often located several kilometers below the surface. Active methods, although they had long been utilized in terrestrial surveys, have only been used in the marine

realms since the late 1970's, after researchers began to overcome the difficulties arising from the conductive properties of seawater (Cox et al., 1971; Cox, 1981). These controlled source electromagnetic (CSEM) systems are mainly used in the search for ore bodies, aquifers, and hydrocarbon reservoirs.

Today, the standard used in the oil and gas industry for deep water exploration consists of a long horizontal electric dipole transmitter towed close to the bottom and a series of stationary receivers installed on the seafloor; theory and examples for applications are found e.g. in Cheesman et al. (1987); Edwards & Chave (1986); Edwards (1997, 2005); Schwalenberg et al. (2009). Typical targets are located in the range of hundreds of meters below the seafloor. A fully mobile system for measurements of the shallow seafloor (10s of meters) consists of a magnetic field transmitter and a string of receivers (Evans et al., 1999; Edwards, 2005).

The nature of the research presented in this thesis came with special constraints that impacted the choice of system: it had to be compact and fully mobile to be used from a small ship in shallow coastal waters and to target very shallow subsurface depths in the range of ca. one meter to capture the effects of active sediment transport processes, and it had to measure not only electrical, but also magnetic properties of the seafloor in order to assess heavy magnetic minerals. The used system was originally modified from the GEM-3 design (Won et al., 1997) for use in the marine environment by Müller (2009) and developed further in the following years (Müller et al., 2012). It makes use of pressure-resistant housings and an increased amplitude for better signal-to-noise ratio and is installed on a bottom-towed benthic profiler. This series of systems is called *NERIDIS* (short for Neritic Discoverer), with the newest model being named *NERIDIS III*. It uses an induction coil sensor with a compact design consisting of three concentric and coplanar coils, which allows to target very shallow depths (ca. 1 m) in the sediment column. Measurements are made in the frequency domain[4] So far, this system has been used to identify freshwater

[4]Phase and amplitude of the received signal are recorded, the alternative time domain method records the amplitude only. Theoretically, both a fully convertible by Fourier transformation, but real measurements always have some form of experimental error attached that may be smaller in a direct measurement than in a converted property (Cheesman et al., 1987).

seeps in pockmarks and classify sediments on the immediate surface of the seafloor based on their magnetic properties and porosity (Müller et al., 2011), and for reconstruction of layering in marine deposits by inversion of sediment conductivity (Baasch et al., 2015).

The induction process is governed by Maxwell's equations, especially important for a brief description are the extended circuital law, also known as Ampere's law, and the law of induction, or Faraday's law (Ždanov & Keller, 1994). The circuital law shows that magnetic fields with field strength H [A/m] are created by moving charges in form of conduction currents with free current density J [A/m] and time-varying displacement currents expressed by the electric displacement field D [C/m]

$$\nabla \times H = J + \frac{\delta D}{\delta t} \tag{1.5}$$

The law of induction describes how an electrical field E [V/m] is created by a time-varying magnetic field with flux density B [T] as

$$\nabla \times E = -\frac{\delta B}{\delta t} \tag{1.6}$$

H is related to B by the magnetic permeability of a body μ [H/m] as $H = B/\mu$; the permeability in turn is related to the susceptibility κ and the magnetic permeability of free space μ_0 by $\mu = \mu_0(\kappa + 1)$. E can be equated to D using the dielectric permittivity ϵ [F/m] as $E = D/\epsilon$, and to J by the electric conductivity σ [S/m] with $E = J/\sigma$

The practical application is as follows: According to the circuital law, an alternating current in the transmitter (outer coil) is the source of the primary magnetic field. By the law of induction, this time-varying magnetic field also induces a primary electric field, which is phase shifted at 90° (quadrature) to the magnetic field, and drives eddy currents in conductive media. These currents in turn produce a secondary magnetic field, still in quadrature to the primary field. As the primary field is changing with time, the induced eddy currents and their associated secondary fields are also frequently changing, and this change is opposed by a self-induced a current in the same media. The self-induced current likewise

causes a secondary magnetic field which is again shifted at 90° and thereby in-phase with the primary field, but with reversed sign. Simultaneously, the primary magnetic field is magnetizing particles, which now also cause a secondary magnetic field, in-phase to the primary field Müller (2009). To summarize, an sinusoidal alternating primary field causes a sinusoidal secondary field due to magnetic induction, and both a cosinusoidal and inversed sinusoidal secondary field by electric induction in the seafloor.

The superimposed secondary fields induce a current in the receiver coil, located in the center of the sensor arrangement. This is accompanied by yet another 90° phase shift. What is finally measured is not the current itself, but the associated voltage – and as the change in voltage precedes the current, another phase shift has to be taken into account. The final output is thereby shifted by 180° (reversed signs) in respect to the primary field. To prevent an influence of the transmitter on the receiver, a bucking coil is installed between them. This current is in series with the transmitter, but has half the number of windings and a current flowing in opposite direction to create a magnetic cavity at the center of the sensor (Won et al., 1997).

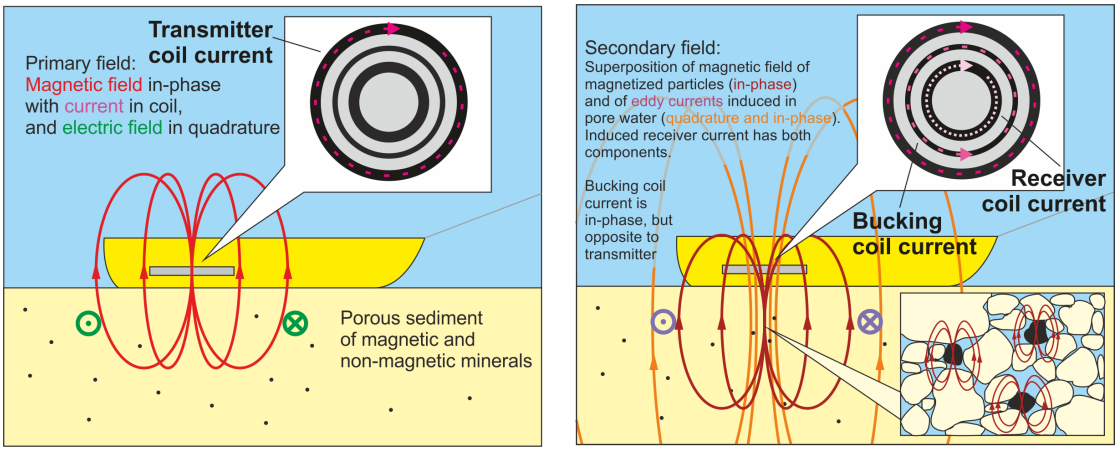

Figure 1.7: Principle of the induction process during benthic profiling.

Electric induction depends on the electric conductivity, and as this property is magnitudes higher in seawater than in any sedimentary components it is almost completely controlled by eddy currents induced in the fluid phase [5]. To

[5] Large metallic bodies or extremely high concentrations (close to 100 %) of metallic particles would also act as an effective conductor, which puts a theoretical limit to the applicability

correctly differentiate the conductivity of the subsurface from the water above, an independent measurement of the seawater conductivity is performed with a CTD. Magnetic induction depends on the magnetic susceptibility, which is much higher in the solid than in the fluid phase, and dominant in magnetic materials. By this, the conductivity is related to the seawater-filled pore space in the sediment, whereas susceptibility is controlled by the amount of magnetic minerals.
The induced current is further dependent on the frequency of the magnetic flux through the medium. At very low frequencies, the resistivity of the medium becomes much greater than the inductance; this is called the resistive limit (Fitterman & Labson, 2005). The induced current and the related secondary field are now extremely small, and the signal is almost completely controlled by the magnetic susceptibility. However, this is a constant value and its contribution is very small in higher frequencies, which are almost completely controlled by the conductivity (most other systems operate well above the resistive limit and susceptibility can be safely neglected). Therefore, low in-phase frequencies are used to pick susceptibility, while a corresponding conductivity is best picked from high frequency quadrature components (Müller et al., 2012).
The received signal is a combined volumetric response and the measured parameters are modeled to fit an equivalent homogeneous half-space. As they are not the real properties of any individual physical object, gradient or layer they are commonly described as ”apparent” conductivity, resp. susceptibility (Fitterman & Labson, 2005).

1.4.2 Numerical sediment transport modelling

The sediment transport model used in chapter 4 is a modified version of the one developed by Coco et al. (2007). The basic functions are based on Murray & Thieler (2004). It is intended as an exploratory model in the sense of Murray (2002, 2003) to investigate general processes and mechanisms involved in the formation of heavy mineral enrichments in a realistically calibrated, but simplified environment rather than a detailed simulation of hydro- and sediment dynamics

this method. This limit is far beyond the concentrations encountered in the study area.

like e.g. Delft3D. The choice of a relatively simple model makes it easier to highlight key processes that might get buried in details in a more complex model. The short computing time allows a great number of different model setups to be tested in a given time. As only a relatively small number of variables are involved, uncertainties in the calibration are reduced. Although more simple models do not consider every aspect of sediment dynamics and thus may only have a limited use for quantitative predictions, the quality of the processes that are included can be more reliable (Merritt et al., 2003).

The model uses a finite-differences approach and tracks sediment concentrations in and across cells, following the Eulerian method [6] (Kombiadou & Krestenitis, 2013). It simulates the transport of two separate sediment fractions that differ in grain size and density. Transport takes place in a three-dimensional grid with cell dimensions $5 \times 5 \times 0.05$ m and with certain initial parameters attributed to each cell. These are the cell's Cartesian location and dimensions, hydrodynamics parameters (wave height/period, current velocities in x and y directions), mean bedslope, concentration of coarse and fine sediments and fullness. A number of cells starting from the bottom is filled with sediment, everything above is left empty. Water depth is determined as the preset depth of the lowest layer minus the height of the sediment column. In every iteration, sediment transport parameters are calculated separately for the fine and coarse fraction (see Fig. 1.8).

In the first step, the critical bed shear stress for the respective fraction in the particular sediment composition in the cell is determined, as well as the bed shear stress in each cell resulting from the hydrodynamic parameters. For later use, the expected height and wavelength of developing ripples and the associated drag is also calculated. Following Soulsby (1997), the drag from ripple-related turbulence is not used for the entrainment of sediment, but for the diffusion of suspended matter.

If the bed shear stress is greater than the critical shear stress, bedload and

[6] Models generally follow the Eulerian or the Lagrangian method, which tracks the paths of individual particles or groups of particles from their origin. A third option are mixed Eulerian-Lagrangian models.

suspended load are calculated separately. Suspension is based on a reference concentration very close to the bed, the ripple-generated drag and the vertical current velocity profile. It is determined by numerically solving an integral over the height above the seafloor until a preset, extremely small concentration is reached. Bedload can be determined more straightforward as a function of the shear stress, current velocity and grain size.

Suspended load and bedload sum up to the local load transported out of the cell, and the difference between the local load and the inflow from adjacent cells makes up the total load Q. Based on the settling velocity of the grain size fraction, a certain percentage P of this load is expected to be deposited. This is calculated by the ratio of the transport time through the cell given by cell length X and a current velocity U_{uv} to the settling velocity W countered by the effective profile height of the ripple-generated drag H_{eff}. As the current has two components u and v in x and y direction, sediment can be transported out of the cell faster in one of these directions than the other. U_{uv} is therefore chosen as the greater of the current components.

$$P = \frac{X/U_{uv}}{W/H_{eff}} \tag{1.7}$$

By definition, $P \leq 1$. The volume of sediment added (or usually, removed) from the cell is thus given by

$$V_{add} = PQ \tag{1.8}$$

The volume of sediment exiting the cell in x and y direction is given by the deposited percentage, the total load and the relative magnitude of u and v (Murray & Thieler, 2004)

$$V_{out,x} = (1-P)Q\frac{u}{u+v}; V_{out,y} = (1-P)Q\frac{v}{u+v} \tag{1.9}$$

The final step is to evaluate the volume of fine and coarse sediment added or removed from each cell and adjust the composition of the cell for the next iteration. If more sediment is removed than was present in the cell, this cell is

now declared as empty and the next deeper cell becomes the active layer. In the reverse case, if the volume of sediment surpasses the volume of the cell, the overflow spills over to the next empty cell above.

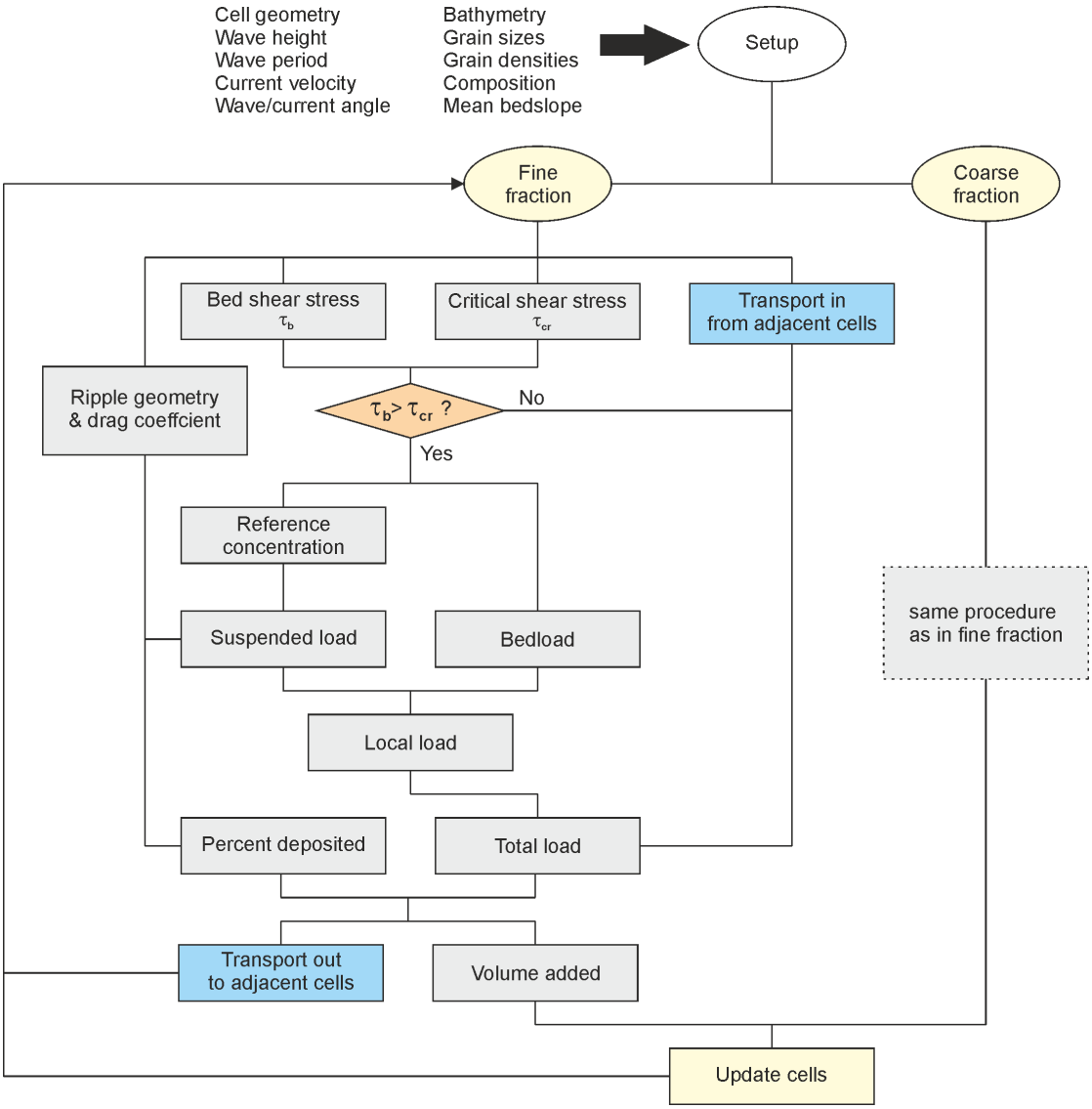

Figure 1.8: Algorithm of the sediment transport model executed for each cell per iteration.

Bibliography

Baasch, B., Müller, H., Oberle, F.K.J., von Dobeneck, T. (2015): Inversion of marine multifrequency electromagnetic profiling data: a new approach to resolve surficial sediment stratification – Geophysical Journal International, Vol. 200, pp. 439-451.

Badesab, F., von Dobeneck T., Bryan, K.R., Müller, H., Briggs, R.M., Frederichs, T., Kwoll, E. (2012): Formation of magnetite-enriched zones in and offshore of a mesotidal estuarine lagoon: An environmental magnetic study of Tauranga Harbour and Bay of Plenty, New Zealand – Geochemistry, Geophysics, Geosystems, Vol. 13, Q06012, doi:10.1029/2012GC004125.

Bagnold, R. A. (1954): Experiments on a gravity-free dispersion of large solid spheres in a Newtonian fluid under shear – Proceeding of the Royal Society London, Series A, Vol. 225, pp. 49-63.

Bagnold, R. A. (1954): The flow of cohesionless grains in fluids – Proceeding of the Royal Society London, Series A, Vol. 265, pp. 315-319.

Bartzke, G., Bryan, K.R., Pilditch, C.A., Huhn, K. (2013): On the stabilizing influence of silt on sand beds – Journal of Sedimentary Research, Vol. 83, pp. 691–703, doi:10.2110/jsr.2013.57.

Bartzke, G., Huhn, K. (2015): A conceptual model of pore-space blockage in mixed sediments using a new numerical approach, with implications for sediment bed stabilization – Geo-Marine Letters, doi:10.1007/s00367-015-0399-1.

Battershill, C., Schiel, D.R., Ross, P.M., Fairweather, R., Culliford, D, Marsh, R., Taiapa, C., Bennett, P. (2013): Rena Environmental Recovery Monitoring Programme: executive summary – Te Mauri Moana, Environmental Research Institute, University of Waikato, Tauranga, New Zealand, 37pp.

Bryan, K.R., Robinson, A., Briggs, R.M. (2007): Spatial and temporal variability of titanomagnetite placer deposits on a predominantly black sand beach – Marine Geology, Vol. 236, pp. 45-59.

Burton, J.P., Fralick, P. (2003): Depositional Placer Accumulations in Coarse-Grained Alluvial Braided River Systems – Economic Geology, Vol. 98, pp. 985-1001.

Byrne, J.M., Klueglein, N., Pearce, C., Rosso, K.M., Appel, E., Kappler, A. (2015): Redox cycling of $\mathrm{Fe(II)}$ and $\mathrm{Fe(III)}$ in magnetite by Fe-metabolizing bacteria.

Cheesman, S.J., Edwards, R.N., Chave, A.D. (1987): On the theory of sea-floor conductivity mapping using transient electromagnetic systems – Geophysics, Vol. 2, No. 2, pp. 2204-217.

Coco, G., Murray, A.B., Green, M.O. (2007): Sorted bed forms as self-organized patterns: 1. Model development – Journal of Geophysical Research, Vol. 112, F03015, doi:10.1029/2006JF000665.

Constable, S., Srnka, L.J. (2007): An introduction to marine controlled-source electromagnetic methods for hydrocarbon exploration – Geophysics, Vol. 72, No. 2, pp. WA3-WA12.

Corbett, I., Burrell, B. (2001): The earliest Pleistocene(?) Orange River fan-delta: an example of succesful exploration delivery aided by applied Quaternary research in diamond placer sedimentology and plaeontology – Quaternary International, Vol. 82, pp. 63-73.

Cox, C.S., Filloux, J.H., Larsen, J.C. (1971): Electromagnetic studies of ocean currents and electrical conductivity below the ocean-floor – In A. Maxwell [ed.](1971): The Sea, Wiley, New York, Vol.4, part 1, pp. 637-693.

Cox, C.S. (1981): On the electrical conductivity of the oceanic lithosphere – Physics of the Earth and Planetery Interiors, Vol. 25, pp. 196–201.

Dunlop, D.J., Özdemir, Ö (1997): Rock Magnetism: Fundamentals and frontiers – Cambridge University Press, Cambridge, 573 pp.

Edwards, R.N. (1997): On the resource evaluation of marine gas hydrate deposits using sea-floor transient electric dipole-dipole methods – Geophysics, Vol. 62, No. 1, pp. 63-74.

Edwards, R.N. (2005): Marine controlled source electromagnetics: Principles, methodologies, future commercial applications – Surveys in Geophysics, Vol. 26, pp. 675–700.

Edwards, R.N., Chave, A.D. (1986): A transient electric dipole-dipole method for mapping the conductivity of the sea floor – Geophysics, Vol. 51, No. 4, pp.984-987.

Evans, R.L. (2007): Using CSEM techniques to map the shallow section of seafloor: From the coastline to the edges of the continental slope – Geophysics, Vol. 72, No. 2, WA105–WA116, doi: 10.1190/1.2434798.

Evans, R.L., Law, L.K., St. Louis, B., Cheesman, S., Sananikone, K. (1999): The shallow porosity structure of the Eel shelf, northern California: results of a towed electromagnetic survey – Marine Geology, Vol. 154, pp. 211–226.

Elsner, H. (1992): Granulometry and mineralogy of some northeastern Florida placers: a consequence of heavy mineral concentration in nearshore bars – Sedimentary Geology, Vol. 76, pp. 233-255.

Elsner, H. (2010): Heavy Minerals of Economic Importance – Bundesanstalt für Geowissenschaften und Rohstoffe (BGR) Assessment Manual, Hannover, 218 pp.

Evans, M., Heller, F. (2003): Environmental Magnetism: Principles and Applications of Enviromagnetics – Academic Press, Elsevier Science, San Diego, 299 pp.

Duk-Rodkin, A., Barendregtb, R.W., Whitea, J.M., Singhrey, V.H. (2001): Geologic evolution of the Yukon River: implications for placer gold – Quaternary International, Vol. 82, pp. 5-31.

Egiazaroff, I.V. (1965): Calculation of nonuniform sediment concentrations – Journal of the Hydraulics Division, Vol. 91, No. 4, pp. 225-247.

Fitterman, D.V., Labson, V.F. (2005): Electromagnetic Induction Methods for Environmental Problems – in: Butler, D.K. [ed.](2005): Near-Surface Geophysics, Society of Exploration Geophysicists, Tulsa, pp. 301-356.

Frihy, O.E. (1994): Discrimination of accreted and eroded coasts using heavy mineral compositions of the Nile Delta beach sands, Egypt – Sedimentology, Vol. 41, pp. 905-912

Frihy, O.E., Komar, P.D. (1993): Long-term shoreline changes and the concentration of heavy minerals in beach sands of the Nile Delta, Egypt – Marine Geology, Vol. 115, pp. 253-262.

Frihy, O.E., Lotfy, M.F., Komar, P.D. (1995): Spatial variations in heavy minerals and patterns of sediment sorting along the Nile Delta, Egypt – Sedimentary Geology, Vol. 97, pp. 33-41.

Gallaway, E., Trenhaile, A.S., Cioppa, M.T., Hatfield, R.G. (2012): Magnetic mineral transport and sorting in the swash-zone: northern Lake Erie, Canada – Sedimentology, Vol. 59, pp. 1718-1734.

Halgedahl, S.L. (2007): Magnetic Domains – in: Gubbins, D., Herrero-Bervera, E. [eds.](2007): Encyclopedia of Geomagnetism – Springer, Berlin, pp. 490-502.

Hamilton, N.T.M., Collins, L.B. (2001): Placer Formation in a Holocene Barrier System, Southwestern Australia – Journal of Coastal Research, Vol. 14, No. 1, pp. 240-255.

Hjulstroem, F. (1935): Studies in the morphological activity of rivers as illustrated by the River Fyris – Bulletin of the Geological Institute of Uppsala, Vol. 25, pp. 221–527.

Hjulstroem, F. (1939): Transport of detritus by moving water recent marine sediments – in: Trask, P.D. [ed.](1939): Recent Marine Sediments, a symposium, Tulsa, Oklahoma: American Association of Petroleum Geologists: New York, London, T. Murby & Co.; Reprinted 1968 by Dover Publications, pp. 3-31.

Just, J., Schefuß, E., Kuhlmann, H., Stuut, J.-B.W., Pätzold, J. (2014): Climate induced sub-basin source-area shifts of Zambezi River sediments over the past 17 ka – Palaeogeography, Palaeoclimatology, Palaeoecology, Vol. 410, pp. 190–199.

Komar, P.D., Wang, C. (1984): Processes of selective grain transport and the formation of placers on beaches – Journal of Geology, Vol. 92, pp. 637-655.

Kombiadou, K., Krestenitis, Y.N. (2013): Modelling Cohesive Sediment Dynamics in the Marine Environment – in: Manning, A. [ed.](2013): Sediment Transport Processes and Their Modelling Applications, InTech, doi: 10.5772/51061.

Krippner, A., Meinhold, G., Morton, A.C., Schönig, J., von Eynatten, H. (2016): Heavy minerals and garnet geochemistry of stream sediments and bedrocks from the Almklovdalen area, Western Gneiss Region, SW Norway: Implications for provenance analysis – Sedimentary Geology, Vol. 336, pp. 96–105.

Kulgemeyer, T. (2013): Distribution of Magnetic Minerals in the Bay of Plenty – Master thesis, lodged at the library of the University of Bremen, Bremen, Germany.

Li, G., Yan, W., Zhong, L., Xia, Z., Wang, S. (2015): Provenance of heavy mineral deposits on the northwestern shelf of the South China Sea, evidence from single-mineral chemistry – Marine Geology, Vol. 263, pp. 112-124.

Maher, B.A. (1986): Characterization of sold by mineral magnetic measurements – Physics of the Earth and Planetary Interiors, Vol. 42, pp. 76-92.

May, J.P. (1973): Selective transport of heavy minerals by shoaling waves – Sedimentology, Vol. 20, pp. 203-211.

Merritt, W.S., Letcher, R.A., Jakeman, A.J. (2003): A review of erosion and sediment transport models – Environmental Modelling & Software, Vol. 18, pp. 761–799.

Miedema, S.A. (2010): Constructing the Shields curve, a new theoretical approach and its applications – WODCON XIX, Beijing.

Müller, H. (2009): Characterization of marine near-surface sediments by electromagnetic profiling – Ph.D. Thesis, lodged at the library of the University of Bremen, Bremen, Germany 152 pp.

Müller, H., von Dobeneck, T., Nehmiz, W., Hamer, K. (2010): Near-surface electromagnetic, rock magnetic, and geochemical fingerprinting of submarine freshwater seepage at Eckernförde Bay (SW Baltic Sea) – Geo-Marine Letters, Vol. 31, No. 2, pp. 123–140, doi: 10.1007/s00367-010-0220-0.

Müller, H., von Dobeneck, T., Hilgenfeldt, C., SanFilipo, B., Rey, D., Rubio, B. (2012): Mapping the magnetic susceptibility and electric conductivity of marine surficial sediments by benthic EM profiling – Geophysics, Vol. 77, No. 1, pp. 1-14.

Murray, A.B. (2002): Seeking explanation affects numerical modeling strategies – EOS, Transactions, American Geophysical Union, Vol. 83, pp. 418-419.

Murray, A.B. (2003): Contrasting the goals, strategies, and predictions associated with simplified numerical models and detailed simulations – in: Iverson, R.M., Wilcock, P.R. [eds.](2003): Predictions in Geomorphology, American Geophysical Union, Geophysical Monograph, No. 135, pp. 151-165.

Murray, A.B., Thieler, E.R. (2004): A new hypothesis and exploratory model for the formation of large-scale inner-shelf sediment sorting and "rippled scour depressions" – Continental Shelf Research, Vol. 24, pp. 295-315.

Oldfield, F., Rummery, T.A., Thompson, R., Walling, D.E. (1979): Identification of Suspended Sediment Sources by Means of Magnetic Measurements: Some Preliminary Results – Water Resources Research, Vol. 15, No. 2, pp. 221-18.

Petrovsky, E. (2007): Susceptibility – in: Gubbins, D., Herrero-Bervera, E. [eds.](2007): Encyclopedia of Geomagnetism, Springer, Berlin, pp. 931-933.

Razik, S., Chiessi, C.M., Romero, O. von Dobeneck, T. (2013): Interaction of the South American Monsoon System and the Southern Westerly Wind Belt during the last 14 kyr – Palaeogeography, Palaeoclimatology, Palaeoecology, Vol. 374, pp. 28–40.

Razik, S., Govin, A., Chiessi, C.M., von Dobeneck, T. (2015): Depositional provinces, dispersal, and origin of terrigenous sediments along the SE South American continental margin – Marine Geology, Vol. 363, pp. 261–272.

Schwalenberg K., Haeckel, M., Poort, J., Jegen, M. (2009): Evaluation of gas hydrate deposits in an active seep area using marine controlled source electromagnetics: Results from Opouawe Bank, Hikurangi Margin, New Zealand – Marine Geology, Vol. 272, pp. 79-88, doi:10.1016/j.margeo.2009.07.006.

Shields, A. (1936): Anwendung der der Ähnlichkeitsmechanik und der Turbulenzforschung auf die Geschiebebewegung – Mitteilungen der Preußischen Versuchsanstalt für Wasserbau und Schiffbau, Vol. 26, Berlin, 26 pp.

Slingerland, R., Smith, N.D. (1986): Occurence and formation of water-laid placers – Annual Review of Earth and Planetary Sciences, Vol 14, pp. 113-47.

Soulsby, R.L. (1997): Dynamics of Marine Sand – Thomas Telford Publishing, London, 272 pp.

Soulsby, R.L., Whitehouse, R.J.S.W. (1997): Threshold of sediment motion in coastal environments – Proceedings of Pacific Coasts and Ports '97 Conference Christchurch, Vol.1, pp. 149-54. University of Canterbury, New Zealand.

van Rijn, L.C. (1993): Principles of Sediment Transport in Rivers, Estuaries and Coastal Seas – Aqua, Amsterdam.

van Rijn, L.C. (2007 a): Unified View of Sediment Transport by Currents and Waves. I: Initiation of Motion, Bed Roughness and Bed-Load Transport – Journal of Hydraulical Engineering, Vol. 133, No. 6, pp. 649-667.

van Rijn, L.C. (2007 b): Unified View of Sediment Transport by Currents and Waves. II: Suspended Transport – Journal of Hydraulical Engineering, Vol. 133, No. 6, pp. 668-689.

van Rijn, L.C. (2007 c): Unified View of Sediment Transport by Currents and Waves. III: Graded Beds – Journal of Hydraulic Engineering, Vol. 133, No. 7, pp. 761-775.

Wilson, G.S., Roberts, A.P. (1999): Diagenesis of magnetic mineral assemblages in multiply redeposited siliciclastic marine sediments, Wanganui basin, New Zealand – in: Tarling, D.H., Turner, P. [eds.](1999): Palaeomagnetism and Diagenesis in Sediments, Geological Society, London, Special Publications, Vol. 151, pp. 95-108.

Won, I.J., Keiswetter, D.A., Hanson, D.R., Novikova, E., Hall, T.M. (1997): GEM-3: A monostatic broadband electromagnetic induction sensor – Journal of Environmental and Engineering Geophysics, Vol. 2, No. 1, pp. 53-64.

Wright, J., Colling, A., Park, D. [eds.] (1999): Waves, tides and shallow water processes – Butterworth Heinemann, Oxford, 227 pp.

Zhang, S., Cioppa, M., Zhang, S. (2010): Spatial Variations in Particle Size and Magnetite Concentration on Cedar Beach: Implications for Grain-Sorting Processes, Western Lake Erie, Canada – Acta Geologica Sinica (English Edition), Vol. 84, No. 6, pp. 1520-1532.

Ždanov, M.S., Keller, G.V. (1994): The Geoelectrical Methods in Geophysical Exploration – Methods in Geochemistry and Geophysics, Vol. 31, Elsevier, New York, 884 pp.

Chapter 2

Lithofacies distribution and sediment dynamics on a storm-dominated shelf from combined photographic, acoustic and sedimentological methods (Bay of Plenty, New Zealand)

Tobias Kulgemeyer[a], Tilo von Dobeneck[a], Hendrik Müller[a], Karin Bryan[b], Willem de Lange[b], Christopher Battershill[b]

[a]Faculty of Geosciences and MARUM - Center for Marine Environmental Sciences, University of Bremen, Klagenfurter Straße, 28359 Bremen, Germany

[b]School of Science, University of Waikato, Private Bag 3105, Hamilton, New Zealand

Published in:
Marine Geology, Vol. 376, pp. 158-174, doi:10.1016/j.margeo.2016.03.005

Abstract

Sediment dynamics a storm-dominated shelf (western Bay of Plenty, New Zealand) were examined using the newly developed benthic profiler MARUM *NERIDIS III*. An area of 60 km $\times$ 7 km area between 2-35 m water depth was surveyed with this bottom-towed sled equipped with a high-resolution camera for continuous close-up seafloor photography and a CTD with connected turbidity sensor. Here we introduce our approach of using this multi-parameter dataset combined with sidescan sonography and sedimentological analyses to create detailed lithofacies and bedform distribution maps and to derive

regional sediment transport patterns.

For the assessment of sediment distribution, photographs were classified and their spatial distribution mapped out according to associated acoustic backscatter from a sidescan sonar. This provisional map was used to choose target locations for surficial sediment sampling and subsequent laboratory analysis of grain size distribution and mineralogical composition. Finally, photographic, granulometric and mineralogical facies were combined into a unified lithofacies map and corresponding stratigraphic model. Eight distinct types of lithofacies with seawards increasing grain size were discriminated and interpreted as reworked relict deposits overlain by post-transgressional fluvial sediments.

The dominant transport processes in different water depths were identified based on type and orientation of bedforms, as well as bottom water turbidity and lithofacies distribution. Observed bedforms include subaquatic dunes, coarse sand ribbons and sorted bedforms of varying dimensions, which were interpreted as being initially formed by erosion. Under fair weather conditions, sediment is transported from the northwest towards the southeast by littoral drift. During storm events, a current from the southeast to the northweast is induced which is transporting sediment along the shore in up to 35 m water depth. Shorewards oriented cross-shore transport is taking place in up to 60 m water depth and is likewise initiated by storm events.

Our study demonstrates how benthic photographic profiling delivers comprehensive compositional, structural and environmental information, which compares well with results obtained by traditional probing methods, but offers much higher spatial resolution while covering larger areas. Multi-sensor benthic profiling enhances the interpretability of acoustic seafloor mapping techniques and is a rapid and economic approach to seabed and habitat mapping especially in muddy to sandy facies.

2.1 Introduction

Coastal regions are the most heavily populated and most dynamic environments on the planet. They are constantly undergoing both natural and man-made changes on time scales from hours (storms, tsunamis, oil spills) over decades (settlement and coastal engineering projects, coastal erosion) to centuries (climate and sea level change) and longer (subsidence, rifting). A thorough under-

standing of the processes at work is crucial for the prediction and mitigation of their future development (Gao & Collins, 2014; Schwab et al., 2014; DeFalco et al., 2015). Although in populated regions the shores themselves are often regularly or even permanently monitored, substantial research also has to include the adjacent areas of the inner continental shelf. The composition and distribution of sediment facies (Bradshaw et al., 1994; Hanquiez et al., 2007; Thieler et al., 2014) including shell and mineral enrichments (Frihy, 1994; Badesab et al., 2012; Li et al., 2015) as well as morphological features of the seafloor like sorted bedforms (Cacchione & Drake, 1984; Green et al., 2004; Coco et al., 2007; Trembanis & Hume, 2011; DeFalco et al., 2015) and subaquatic dunes or sand ridges (Duane et al., 1972; Swift et al., 1972; Figueiredo et al., 1982; Parker et al., 1982; Bradshaw et al., 1994; Lobo et al., 2000; Simarro et al., 2015) are indicators of hydro- and sediment dynamics of coastal systems.

On wave dominated shelves, sediment transport is controlled by the action of waves in contrast to tides. Storm-dominated shelves are a subset where net sediment transport is mostly driven by high-energy storm waves (Heward, 1982). Most parts of the New Zealand shelf falls under this definition (Carther & Heath, 1975). The study area in the Bay of Plenty (Fig. 2.1) gained the attention of the international media when a container ship, the MV *RENA*, ran aground on Astrolabe Reef in October 2011. For the "*RENA* Long Term Environmental Recovery Monitoring Program" a quick assessment of the state of the seafloor by various bio- and geoscientific studies was necessary (Battershill et al., 2013). This was an opportunity for the first large-scale deployment of the new benthic profiler *NERIDIS III* (Fig. 2.2) that was developed at the University of Bremen/MARUM. A survey in November 2012 was initiated by INTERCOAST, a cooperative graduate school of the Universities of Bremen and Waikato.

The main instrument of *NERIDIS* is an induction coil sensor that measures the magnetic susceptibility and electric conductivity of the surficial sediment down to $\sim$50 cm giving an insight into the petrology and porosity of the seafloor. Additional instruments include a digital flash camera system for continuous high-resolution seafloor photography, and a conductivity, temperature and depth probe (CTD)

with turbidity sensor. This paper examines the sedimentological environment by analyzing seafloor images and accompanying sidescan sonography as well as sample material that was collected during a later survey in December 2013; size and complexity of the electromagnetic data will require a separate publication.

The ability to gain continuous data on large areas has made hydroacoustic methods the standard approach for seafloor mapping (Mayer, 2006). However, the acoustic response of the seafloor is not unique and an accurate interpretation requires ground truthing by independent methods (Barnhardt et al., 1998; Pandian et al., 2009). This is achieved by sampling or by optical examination through videos and still photographs (the latter often in a biological context as it allows the identification of biota and corresponding substrate sediments). Most optical systems are installed in ship-towed platforms or ROVs and operate in a distance of 1-4 m from the seafloor (Milkov et al., 1999; Rooper et al., 2007; Erdey & Cochrane, 2015; Williams et al., 2015). Common classifications make use of a descriptor (mud, sand, pebble etc.) and differentiate primary and secondary substrates for a given area (Stein et al., 1992; Yoklavich et al., 2000). In contrast, the camera on board of *NERIDIS* operates from a ground distance of 40 cm, and the high resolution enables the differentiation of fine, medium and coarse sand. Although close-up seafloor photography has been done in the past (Kostylev et al., 2001), it is mostly punctual. The camera installed on *NERIDIS* operates with a high frequency and produces a continuous coverage of the profile. As it is rarely used, no standard approach for the classification of this kind of imagery exists so far. The one used here builds on the strengths of high resolution close-up photography. Theoretically, individual grains can be distinguished in sediments larger then medium sand (although practically, motion blur is hindering accurate grain size estimation). This allows for a classification oriented on classical sedimentological methods as they are used e.g. for the description of cores. On this basis, an approach for sedimentological seafloor mapping is developed.

Through this novel multiproxy strategy of geophysical benthic profiling combined with sedimentological laboratory analyses, this study provides insights into bed-

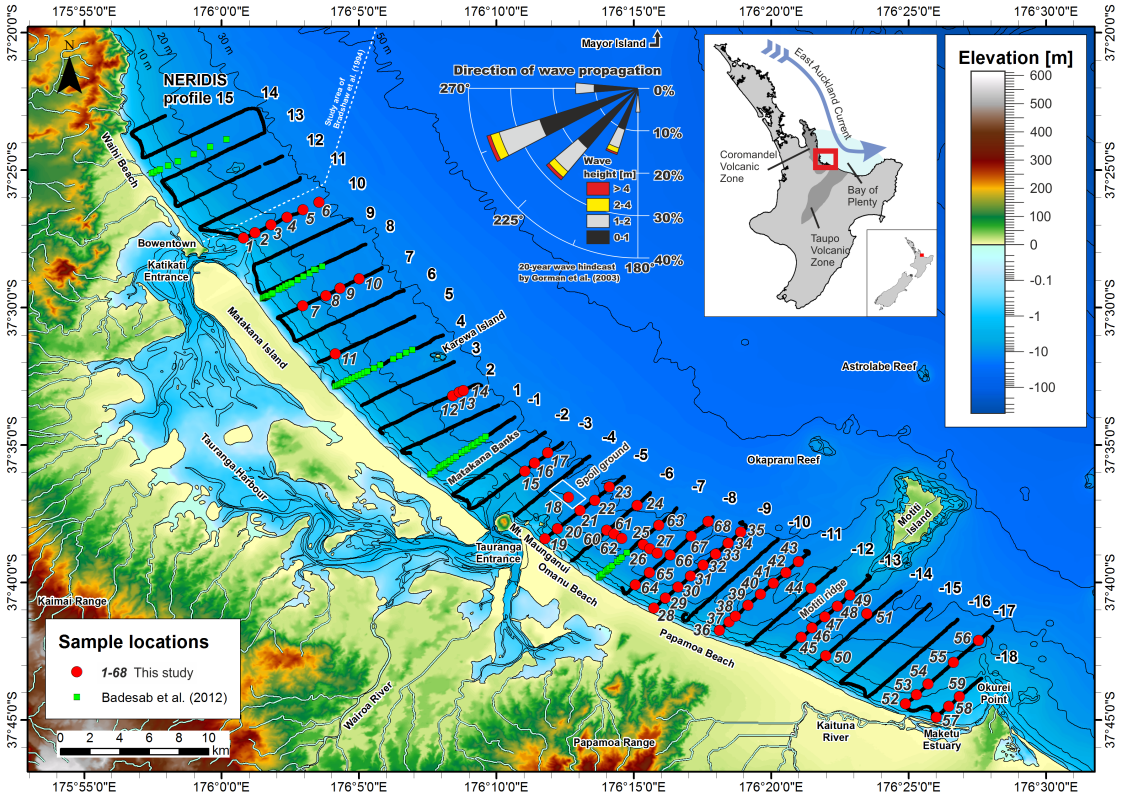

Figure 2.1: Overview of the study area with sample locations and *NERIDIS* survey profiles. Topographic data from Land Information New Zealand (LINZ) database. The bathymetry is interpolated from combined LINZ data and own multibeam sonar measurements. Extent of CVZ and TVZ from Briggs et al. (2005), wave hindcast by Gorman et al. (2003).

forms, sediment distribution and transport in a storm-dominated coastal system from the shoreface to the inner shelf. This includes: 1) the definition and mapping of sediment facies using combined photographic, hydroacoustic, granulometric and mineralogical evidence; 2) classification and examination of seafloor morphology on the basis of sidescan sonography; 3) integration of 1 and 2 together with additional information provided by bottom-water turbidity; 4) the development of a conceptual sediment transport model.

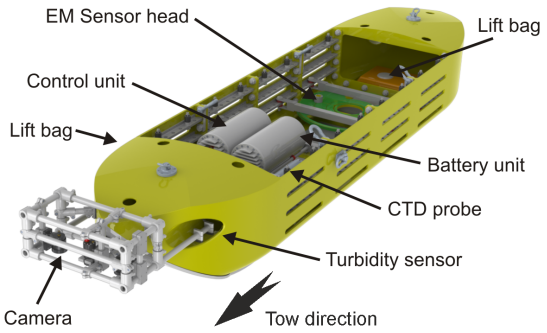

Figure 2.2: Schematic view of the benthic profiler *NERIDIS III* and incorporated systems.

2.2 Study area

2.2.1 Geographic and geological setting

The Bay of Plenty (BoP) is located on the northern coast of New Zealand's North Island (Fig. 2.1). It is confined to the east by the East Cape region and to the west by the Coromandel Peninsula. On a regional scale, oceanic water masses in the BoP are subject to the northwest-southeast flowing East Auckland Current (Brodie, 1960). The study area comprises the coastal region of approximately the western third of the bay and spans 60 km from the northern end of Waihi Beach to Okurei Point (Town Point) (Fig. 2.1). The cross-shore extent of the survey area is 7 km with water depths ranging from 2 m to 35 m.

The most prominent landmark of this region is the Tauranga Harbour estuary, a mesotidal lagoon that is shielded from the sea by the barrier island of Matakana (Healy & Kirk, 1982; Healy et al., 1996). The main freshwater input of Tauranga Harbour is Wairoa River (Park, 2004), which transports sediments from rhyolitic source rocks in the Taupo Volcanic Zone (TVZ) northwards into the southern basin (Briggs et al., 2005). The hydrologically independent (De Lange, 1988) northern basin is supplied by smaller local streams draining the Kaimai Ranges, which mark the transition of the older dacitic to andesitic Coromandel Volcanic Zone (CVZ) to the younger TVZ (Briggs et al., 2005). Two entrances north (Katikati Entrance) and south (Tauranga Entrance) of the island connect Tauranga

Harbour to the BoP. At both entrances, the side opposite to Matakana is confined by an outcrop of rhyolitic volcanic rock (Briggs et al., 2005) which is connected to the mainland by a narrow tombolo (Healy et al., 1996). In the north, this is the 88 m high Bowentown dome while in the south the 231 m Mt. Maunganui is the highest topographic feature. Both domes were formed TVZ 2 - 3 Ma ago in association with the (Briggs et al., 2005; Cole, 1979). At both entrances, sediment export is driven by ebb-tidal currents (Davies-Colley & Healy, 1978a; Hicks & Hume, 1996, 1997). Sediment exiting Tauranga Entrance forms the ebb-tidal delta of the Matakana Banks. Shell-lag is covering parts of the entrance channel (Krüger & Healy, 2006). A large portion of the sediment is recirculated by a system of tide-induced eddies and returns in a southwesterly direction into the estuary, along with material derived from the inner shelf (Davies-Colley & Healy, 1978a,b; Spiers et al., 2009). To allow larger vessels to reach the port of Tauranga, the natural ebb tidal delta of Tauranga Entrance has been dredged and deposited in dumping grounds between 4-7 m, 15-25 m and 28-33 m depths offshore Mt. Maunganui (Healy et al., 1991; Davis & Healy, 1993; Foster et al., 1994, 1996; Michels & Healy, 1999).

Another source of sediment for the western BoP are the Maketu estuary and the mouth of Kaituna River at the southeastern end of the study area. The Kaituna derives sediment from nonwelded rhyolitic ignimbrites north of Lake Rotorua and Lake Rotoiti, which originate from the TVZ (Leonard et al., 2010). The river originally discharged into the estuary, but was artificially diverted in 1956 (Burton & Healy, 1985).

The coastline in the western BoP consists of long, sandy beaches. In general, the littoral drift in the study area is directed towards the southeast (Healy, 1977; Healy et al., 1977; Harray & Healy, 1978; Hicks et al., 1999). The northernmost part of the study area at Waihi Beach is prone to erosion (Harray & Healy, 1978; Bear et al., 2009), although onshore transport of sediment has been recorded at the southern end of Waihi Beach (Bear et al., 2009). The 24 km long barrier island of Matakana has been formed by the building and later convergence of two to three smaller bars during the Holocene on a Pleistocene proto-barrier

(Shepherd et al., 1997, 2000). Nowadays the coastline shows little change apart from short-term fluctuations (Gibb, 1994). Omanu and Papamoa Beach are described as in a state of dynamic equilibrium (Iremonger et al., 2011).
Ten kilometers offshore of the southeastern end of Papamoa Beach is Motiti Island, an andesitic lava dome (Briggs et al., 2005) that was formed between 4.32 Ma and 3.42 Ma (Henry, 1991) and has been eroded down to only a flat remnant.

2.2.2 Regional sediment composition

Bradshaw et al. (1994) provide a general model for Holocene sedimentation on the inner Coromandel shelf directly north of the study area where they describe two main lithofacies groups. The underlying bed of about 5m thickness is an autochthonous deposit (Bradshaw & Nelson, 2004) formed by the erosion of Pleistocene sands during the post-glacial transgression between 12 and 6.5 ka. This sediment has a high content of plagioclase (48 %) and quartz (20 %); additional components are lithic fragments (15 %), volcanic glass (8 %) and some heavy minerals (9 %). After sealevel stabilization, these sands were reworked; while their finer fractions moved towards the beach, the coarse fraction remained as lag deposit on the inner shelf. In the late Holocene, the second lithofacies group entered the system when fine and very fine sands were allochthonously delivered from infilled estuaries and started to cover the autochthonous deposits. This overlying bed of less than 5 m thickness (Bradshaw & Nelson, 2004) is rich in volcanic glass (48 %) and consists otherwise of 31 % plagioclase, 15 % lithic fragments, 9 % quartz and 2 % heavy minerals. For both types of sediment the heavy mineral fraction is made up of hypersthene, opaque minerals, green and brown hornblende, cummingtonite and augite (in decreasing order of percentage).

2.2.3 Oceanographic conditions and sediment transport

The shelf of northeastern New Zealand is generally seen as a storm-dominated environment. Tidal currents play only a minor role in the inner shelf dynamics

(Bradshaw et al., 1991); an exception in the study area are the entrances to Tauranga Harbour (Spiers et al., 2009). Most wave energy arrives from the open sea from the northeast sector (Pickrill & Mitchell, 1979; Macky et al., 1995; Gorman et al., 2003). Shelf currents in the western BoP have been investigated north of the study area, on the Coromandel shelf (Bradshaw et al., 1991). This system is controlled by two opposing along-shelf currents that develop under different weather conditions: during fair weather, a weak southerly directed current is observed, which Bradshaw et al. (1991) linked to the influence of the East Auckland Current (see also Fig. 2.1). This remotely forced current is by itself incapable of sediment transport, most transport occurs cross-shore either by wave action in the surf zone (onshore) or rip currents (offshore) (Bradshaw et al., 1994). Under storm conditions, onshore waves pile up water on the shore. This creates a cross-shore pressure gradient, which initiates a downwelling bottom return flow. In balance with Coriolis forces, this leads to a northerly geostrophic current which transports sediments in up to to 80 m depth (Bradshaw et al., 1991, 1994). In principle, this bidirectional current regime also acts in the study area. Wave modeling shows that average waves are only capable to entrain sediment in water depths less than 10 m and transport it onshore and to the southeast. Sediment in deeper water is only affected by storm waves (Badesab et al., 2012).

2.3 Materials and methods

2.3.1 Benthic profiling

The benthic profiler *NERIDIS III* (Fig. 2.2) was used for an extensive survey of the inner western BoP in November 2012. The system operates as a ship-towed sled and requires ground contact for proper operation. The workboat for the survey was the 14 m long aluminium hulled MV *MACY GRAY*, owned and operated by Western Work Boats Ltd. *NERIDIS* is 5.2 $\times$ 1.2 $\times$ 0.8 m in size, and made from non-magnetic, non-conductive materials. Its weight is 900 kg in air and ca. 250 kg in water (Müller et al., 2012).

The profiler's position was determined from the shipboard GPS system by taking

the length and angle of the tow cable into consideration. Head, pitch, roll and acceleration were recorded for later correction. With a typical towing speed of 2-4 kn (1-2 m/s) and a capacity of the two internal 40 Ah 24 V/12 V lithium ion batteries for 7-12 h operation (depending on the instruments used), one dive between battery changes can cover ca. 50-85 km. The operation was monitored via a coax link SHDSL.

2.3.2 CTD and measurement of turbidity

The profiler was equipped with a Sea & Sun Technology CTD 60M multiparameter probe. A connected Seapoint Sensors turbidity sensor monitored the light scattering at 0.5 m above the seafloor. The acquired data were expressed in Formazine Turbidity Units (FTU) on a limited linear scale from 0-25 in 0.001 FTU increments.

2.3.3 Seafloor photography

An AVT Prosilica GC2450C camera system provided by the German Research Center for Artificial Intelligence (DFKI) was installed in a downward orientation in the bow of the profiler from where it could take pictures with a resolution of 1900 $\times$ 1900 on a 40 cm $\times$ 40 cm area. Pictures were taken with a frequency of 5 Hz at a towing speed of 2 m/s which leads to an overlapping coverage of the seafloor's appearance. Two LED flashlights with 200 µs flash exposure time on both sides of the camera ensure balanced lighting conditions and avoid motion blur. Overall, about 800,000 colour photographs of the seafloor were taken. As no automated scheme for the sedimentological evaluation of these photographs has been developed so far, a subset of ca. 6000 photos (one picture every 20 s $\approx$ every 30 m) was analyzed by visual observation.

2.3.4 Sidescan and multibeam sonography

Multibeam bathymetry was continuously recorded during the profiling using by a WASSP WMB-3250 echosounder installed on MV *MACY GRAY*. The system

operated at a frequency of 160 kHz with a swath width of 120°× 4°.
Acoustic backscatter data was previously acquired by Seaworks Ltd. with an EdgeTech sidescan sonar and covered the entire study area deeper then 10 m. Overlapping lines were surveyed with a separation of ca. 500 m. The data was processed using the software CARIS and later mosaiced into a single map.

2.3.5 Sampling

The sampling campaign took place about one year after the survey using preliminary results for targeting locations. Additional samples collected in early 2010 were study by Badesab et al. (2012) were added to the sample set. All samples were collected with a Van Veen grab sampler representing the uppermost 1-3 cm of seafloor.

2.3.6 Grain size analysis

About 4 g of each sample were dried and treated with 10 % H_2O_2 for 8-9 days to remove organic matter. Carbonate was kept in the samples as shell and sponge fragments were in some cases the main sedimentary constituents and, furthermore, to allow direct comparison of physical and visual grain sizes. Volumetric grain size distributions were measured by laser diffraction with a Malvern Instruments Mastersizer 2000 which can measure grains up to 2 mm in diameter. To prevent large particles from blocking the instrument, all samples were sieved at 1 mm. The sub-millimeter fraction was measured with the laser particle sizer. The coarser fraction was separated again by dry sieving in 1-2 mm and $\geq$ 2 mm fractions. These were weighed and the approximate volume percentage calculated using an estimated density of 2.7 g/cm^3. For a general classification of sediments, a slight error in the smallest fractions due to the presence of iron oxides can be neglected. The obtained data was analyzed with the software GRADISTAT from Blott & Pye (2001).

2.3.7 Mineralogical analysis

Sediments were micro-optically analyzed with a Zeiss Stemi 2000 binocular. As far as possible, minerals were identified based on colour, lustre and morphology. Also, the quantity of mafic (dark) minerals was estimated using reference charts. Additionally, some X-ray powder diffractometry was performed with a PANalytical Empyrean diffractometer equipped with a copper tube as radiation source where 2-Theta ranged from 10°-80° in increments of 0.02°. These data was examined using the PANalytical HighScore software with the PDF-2 database as reference.

2.4 Strategies and principles of investigation

The general scheme used for the lithofacies classification is outlined on the left side of Fig. 2.3: first, sediments were classified based on their photographic appearance (”photofacies”). Wherever possible, the respective facies boundaries were determined by associated acoustic backscatter data. However, this approach is not suitable for distinguishing adjacent facies of similar grain size. Where bedforms were observed between profiles, boundaries were drawn so that a single bedform was completely enclosed within one photofacies. Sampling stations were chosen according to the photofacies, and with consideration of existing samples from Badesab et al. (2012). From the samples, a mineralogical and a grain size related classification was created. In the second step, these mineral-, granu- and photofacies were combined into a single lithofacies scheme. The spatial extent was again based on the existing boundaries of the photographic facies map; final adjustments according to the methodology above were made if necessary.

The lithofacies map is one of the required inputs for the development of a conceptual sediment transport model as seen on the right side of Fig. 2.3. Along with turbidity, it allows to delineate erosive and non-depositional environments. Transport directions can be derived from the examination of the type and orientation of bedforms based on their acoustic backscatter patterns; turbidity provides some additional insight into these processes. The information about the apparent

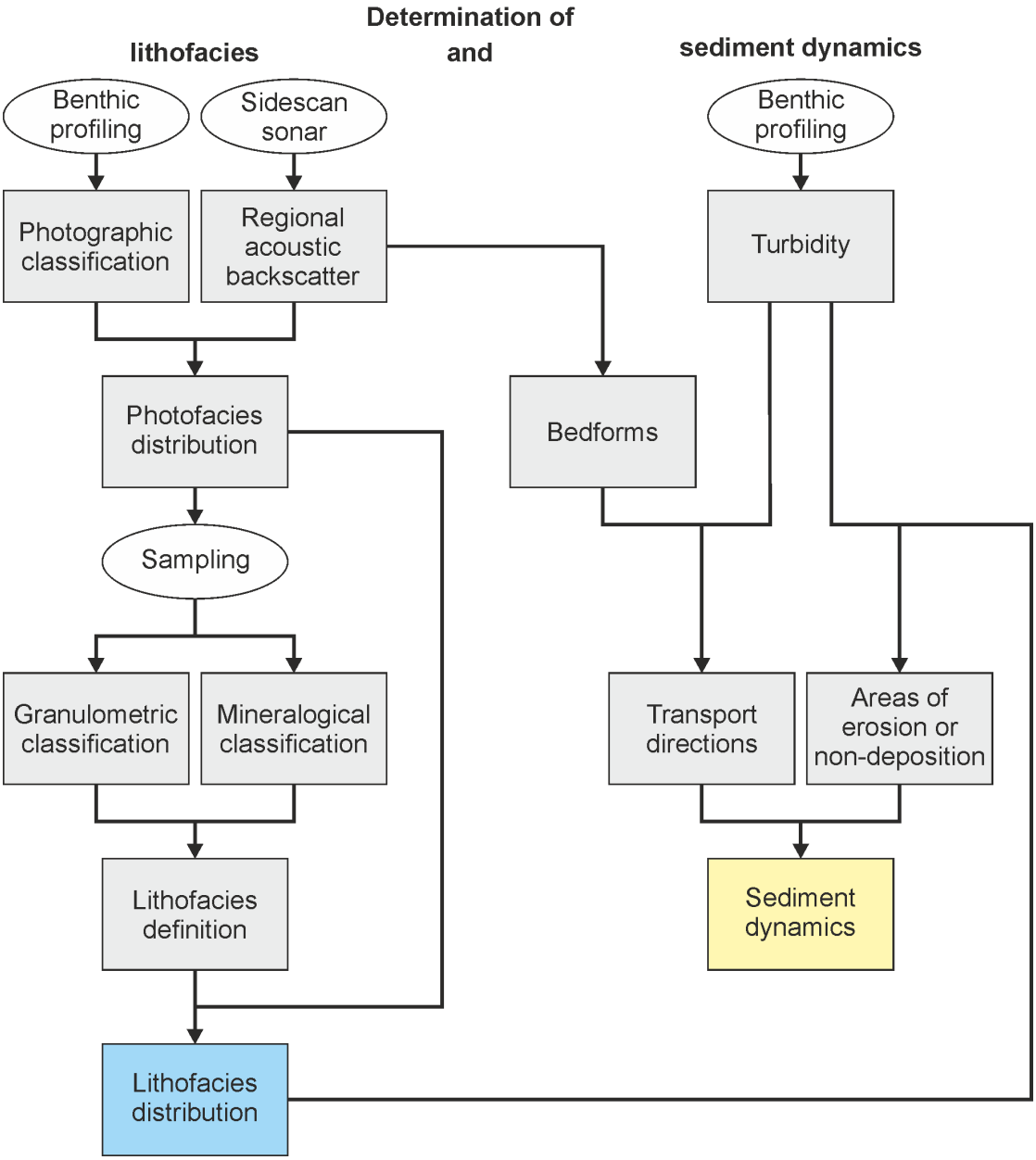

Figure 2.3: Classification scheme for the definition and mapping of the lithofacies and the deduction of sediment dynamics (explained in text, section 2.4).

sediment dynamics and direction of sediment transport are combined into a final conceptual model.

2.4.1 Photographic sediment classification

Three parameters were taken into account for the definition of photographic facies: colour according to the Munsell colour chart, apparent grain size and apparent composition. For an optical estimate of the grain size, an area of 1

cm^2 was selected in a representative image and every apparent grain marked by a rectangle. Following Fernlund (2005), the underlying assumption is that particles in the image are lying in a stable position and the visible part is close to the maximum projected area of the grain. In this position, the long side of the minimum bounding rectangle represents the long axis and the short side the intermediate axis of the particle (the short axis would be perpendicular to both). For an overall classification of grain size as fine to very coarse sand, the median of the intermediate axis (rounded to 10 µm) were used.

2.4.2 Mineralogical sediment classification

The mineralogical classification was based on microscopic optical observation referring to literature on the adjacent coastal areas (Bradshaw et al., 1994) and regional terrestrial geology (Ewart, 1965). Supporting XRD scans were performed on an instrument equipped with a Cu anode; this is problematic as Cu radiation leads to fluorescence in Fe which results in a high background level. It was also difficult to properly grind the samples with the available equipment. As a result, only quartz and plagioclase could clearly be identified while most of the mafic phases were either below the limit of detection or show distorted diffraction patterns.

However, the presence and a rough estimation of the amount of amorphous phases in the sample (probably volcanic glass) was deliverable with the technique. Although amorphous phases do not diffract radiation in a specific pattern, they lead to a characteristic increase of background radiation ("glass bulge") between a $2-\theta$ of about 10° and 30°(Zevin et al., 1995). The appearance of this bulge has been used to determine which samples contain glass. If it has been observed, we assume that the amount of glass in the sample is relatively high; Pawlowski (1985) gives 40 % (weight) as the minimal detectable amount of volcanic glass.

2.4.3 Granulometric sediment classification

The grouping of sediment samples based on grain size distributions was accomplished in three steps: the first step was a broad classification according to the

median grain size into fine, medium and coarse or very coarse sand. The second step accounted for the position of the main mode and, if necessary, a third step was conducted to find the position of a secondary mode. The second and third sorting steps were based on the far more detailed sub-millimeter distribution curves for fine and medium sand, whereas the complete distribution curves were used for coarse and very coarse sand.

2.4.4 Definition of bedforms

Bedforms were identified based on characteristic shapes and include coarse grain bands or patches, sorted bedforms as well as subaquatic dunes. Dunes were identified as elongated areas of high backscatter located next to a more or less strongly developed zone of low backscatter or acoustic shadow. The width (meaning the extension parallel to the crest/trough) and strike angle of each dune were measured in ArcGIS.

The defining characteristic of sorted bedforms is the grain size gradient in long-shore direction, where coarser grains are located at the up-current side (but not necessarily confined to the bathymetric low point (Murray & Thieler, 2004)) and form a sharp contrast to the surrounding finer grained sediments (Stark et al., 2012). The down-current side is usually more diffuse and can take the form of a series of ”fingers” extending from the main bedform (Spiers & Healy, 2007).

2.4.5 Interpolation and gridding of *NERIDIS* data

Turbidity data obtained by benthic profiling with *NERIDIS* were interpolated in ArcGIS via Universal Kriging. The dataset was not interpolated entirely as a whole but instead was divided into 10 overlapping areas which contain 4-5 profiles each. Thereby, Kriging parameters could be adapted by automatic as well as manual settings to each environment in a way that is physically reasonable and minimizes statistical errors.

2.5 Results and initial classifications

2.5.1 Photographic Facies

The photographic sediment classification led to the differentiation of six different classes (examples shown in Fig. 2.4, spatial distribution in Fig. 2.5). Due to technical problems, no photographs are available between profiles -6 and -8. Furthermore, large amounts of lea lettuce (*Ulva spp.*) covering the camera lens on profiles -2 and -3 made most of the photographs unsuitable for interpretation.

- **Photofacies 1** is a greyish black (Munsell colour N2) sand with an optical grain size in the medium sand fraction (400 µm). This photofacies occurs in water depths of 5-20 m. Close to the shoreline ripples are abundant as well as settlement by sand dollars, a species of echinoderms related to sea urchins. Occasionally bivalves occur within facies 1, but shells and shell fragment only make up a minor fraction of the sediment composition. Close to the southern entrance to Tauranga Harbour this sediment is covered with vegetation.

- **Photofacies 2** has a similar greyish black (N2) colour, but larger optical grain size than photofacies 1 (medium to coarse sand, 500 µm) and appears to be less well sorted. It is mostly found at 15-25 m water depth and commonly contains shell material.

- **Photofacies 3** has a greenish black colour (5GY 2/1) and a visual grain size of coarse sand (700 µm). This photofacies contains some very dark to completely black grains and often large amounts of shell material.

- **Photofacies 4** is a visually coarse to very coarse sand (1000 µm). This sediment is made up of medium dark grey (N4) as well as light olive (10Y 5/4) particles, most likely due to a large amounts of shell material. Photofacies 4 has only been observed on two distant locations in the study area, in front of the northern entrance to Tauranga Harbor and at the Maketu estuary. The variant in the southeast appears associated with black sand,

but these two types of sediment are not homogeneously mixed. Instead the black sand usually forms distinct dark deposits elongated parallel or at an angle up to 45° to the coastline within the light surrounding sediment. This feature is not present at the northern entrance.

- **Photofacies 5** occurs only southwest of Motiti Island and is clearly connected to the island itself. It is mostly made up of visually very coarse sand (1150 µm), that appears alongside larger clasts (pebbles and larger). The sediment has a medium dark grey (N4) colour and is frequently densely colonised by diverse biota including sea lettuce (*Ulva spp.*) and several species of bivalves.

- **Photofacies 6** is not a distinct sediment photofacies but describes areas where the seafloor is mostly covered with shells. This mainly occurs directly inside the southern entrance to Tauranga Harbour, but also on smaller, isolated patches south east of Motiti Island. While the former is made up of very large unbroken shells, the deposit in the southeast contains mostly fragments and some small unbroken shells.

2.5.2 Mineralogical composition

Sediments have been classified in four types of mineral compositions. Due to problems regarding XRD data, the definition of these types is mostly based on optical examination. Their spatial distribution is displayed in Fig. 2.5.

- **Type I** consists mostly of white or transparent minerals with glassy luster, either quartz or plagioclase feldspar. The sphericity of grains makes it difficult to differentiate based on cleavage. Mafic minerals make up about 2.5 % of the entire assemblage. They are mostly prismatic, occasionaly bladed and in some isolated cases, hexagonal and platy. Colours are black and dark green. In accordance with regional geology, they can be interpreted as pyroxene and hornblende, while the platy minerals are likely to be biotite. Additional components are irregularly shaped, transparent particles with very sharp edges; these are probably glass shards (see

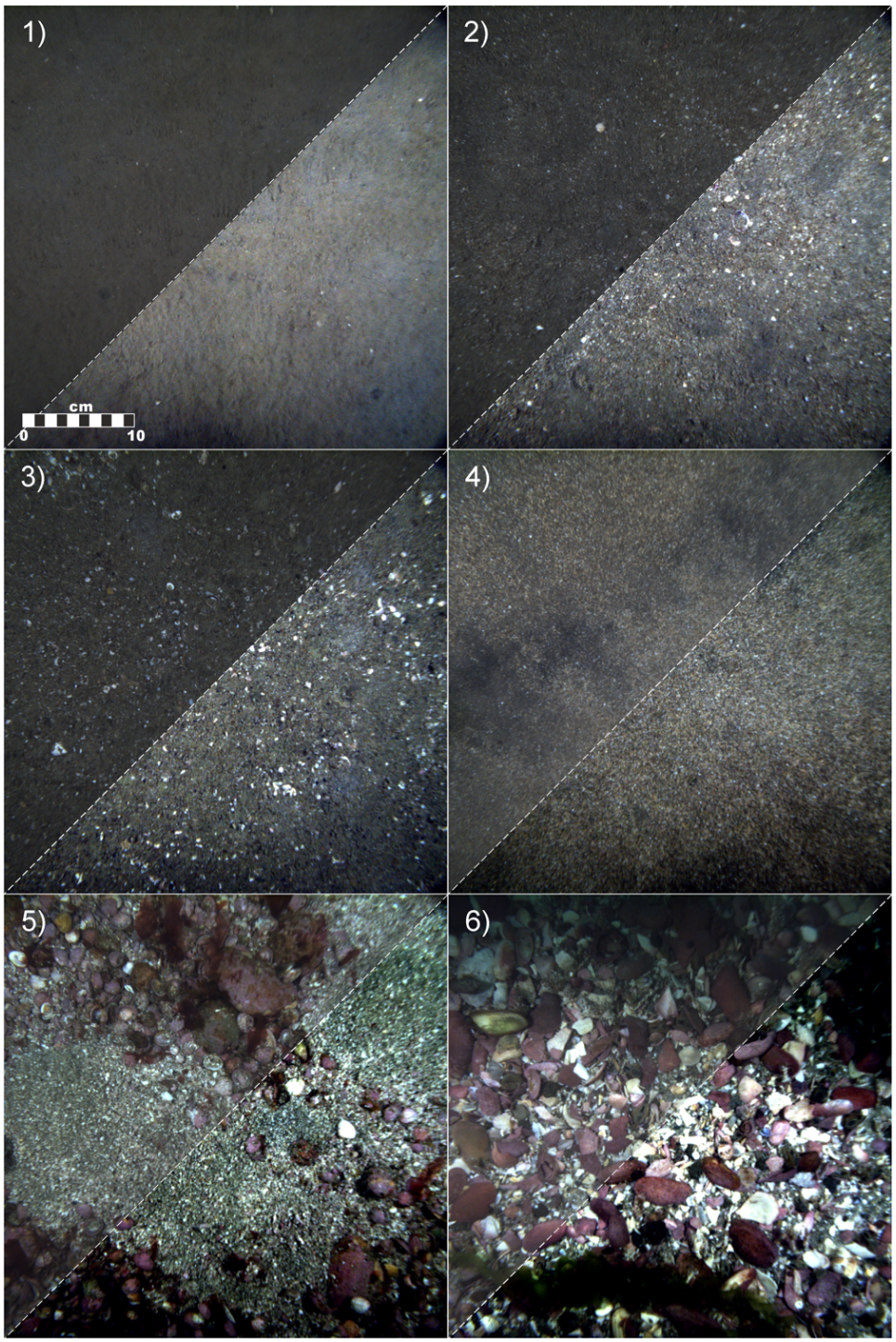

Figure 2.4: Examples of seafloor photos used for the classification of photofacies 1-6. The images shown are considered as typical representations, although every facies has a degree of variance. The upper left corner of each image is the original appearance, the lower right shows the photo with enhanced brightness, contrast and intensity. All photos are of the same scale (40 $\times$ 40 cm).

Bradshaw et al. (1994)). This interpretation is supported by the existence of the typical glass ”bulge” in the diffractogram of 15 out of the 21 samples belonging to this type. The very fine fraction of this type of sediment gives it an overall ”dusty” appearance.

- **Type II** The mafic fraction is more prominent in this type of sediment. It comprises about 5 % of all minerals, which are not only black but also brown in colour. These are again identified as mostly pyroxene and hornblende; biotite has not been found. In addition to single phases, this type also contains rock fragments. Glass shards could not be identified optically, although the shape of the diffractogram indicates an amorphous phase in 7 out of 41 samples. These seven samples belong to the more fine grained examples of type II and have a similar ”dusty” appearance to type I.

- **Type III** appears to be similar in composition to type II, but is mixed with a large amount of shell material (estimated around 25 %). Macroscopically this leads to an easily recognized brownish colour.

- **Type IV** is set apart from other sediment by its large amount of shell, sponge and other organic carbonate fragments (ca. 50 %). Terrestrial components seem to be similar to type II, including rock fragments. Mafic minerals, although negligible when the overall composition of the sediment is concerned, make up slightly more than 5 % of terrestrial components. A pebble-sized rock fragment is part of the sample and is consistent with this estimate. A petrographic analysis has not been conducted for this single piece, but judging from the outer appearance, it is made of andesite (which is to be expected given the proximity to Motiti Island).

2.5.3 Granulometry

All samples have been classified into six distinct groups (Fig. 2.6). Median grain sizes range from 132 µm to 919 µm. The spatial distribution map shows that the majority of the coarser grains are concentrated southwest of Motiti Island and as

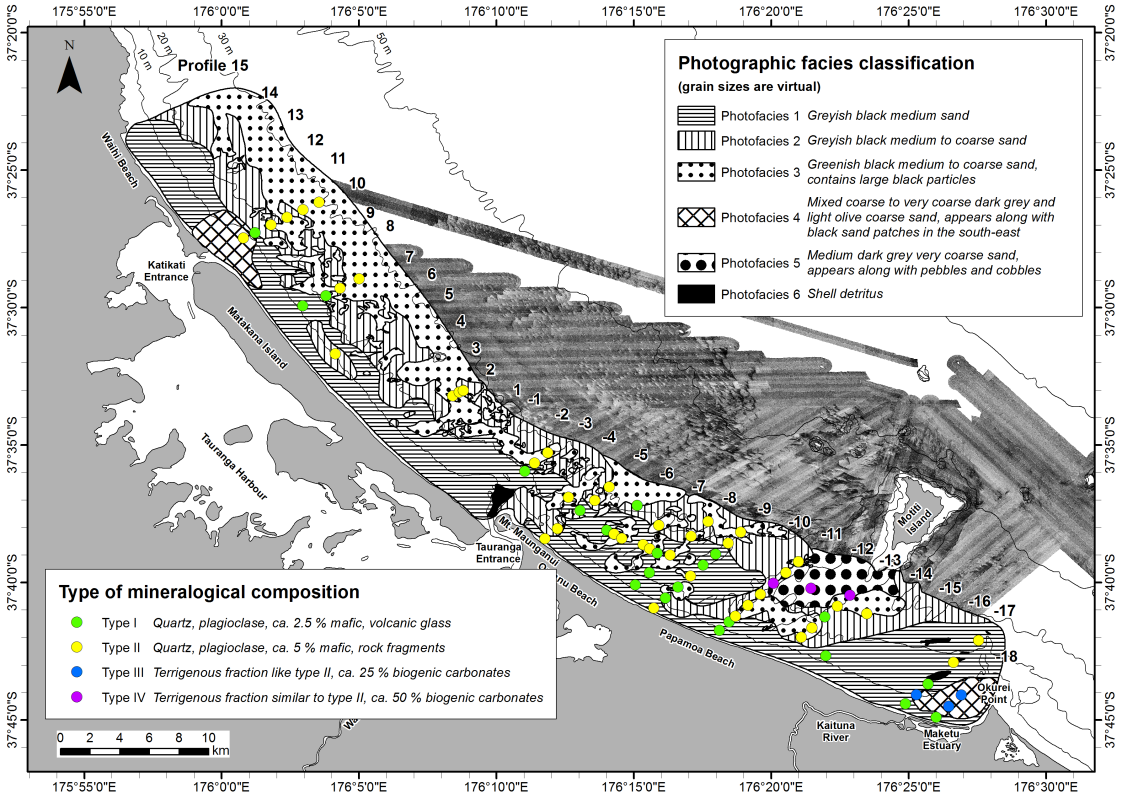

Figure 2.5: Spatial distribution of mineralogical composition derived from samples and photographic facies. Where possible, facies boundaries are based on acoustic backscatter; facies 3 and 5 have a notably high backscatter and strong contrast to surrounding sediments of smaller grain sizes. Because of a camera defect, no photographs are available between profile -6 and -8; due to their high backscatter, sorted bedforms in this area have been marked as photofacies 3.

part of sorted bedforms in the area along Omanu Beach. Additional locations are close to the Maketu Estuary and the northern entrance to Tauranga Harbor. Furthermore, a gradient from fine to coarse grains exists with growing distance from the shore, which is consistent with observations from earlier studies in the BoP (Bradshaw et al., 1994; Badesab et al., 2012).

- **Group A** is a bimodal fine sand. The median grain size is 178 µm and the main mode is at 194 µm. A small secondary mode (ca. 1 % of particles) is positioned at 34 µm. Sediments of this group are found in the entire study area in a water depth of up to 20 m, at Omanu Beach they even reach 30 m. The distribution of this group is for the most part identical to photofacies 1.

- **Group B** is a medium sand ($d_{50} = 237$ µm) with a slight bimodal distribution.

The main mode is at 325 µm, the second mode is located at the same grain size as in group A (34 µm), but is much less pronounced (ca. 0.5 %). Group B sediments appear to make up the largest portion of photofacies 2.

- **Group C** is a medium sand with median grain size of 360 µm. The mode of this distribution is often split into two almost equally high maxima at 325 and 460 µm with only a slight decrease between, but this form does not appear distinctive enough to constitute true bimodality.

- **Group D**, a unimodal coarse sand, is often encountered in the western BoP. The closest it has been found to the beach is at Maketu Estuary in a depth of 6 m; otherwise it appears to be more widespread in the deeper parts of the study area (below 20 m). It has a d_{50} of 640 µm and a mode of 750 µm. This group encompasses most of photofacies 3 and 4.

- **Group E** can not be easily distinguished from group D by the distribution curve alone. The median grain size is 692 µm and the mode is again at 750 µm. However, this sediment contains some particles that are even coarser than the 4 mm limit that was used for the distribution curves. The largest of these is a pebble with a diameter of 3 cm. Sediments of this group are identical to the mineralogical type IV and photographic facies 5.

- **Group F** is similar to group D, but contains a larger portion of coarser grains. The median grain size is considerably higher - 832 µm- and although the sole mode is also located at 750 µm, it is much less pronounced than in group D. This group also contains the coarsest sediment that was found during the sampling campaign: a very coarse sand from the center of a sorted bedform between profile -7 and -8.

2.5.4 Backscatter and bedforms

Regional acoustic backscatter generally increases towards the southeast. A particularly high backscatter can be observed on the ridge southwest of Motiti Island. Another noteworthy location is north of Tauranga Entrance, where the

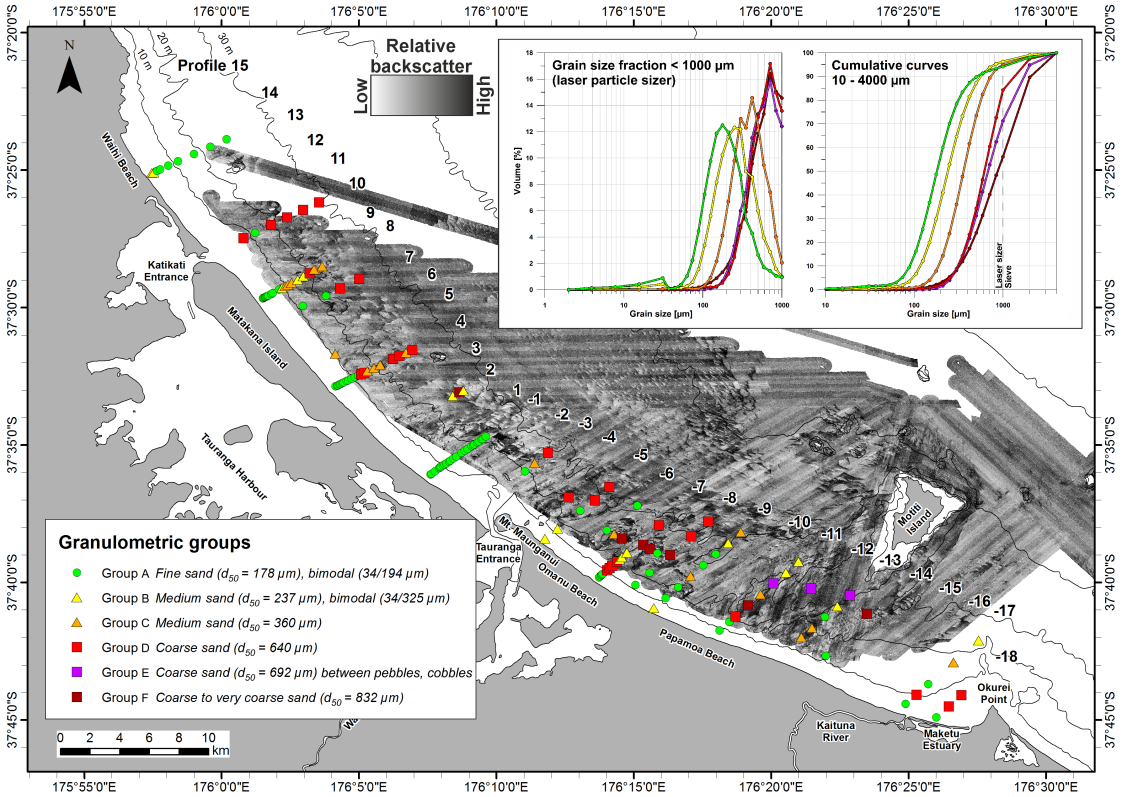

Figure 2.6: Spatial distribution of median grain sizes and granulometrical groups. These data include median grain sizes from Badesab et al. (2012). Given as an example are stacked curves of the six groups of grain size distribution curves. Group 1-3 are differentiated in the sub millimeter fraction (left) while group 4-6 contain larger grains and require the entire grain size spectrum.

otherwise very weak backscatter is interrupted by a structure with extremely high values below the 20 m isobath.

Sand patches and ribbons were found either as singular features or coupled with large, shore-normal striking dunes. In most cases, these features have a higher acoustic backscatter than the surrounding sediments, thus indicating coarser grain sizes. They are almost always oriented parallel to the coastline. On some occasions a single bedform bifurcates into a pattern of multiple bands (Fig. 2.7 a). In every observed case the bifurcation was oriented so that the scale decreased toward the northwest. Of special interest are long and very thin coarse sand ribbons south-southeast of Motiti Island in 20-25 m water depth (Fig. 2.7 c). They extend perpendicular to the mainland coast and parallel to the extent of the submarine ridge. The adjacent area also shows high and low backscatter features alternating without one of them being clearly dominant. These features

are concentrated in a bathymetric depression and follow the steepest gradient towards the 30 m isobath. Below this point, the sand ribbons disappear and instead a series of shore-parallel dunes is observed.

Sorted bedforms (500-650 m cross-shore, 200-300 m long-shore) were found along the coast of Matakana Island (Fig. 2.7 a). These structures are relatively poorly developed; the shape is not as distinctive and the boundaries not as sharp as described in literature. They strike perpendicular or at a slight angle to the coast and are oriented with the more diffuse end toward the northwest. Well developed sorted bedforms could be identified offshore of Omanu Beach. They extend perpendicular to the shoreline from southwest to northeast and stand out from their surroundings by a very high acoustic backscatter (Fig. 2.7 b). The structures are approximately 1 km long-shore and 2.5 km cross-shore. While their southeastern boundaries are abrupt with very strong backscatter, the northwestern limits have a ”feathered-out” appearance. Unfortunately, only few shore-parallel profiles were recorded, and only the shoreward end of one of the bedforms has been covered by the ship’s multibeam sonar. While this is not sufficient for conclusive observations, it appears that the bedforms coincide with slight depressions of the seafloor and the strongest backscatter occurs on their lowest point.

Subaquatic dunes are marked by a line parallel to their strike. While the region between 10 and 30 m water depth is densely covered in dunes, almost no bedforms could be found between 35 m and 40 m depth. However, a large dune field is again located between 40 m and 55 m. The majority of these deep-water bedforms strike parallel to the coast of the mainland. With decreasing distance to the shore, the angle changes to a more shore-normal orientation and dune width (meaning the extent parallel to the crest) increases. Towards the southeast, the strike angle changes and dunes become aligned parallel to the coast of Motiti Island (Fig. 2.8).

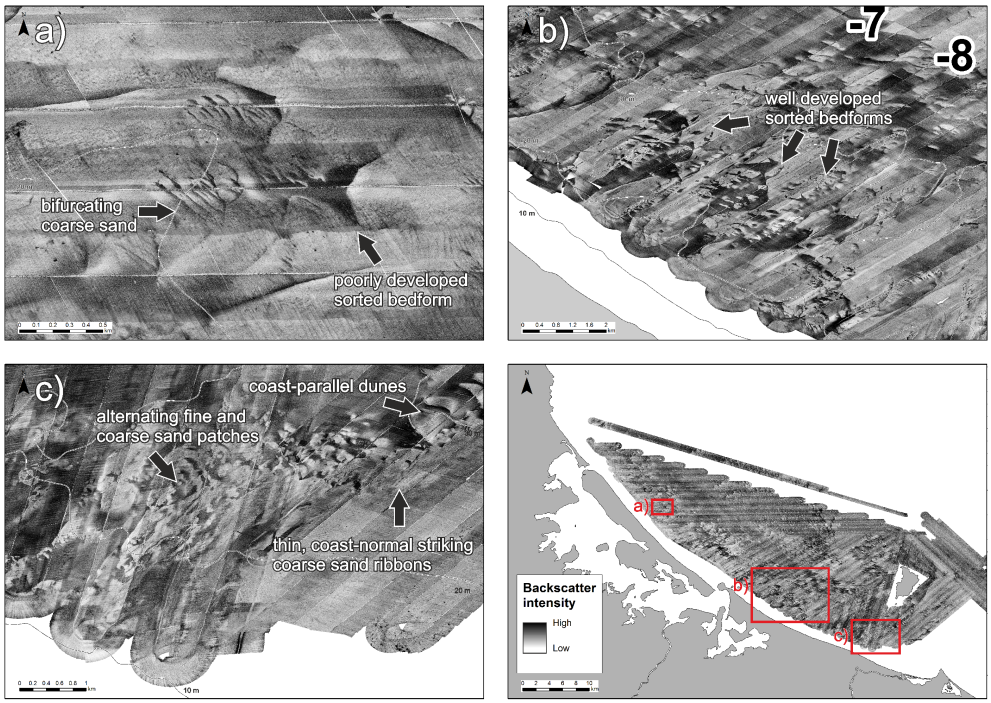

Figure 2.7: Examples of bedforms in the study area. These include coarse sand patches and ribbons as well as sorted bedforms of various dimensions and distinctiveness.

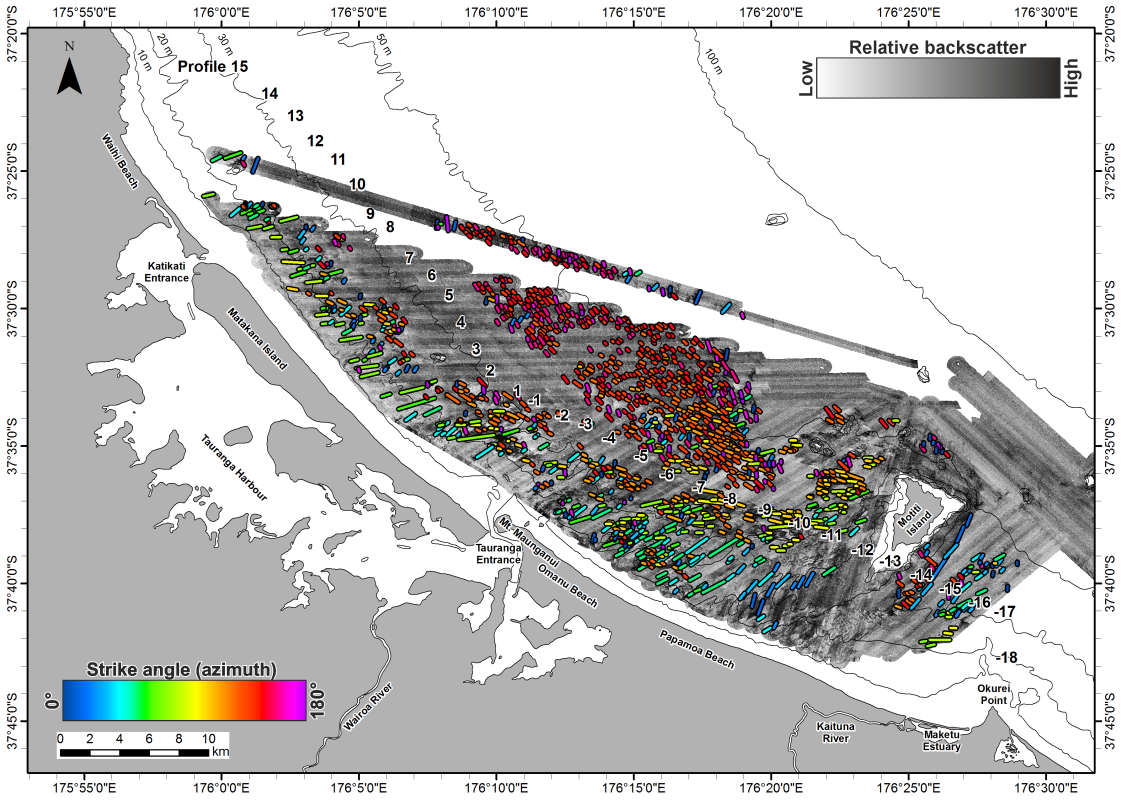

Figure 2.8: Strike angle of dunes in the western BoP in 10-60 m water depth. The angle changes with proximity to the coastlines of the mainland and a submarine ridge southwest of Motiti Island.

2.5.5 Turbidity

The turbidity of bottom water spans a wide range from 0.027 to 24.744 FTU, but the distribution is strongly right-skewed. With a median of 0.508, values higher than ca. 1 are confined to only a narrow section close to the beach where the water depth is less than 5 m. The only places where a turbidity in the higher range was measured was directly at Katikati Entrance and northwest of Tauranga Entrance (profile -3 to 2). The section along Omanu and Papamoa beach has a relatively low turbidity compared to similar water depths along the Matakana coastline. This only changes again east of the submarine ridge between Motiti and the mainland coast.

According to the records of the National Institute of Water and Atmospheric Research (NIWA), the weather conditions were stable over the duration of the *NERIDIS* survey. A part of profile -3 had to be removed from the dataset, in this case turbidity exceeded the sensor range which was probably the result of sea lettuce coverage on the profiler (see Fig. 2.9).

2.6 Discussion

2.6.1 Lithofacies

The lithofacies classification of seafloor sediments was achieved by combining the different datasets of photographic facies, grain size characteristics and mineral content in a joint model (see Table 2.1). This was done by matching the corresponding mineral facies type and grain size distribution groups. The final nomenclature is oriented on the existing photographic facies to take the appearance on a larger scale into account and simplify the comparison of these two schemes in the final lithofacies map.

The physical properties of sediment as determined from samples fit generally well to the initial frame provided by optical appearance. This is especially clear for grain sizes, the major criterion for the definition of photofacies. However, grain sizes detectable from photographs are considerably coarser than those

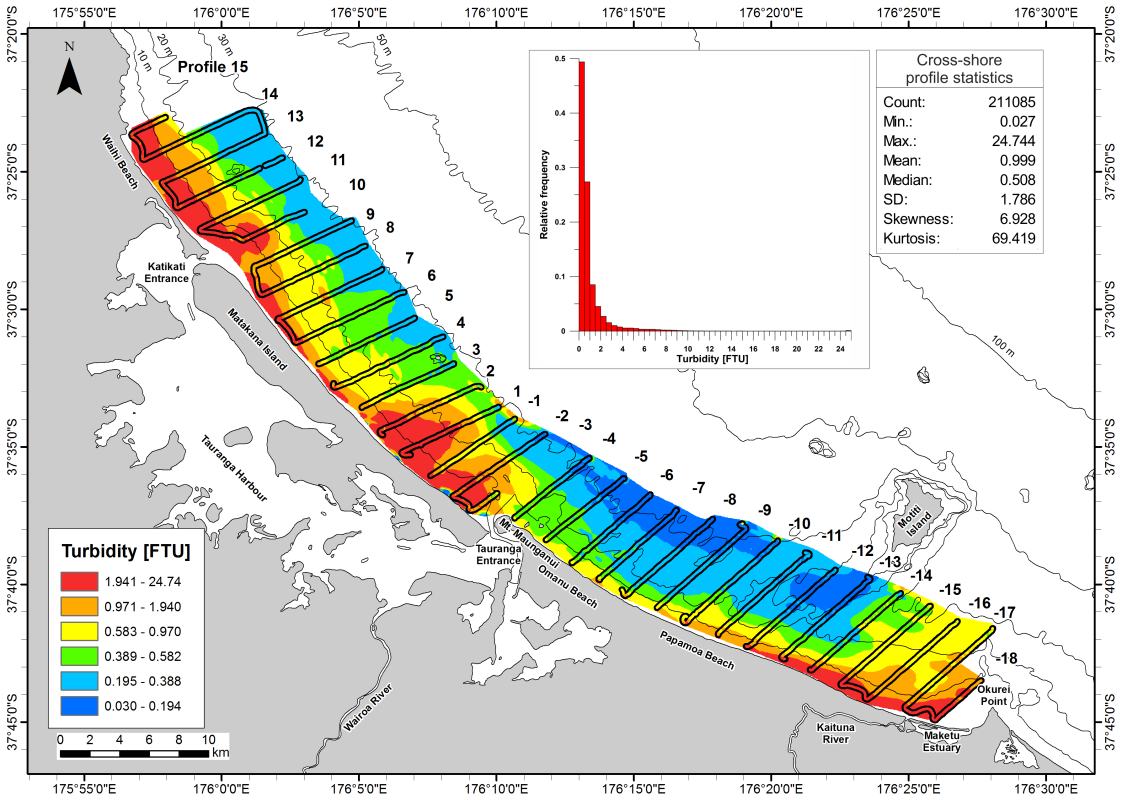

Figure 2.9: Bottom water turbidity (0.5 m above the seafloor) in the study area on a quantile scale.

Table 2.1: Relation of photographic, granulometric and mineralogical classifications to lithofacies.

Photofacies (grain sizes are optical)		Grain size distribution		Mineral composition		Lithofacies	
1	greyish black, medium sand	A	bimodal fine sand	I	ca. 2.5 % mafic, volcanic glass	1	widespread, late Holocene deposit
2	greyish black, medium to coarse sand	B	bimodal medium sand	II	ca. 5 % mafic, rock fragments, rare volcanic glass	2a	widespread, early Holocene deposit, some mixing with facies 1
		C	medium sand			2b	patches, early Holocene deposit
3	greenish black, coarse sand	D	coarse sand			3a	widespread, early Holocene deposit
		F	coarse to very coarse sand			3b	patches, the oldest early Holocene deposit
4	medium dark grey + light olive, coarse to very coarse sand	D	coarse sand (terrestrial: medium sand)	III	terrigenous fraction like II, ca. 25 % biogenic carbonates	4	only at Okurei Point, transported shells mixed with facies 2b
5	medium dark grey, very coarse sand; pebbles, cobbles	E	coarse sand between pebbles, cobbles	IV	terrigenous fraction similar to II, ca. 50 % biogenic carbonates	5	only south of Motiti Island, facies 2a/3a influenced by local sources
6	shell detritus					6	shell detritus

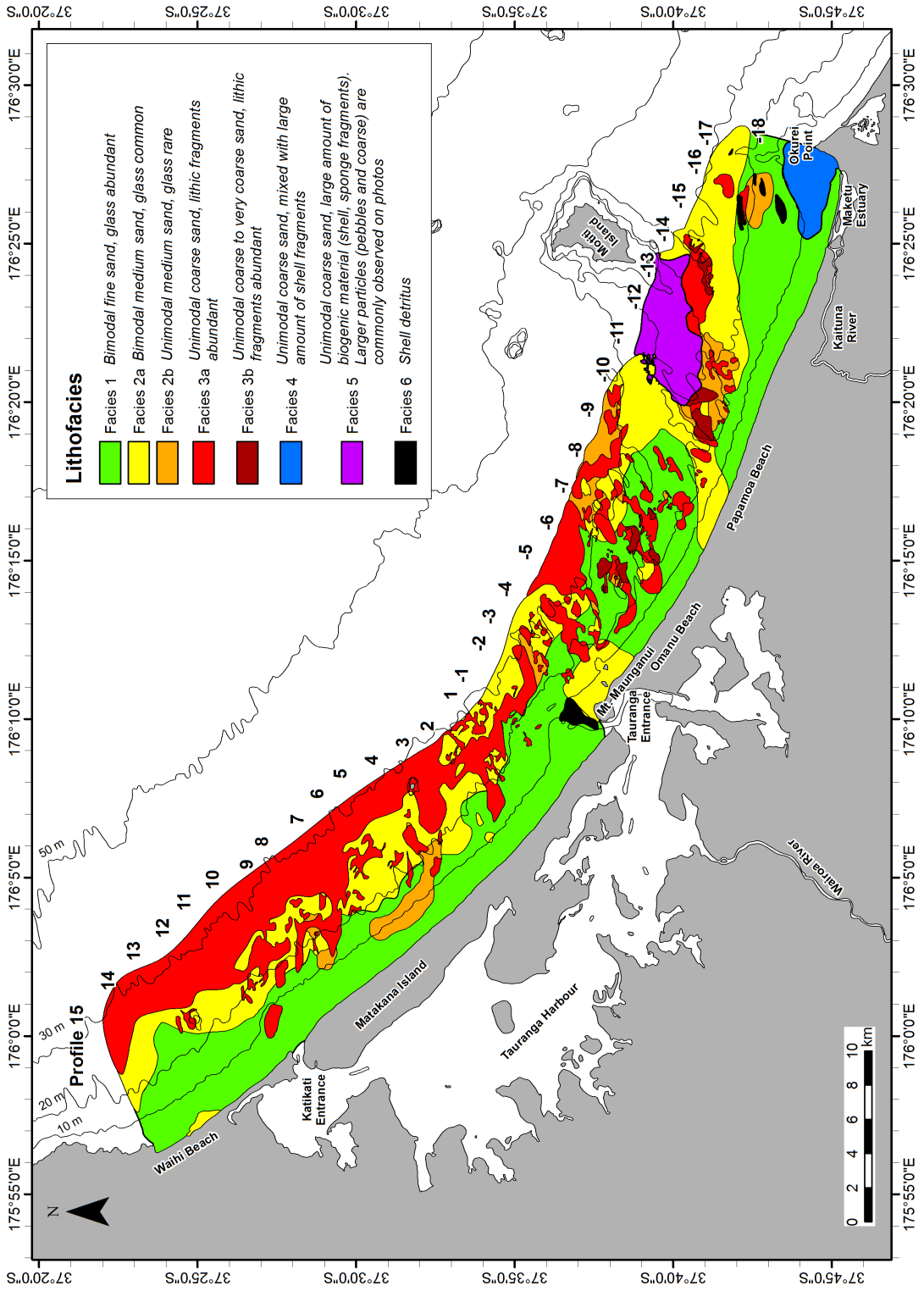

Figure 2.10: Lithofacies inferred from granulometry, mineralogical composition and photographic appearance, spatial extent mapped by associated acoustic backscatter.

measured from sample material. The optical examination of grain sizes is limited by resolution and noise level of the photographs, motion blur due to the movement of the profiler and a lack of contrast between overlapping grains of similar colour, which can often not properly be distinguished from each other. As a result, there is a bias toward the largest particles or aggregates.

While other optical techniques that make use of images taken from a larger ground distance allow a good qualitative assessment of changing seafloor coverage especially of heterogeneous areas (Stein et al., 1992; Yoklavich et al., 2000; Rooper et al., 2007; Erdey & Cochrane, 2015), close-ups enable a more detailed look on small-scale characteristics. Despite the discussed limitations, the facies determined from close-up seafloor photography is remarkably similar the ones based on sedimentological evidence. The definition of lithofacies allows for a more detailed differentiation, but does not require the creation of entirely new facies boundaries as far as the spatial distribution is concerned (Fig. 2.10). With this as link to the acoustic facies, the number of samples necessary for reliable ground truthing can be kept small. Provided environmental circumstances do not prevent of use of benthic profiler, e.g. through a rugged terrain, rock outcrops or coral reefs, this approach can a a valuable addition to seafloor mapping efforts. In total, eight different lithofacies were defined:

- **Lithofacies 1** This fine, mostly felsic sediment encompasses all instances of the granulometric group A as well as the compositional type I. Through these two parameters it differs from all other sediments in the study area. The distribution is limited to a water depth of up to 20 m and matches up with the allochthonous Holocene deposits described by Bradshaw et al. (1994). This sediment, derived from fluvial infills of estuaries, has been deposited after the end of the sealevel rise 6.5 ka ago. On lines that show a change from steeper to flatter slope profiles, the deeper limit of lithofacies 1 usually also coincides with a distinct bathymetric break at around 20 m depth. This is also the limit on generally flat profiles, such as those near the Maketu estuary). Only at Omanu Beach does it reach down to 30 m. This area has a very steep bathymetric gradient between the beach and

20 m water depth, although the distance between the beach and the outer limit of the deposit is with ca. 5.5 km roughly the same as in the adjacent area on southern Papamoa Beach/Maketu. Presumably, this sediment has been mobilized in shallow water and transported in suspension over this distance until it could settle down.

- **Lithofacies 2a** belongs to the slightly more mafic compositional type II and is distinguished from other sediment of this type by the grain size distribution (group B, medium sand). Traces of volcanic glass are sometimes present, most likely in the finer grain sizes that make up the second mode of the distribution curve around 34 µm. This is probably an influence of lithofacies 1 as the finest and lightest particles can easily be entrained by waves and dispersed to a greater distance from the shore than the bulk of this deposit. If lithofacies 1 is identified with the allochthonous deposits, 2a (and indeed all other sediments belonging to this type of mineral composition) is equivalent to the early Holocene transgressionally reworked Pleistocene sands described by Bradshaw et al. (1994).

- **Lithofacies 2b** is also part of the compositional type II and constitutes the granulometric group C. The sediment is a bit coarser than 2a, and almost never contains volcanic glass. It appears that the unconnected locations where lithofacies 2b is found are either too distant from lithofacies 1 to mix with finer younger sediments, or wave energy is too high to allow their deposition. The latter is the most likely case in the surroundings of sample 11 (see Fig. 2.1), an area in about 10 m water depth that would otherwise be typically occupied by lithofacies 1.

- **Lithofacies 3a** is a coarse sand (group D) variety of mineral composition type II. The spatial distribution coincides with the deepest parts of the study area or bedforms that reflect erosional conditions like the center of the sorted bedforms at Papamoa Beach. It appears to be an older stage of the transgressional deposits underlying the previously described lithofacies.

- **Lithofacies 3b** differs from 3a by an even coarser grain size (group F). It

occurs only in relatively small erosive areas within sorted bedforms and south of Motiti Island. As described above, much of the BoP sediments have been deposited during or after the Holocene transgression, which results a fining-upwards sequence. Therefore the coarse grain size of lithofacies 3a indicates that this likely belongs to the oldest deposit in the study area. Judging from the samples it is not entirely clear if this facies constitutes a separate layer under facies 3a or is merely a local variation depending on a more energetic sorting process.

- **Lithofacies 4** complies with nearly the same grain size group as lithofacies 3a (group D) as far as the bulk sediment is concerned. The largest components are shell fragments; all samples of compositional type III fall within this lithofacies. The terrigenous component is a medium sand of comparable composition as lithofacies 2b. This sediment is confined to a location at Okurei Point, which supports the assumption of a net littoral drift towards the southeast: the rocky headland is a natural barrier, where shell material fractured during transport accumulates along the coast. Waves reflected on the steep outcrop could prevent finer material from deposition.

- **Lithofacies 5** consists mainly of coarse sand, but photographs of the the surrounding seafloor commonly show larger particles up to the range of a decimeter (grain size group E). The material includes all examples of compositional type IV. The high biogenic component includes shells in all stages of disaggregation from complete halves to fragments, as well as parts of sponges. The terrigenous component is similar to lithofacies 3a, but it includes pebble-sized components that are significantly larger than anything found in 3a or 3b. It can be assumed that this sediment is mixed with material originating from the nearby Motiti Island.

- **Lithofacies 6** A shell detritus deposit, the underlying sediment could not be determined.

2.6.2 Bedforms and sediment dynamics

The littoral drift of sediment in the study area has been repeatedly determined at multiple locations in past studies ((Healy, 1977; Harray & Healy, 1978; Hicks et al., 1999; Healy & De Lange, 2014) as essentially bidirectional but with the net component directed towards the southeast. According to the model for the neighboring inner Coromandel shelf by Bradshaw et al. (1994), sediment transport in fair weather conditions is limited to on- and offshore transport by waves and rip currents, with a SE flux component up to 10 m water depth (Badesab et al., 2012). The datasets used in this study contain little additional information about the situation in shallow water as the sidescan sonar map only starts at 10-15 m. However, the observed bedforms below that depth agree with Bradshaw et al. (1994): All indications point to a northwesterly-directed transport between 10-15 m and 30 m water depth between Papamoa and Waihi Beach.

Subaquatic dunes

The first piece of evidence for this interpretation comes from the orientation of bedforms. A closer examination of strike angles shows that dunes can be placed into one of two groups: the first includes dunes striking - in first approximation - perpendicular to the coastline (”shore-normal” in Fig. 2.11). Their strike angle is on average 51° to true north, although this is mostly due to a large number small-scale structures; the larger dunes in close proximity to the shore are closer to 75° azimuth – ca. 60° to the shoreline. Those in the second group strike along the coastline (”shore-parallel”, 125°) and are less varied in their orientation.
Dunes belonging to the ”shore-normal” group are concentrated in the depth range from 10 to 30 m, but no such restriction could be found for ”shore-parallel” dunes. As our survey was limited to a maximum depth of up to 35 m, only the bedforms within this range have been statistically examined. A total number of 285 structures with an average width of 428 m (parallel to the crest) and wavelength between 0.5 and 1.3 km have been classified as ”shore-normal”. Examples of ”shore-parallel” dunes appear in almost equal numbers (273 dunes) but are much smaller with an average width of 256 m and a wavelength of 0.1-0.3

km.

Backscatter usually decreases at first gradually towards the northwestern side of ”shore-normal” and on the southwestern side of ”shore-parallel” dunes, then decreases again rapidly to an area of minimal backscatter, then increases again abruptly to another maximum. In some cases, photographs and multibeam data are available on or reasonably close to these areas of high backscatter. It appears that the high backscatter is caused by the accumulation of large shells and shell fragments close to the dune trough. The material gets sorted out on the stoss slope of the dune and disappears completely before the change to minimum backscatter; this point marks the dune crest (Fig. 2.12).

Shore-oblique nearshore bedforms of similar dimensions have been observed on storm-dominated shelves of the north (Duane et al., 1972; Swift et al., 1972) and south Atlantic (Figueiredo et al., 1982; Parker et al., 1982). However, the Atlantic sand ridges have a much smaller angle to the shore than the bedforms in the BoP, between 1-50°(McKinney et al., 1974; Swift & Field, 1981) and on average ca. 30 °(Figueiredo et al., 1982; Parker et al., 1982; Goff et al., 1999). The responsible longshore current responds faster to wind stress and is consequently stronger in shallow water, sediment is transported faster here than in greater depth Swift & Field (1981); Goff et al. (2015). These structures are maintained by the offshore deflection of storm-driven longshore currents at their crests (Trowbridge, 1995; Calvete et al., 2001). In all cases, the angle opens in the upcurrent direction: to the north on the North American and to the south on the South American shelf. In the case of the BoP, the obliquity of dunes points to a SE-NW directed current. The unusually large opening angle of the BoP dunes is a striking difference to other storm-dominated shelves. A key difference in the wave and current climate of the North American and the BoP shelf appears to be wind direction during storms. The BoP experiences mostly onshore directed easterly and northeasterly winds of passing tropic cyclones. According to Bradshaw et al. (1991), these first lead to a downwelling current which is subsequently deflected to the northwest by balancing the cross-shore pressure gradient and Coriolis forces. Sediment entrained by storm waves is transported by this current. Depending on the

angle of the incoming waves to the shoreline, an additional and opposite NW-SE directed current may sometimes develop on the upper shoreface (Niedoroda et al., 1985); however, as most wave fronts hit the coast at an almost right angle (see Fig. 2.1) this will seldom be the case. The North American coast is also frequently afflicted by northeasterly storms, but due to the NE-SW orientation of the shoreline those have a stronger longshore component. Subsequent currents follow this direction (Dragos & Aubrey, 1990; Trowbridge, 1995). Goff et al. (2015) predicts that flow-traverse bedforms will over time develop a more acute angle to the shore due to the in cross-shore direction differing flow velocity. As the longshore current is directly forced by the wind stress, the cross-shore velocity gradient is relatively large. In the BoP, the downwelling current is in total losing energy with distance to the shore, but at the same time the remaining energy flux is more and more shifted in longshore direction. This could result in a less varied velocity gradient from shallow to deep water. Unfortunately there are currently no current meter datasets available to test this hypothesis.

Regarding the bedforms in deeper parts of the BoP, the available data provide no indication whether these have been formed by recent or past processes. If these features are still dynamic, the transition of shore-parallel dunes to a featureless section between 30 and 40 m and the recurrence of dunes in shallower water could be explained by the energy distribution of the responsible waves. It is possible that approaching swell transfers its highest shear stress to the seafloor at 30-40 m depth before it loses energy due to friction in shallow water. In that case, the featureless section could represent the plane bed stage of the upper flow regime, which means that sediment would be transported towards the shore from as deep as 60 m.

Sorted bedforms and coarse sand ribbons

A second indicator for transport direction is the uniform shape and orientation of sorted bedforms, which are elongated in cross-shore direction with a sharp boundary towards southeast. This is the case both for small, poorly developed bedforms offshore Matakana Island and for the very large, distinctive features

at Omanu Beach. Similarly developed bedforms, although with dimensions comparable to those along Matakana Island, have been monitored by Spiers & Healy (2007) close to Mt. Maunganui. Spiers & Healy (2007) related these structures to zones of wave convergence created by the offshore dumping grounds in that area. If a similar process is involved in the formation of the well developed Omanu bedforms, Motiti Island or one of the several local elevations in the immediate neighborhood of these sorted bedforms could possibly lend themselves to wave convergence. In any case, considering the water depth and related low wave energy (Badesab et al., 2012), the waves in question have to be storm induced to affect the seafloor; DeFalco et al. (2015) provide another example of sorted bedforms formed during periodic storm events.

As studies like Coco et al. (2007) have shown, it is possible for sorted bedforms to be created by unmixing of a poorly sorted sediment; however, it is unlikely that this process is responsible here for two reasons: 1) there is no source sediment in the system with a wide enough range of grain sizes and 2) the coarse sediment inside the sorted bedforms is identical to other examples of the underlying lithofacies 3a and 3b. With this in mind, it appears that these features were originally formed either by erosion of lithofacies 1 to the point that the underlying strata were exhumed, or alternatively lithofacies 1 was never deposited in these locations in the first place. The low turbidity in the surroundings of the sorted bedforms again indicates that erosion, but also deposition of suspended material is limited during fair weather conditions. Observations of bedforms created in an erosive environment on a coarse bed overlain by finer sediment were also made by other studies, for example on bedforms in Shinnecock Inlet (New York) and Grays Harbor (Washington) by Ferrini & Flood (2005) (there classified as type II rippled scour depressions). Either process can be linked to the mechanism of increased turbulence proposed by Murray & Thieler (2004) and others, that is keeping these bedforms stable.

The orientation of coarse sand ribbons has in the past been interpreted as parallel to the current responsible for their creation (Goff et al., 1999; Feldens et al., 2015). As such, they show coast parallel sediment transport, except south of

Motiti Island (along profile 14). It appears that in this area sediment is transported cross-shore below 10 m water depth.

Turbidity and lithofacies distribution

With consideration of turbidity, it appears that the environment along Matakana is overall more dynamic than the Omanu/Papamoa region. The measurements indicate a link between turbidity and bathymetric gradient between 0 and 20 m water depth. More sediment is in suspension (and in greater depth) in the northern region than along the relatively steep southern coastline of the study area. This is a matter of local entrainment, but also availability of sediment from external sources. Only the southeastern end of the study area, in proximity to the Kaituna River, shows a level of turbidity that is comparable to (or even greater than) the Matakana coast. Sediment in this location appears to be dispersed either offshore or is bypassing Okurei Point. Some minor input may be delivered directly from Motiti, but considering the extent of the different lithofacies in this area and the lack of sediment structures, the submarine ridge appears to act as a barrier for sediment transport in any direction. The low turbidity, but great extent of lithofacies 1 and 2a offshore Omanu Beach (from 5-30 m depth, almost 10 m deeper than anywhere else) could be explained by a periodic entrainment of a large volume of sediment close to the beach, which is transported in suspension offshore by a relatively strong current as described by Niedoroda et al. (1984). A plausible scenario is a storm driven transport initiated by an initially onshore directed current parallel to the Motiti ridge, that is in turn pushing a downwelling current offshore and away from Omanu Beach. After the storm has ended, upwelling can take place, but this current is relatively weak and without wave action unable to re-entrain (Badesab et al., 2012) the deposited sediment (Niedoroda et al., 1984).

Conceptual sediment transport

By combining these observations about the nature and extent of sediment facies, of bedforms, of the distribution of suspended material and the comparison to

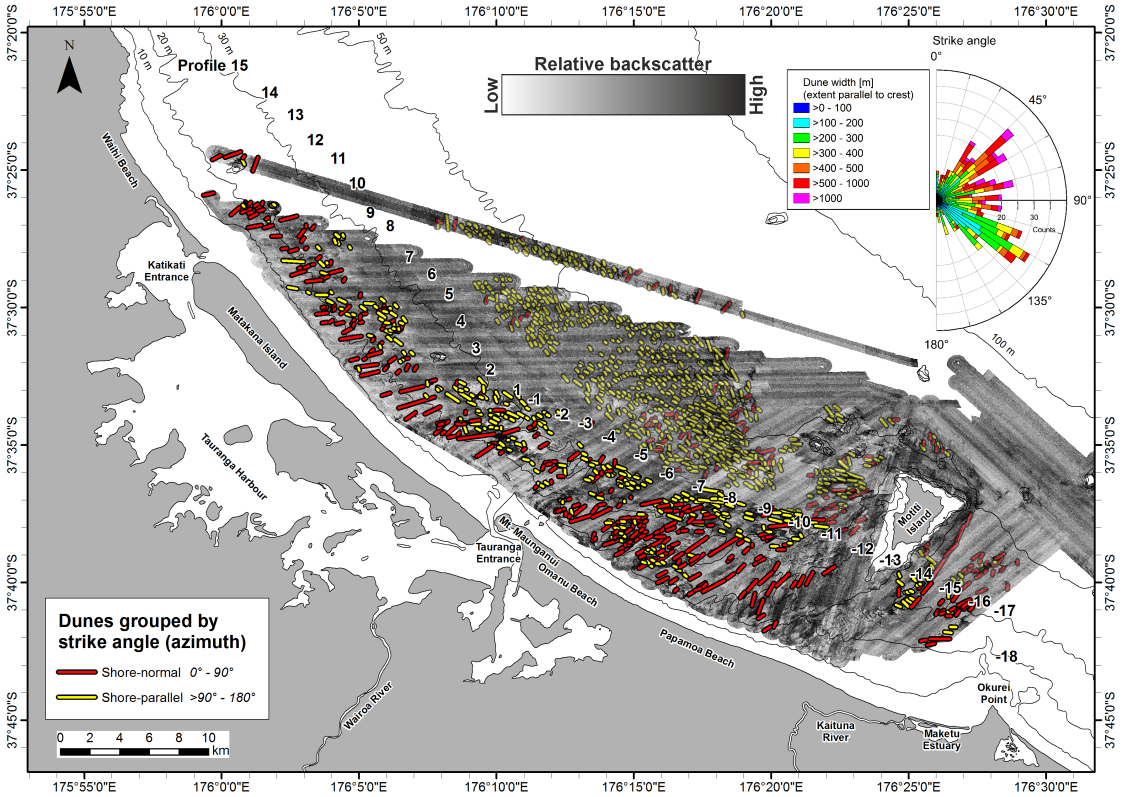

Figure 2.11: Dune structures in the study area fall into one of two groups. One of them strikes perpendicular to the coastline and is almost exclusive to the nearshore area between 10-15 m and 30 m. The other strikes parallel to the coastline and is found in all water depths. Only dunes in the nearshore area (strong colours) are included in the analysis.

the published literature, a general sediment transport model can take the net transport directions as well as the location of hypothesized centers of erosion/non-deposition into account (Fig. 2.13). Using the approximate thickness of seismic units from Bradshaw & Nelson (2004) (sheet-like late Holocene fine sands on top of ca. 5 m early Holocene coarse sand) as a rough guideline, a schematic stratigraphy of the upper 5-10 m of seafloor of the western BoP coastal system could be developed (Fig. 2.12). Of course, for a reliable model of the geologic structure sediment cores would be a necessity. These would also give valuable insight into the internal structure of the large sorted bedforms; at this point it is unclear if these features are in deed purely erosive or if there are periods of fine sand deposition as observed in other places (Murray & Thieler, 2004; Trembanis & Hume, 2011).

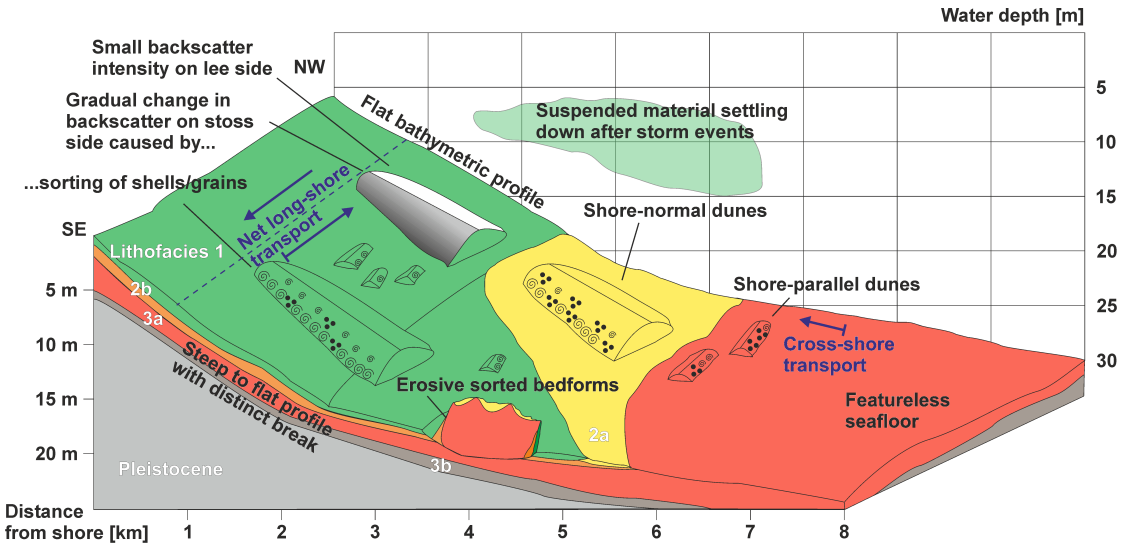

Figure 2.12: Schematic view of the coastal environment of the western BoP with sediment structures and stratigraphic arrangement of lithofacies. The thickness of the individual layers is a rough estimate based on seismic units from Bradshaw & Nelson (2004).

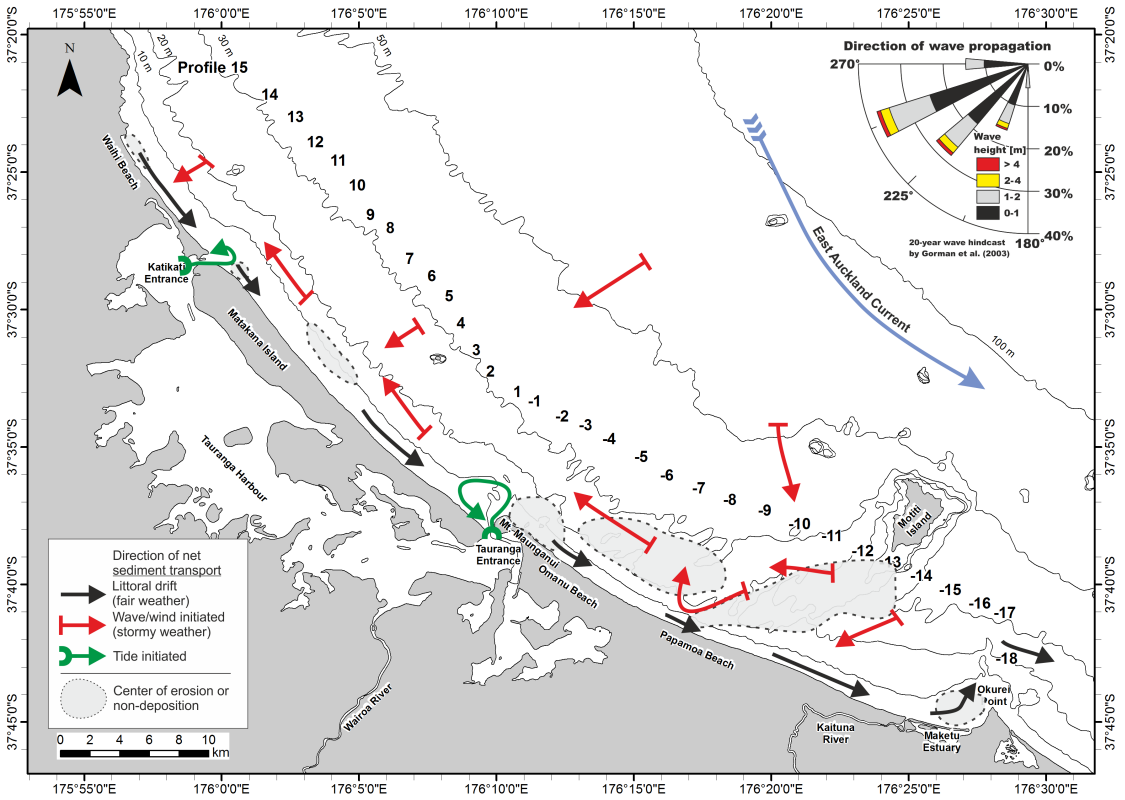

Figure 2.13: Inferred directions of net sediment transport and centers of erosion or non-deposition in the study area. Up to a depth of 10-15 m net transport has a southeasterly direction. Below that depth, net transport is directed towards the northwest. No longshore sediment transport is taking place below 30 m.

2.7 Conclusions

The sedimentology of the western Bay of Plenty has been mapped by a combined optical, acoustic and sampling based approach, which has provided a higher level of resolution than conventional lithofacies mapping studies. The results fit well with the previously established environment of the Bay of Plenty and inner Coromandel shelf. Eight distinct lithofacies categories were defined and mapped. The nearshore area is dominated by fine sand that contains plagioclase, quartz, few mafic minerals and an amorphous phase (presumably volcanic glass). At greater distance from the shore, gradually coarser sediments have been deposited that differ mineralogically from the fine sand by higher amounts of mafics, absence of volcanic glass, and the presence of lithic fragments. These sediment can be linked to similar deposits on the inner Coromandel shelf and are interpreted as early to late Holocene sand reworked from Pleistocene deposits overlain by late Holocene allochthonous sediments.

Net sediment transport is directed from northwest to southeast close to shore, as had been established in this and adjacent regions by earlier studies (e.g. Davies-Colley & Healy, 1978b; Bradshaw et al., 1994; Hicks et al., 1999; Bear et al., 2009; Badesab et al., 2012). In depths greater than 10-15 m, only indications for a northwesterly directed transport were found. These opposing directions are likely due to the transport of wave-entrained sediment by a southeastern littoral drift prevalent under normal weather conditions vs. the usual direction of storm waves approaching the shore from northeast inducing the downwelling of water masses which are deflected to the northwest as a geostrophic current (Harray & Healy, 1978; Bradshaw et al., 1991, 1994). Both transport systems are connected by the cross-shore transport of sediments, only shoreward directed transport appears to lead to the creation of indicative bedforms such as coast-parallel striking dunes. Cross-shore transport is the only process taking place below a depth of 30-35 m, indicators for this process have been observed in a water depth of up to 60 m. The northern half of the study area along the barrier island of Matakana was found to be more dynamic than the region southeast of

Mt. Maunganui. There is little to no deposition of sediment offshore of Omanu Beach which has no sources of riverine input and is located between two natural barriers for sediments: Tauranga Entrance to the northwest and the submarine Motiti ridge to the southeast. Sorted bedforms of various dimensions have been found and their origin interpreted as erosional rather than due to the unmixing of grains.

Overall, the method developed in this study for an assessment of sediment classification, distribution and dispersal by combining datasets of varying dimensions and resolution led to convincing results. The high density of data along benthic profiles enables a detailed delineation of adjacent facies and the association with area covering acoustic backscatter provides the necessary information for two-dimensional mapping. Used as a guidance for targeting specific sampling locations, this approach leads to a highly detailed insight into the local sediment facies. In an environment where no major obstacles (rock outcrops, coral reefs etc.) prevent the use of a benthic sled, the usefulness of close-up seafloor photography is apparent and has potential for future improvements. Considering the time and effort a manual photographic sediment classification requires, an automatic scheme would need to be developed before this method could find widespread application.

2.8 Acknowledgments

We thank Dirk Immenga, Chris Morcom, Chris Eager and Brice Blossier for their guidance and assistance in the sampling campaign and Christian Hilgenfeldt and Benjamin Baasch for their participation in the 2012 *NERIDIS* survey. That survey took place using the Western Workboats vessel *MACY GRAY* with great support by Henry Wolfenden and Sean Kelly. Annette Rodgers, Janine Ryburn, Ganqing Xu and Renat Radosinsky of the University of Waikato technical staff provided valuable help in diverse sedimentological and mineralogical laboratory measurements. Seaworks Ltd. generously provided raw sidescan sonar data. The digital camera used on *NERIDIS* belongs to the German Reserach Center for

Artificial Intelligence (Deutsches Forschungszentrum für Künstliche Intelligenz, DFKI). LED flash systems and pressure housings were funded by MARUM. At the University of Bremen, we thank Michael Wendschuh for advice in the interpretation of XRD data and Konstantin Reeck for the processing of diverse datasets. This work includes LINZ's data which are licensed by Land Information New Zealand (LINZ) for re-use under the Creative Commons Attribution 3.0 New Zealand licence. The deployment of *NERIDIS* was financed by the *RENA* Long Term Environmental Recovery Monitoring Program. This study is a project of the collaborative graduate school INTERCOAST of the universities of Bremen and Waikato, with financing provided by the German Research Foundation (Deutsche Forschungsgesellschaft, DFG). Finally, we thank two anonymous reviewers for their insightful comments.

Bibliography

Badesab, F., von Dobeneck T., Bryan, K.R., Müller, H., Briggs, R.M., Frederichs, T., Kwoll, E. (2012): Formation of magnetite-enriched zones in and offshore of a mesotidal estuarine lagoon: An environmental magnetic study of Tauranga Harbour and Bay of Plenty, New Zealand – Geochemistry, Geophysics, Geosystems, Vol. 13, Q06012, doi:10.1029/2012GC004125.

Barnhardt, W.A., Kelley, J.T., Dickson, S.M., Belknapt, D.F. (1998): Mapping the Gulf of Maine with Side-Scan Sonar: A New Bottom-Type Classification for Complex Seafloors – Journal of Coastal Research, Vol. 14, No. 2, pp. 646-659.

Battershill, C., Schiel, D.R., Ross, P.M., Fairweather, R., Culliford, D, Marsh, R., Taiapa, C., Bennett, P. (2013): Rena Environmental Recovery Monitoring Programme: executive summary – Te Mauri Moana, Environmental Research Institute, University of Waikato, Tauranga, New Zealand, 37pp.

Bear, A.L., Healy, T.R., Immenga, D.K. (2009): Coastal Erosion and Sedimentation Processes at Waihi Beach, New Zealand – Journal of Coastal Research, Special Issue 56, pp. 1721-1725.

Blott, S.J., Pye, K. (2001): GRADISTAT: a grain size distribution and statistics package for the analysis of unconsolidated sediments – Earth Surface Processes and Landforms, Vol. 26, pp. 1237-1248.

Bradshaw, B.E., Healy, T.R., Dell, P.M., Bolstad, W.M. (1991): Inner shelf dynamics on a storm-dominated coast, East Coromandel, New Zealand – Journal of Coastal Research, Vol. 7, No. 1, pp. 11-30.

Bradshaw, B.E., Healy, T.R., Campbell, S.N., Dell, P.M., De Lange, W.P. (1994): Holocene sediment lithofacies and dispersal systems on a storm-dominated, back-arc shelf margin: the east Coromandel coast, New Zealand – Marine Geology, Vol. 119, pp. 75-98.

Bradshaw, B.E., Nelson, C.S. (2004): Anatomy and origin of autochthonous late Pleistocene forced regression deposits, east Coromandel inner shelf, New Zealand: implications for the development and definition of the regressive systems tract – New Zealand Journal of Geology & Geophysics, Vol. 47, pp. 81-99

Brodie, J.W. (1960): Coastal surface currents around New Zealand – New Zealand Journal of Geology and Geophysics, Vol. 3, No. 2, pp. 235-252, doi: 10.1080/00288306.1960.10423596.

Briggs, R.M., Houghton, B.F., McWilliams, M., Wilson, C.J.N. (2005): $^{40}\mathrm{Ar}/^{39}\mathrm{Ar}$ ages of silicic volcanic rocks in the Tauranga-Kaimai area, New Zealand: dating the transition between volcanism in the Coromandel Arc and the Taupo Volcanic Zone – New Zealand Journal of Geology and Geophysics, Vol. 48, pp. 459-469.

Burton, J.H ., Healy, T.R. (1985): Tidal Hydraulics and Stability of the Maketu Inlet, Bay of Plenty – in: 1985 Australasian Conference on Coastal and Ocean Engineering. Barton, A.C.T.: Institution of Engineers, Australia, 1985: pp. 697-702.

Cacchione, D.A., Drake, D.E. (1984): Rippled scour depressions on the inner continental shelf off central California – Journal of Sedimentary Petrology, Vol. 54, No. 4, pp. 1280-1291.

Calvete, D., Walgreen, M., de Swart, H.E., Falqués, A. (2001): A model for sand ridges on the shelf: Effect of tidal and steady currents – Journal of Geophysical Research, Vol. 106, No. C5, pp. 9311-9325.

Carter, L., Heath, R.A. (1975): Role of mean circulation, tides and waves in the transport of bottom sediment on the New Zealand continental shelf – New Zealand Journal of Marine and Freshwater Research, Vol. 9, pp. 423-448.

Coco, G., Murray, A.B., Green, M.O. (2007): Sorted bed forms as self-organized patterns: 1. Model development – Journal of Geophysical Research, Vol. 112, F03015, doi:10.1029/2006JF000665.

Cole, J.W. (1979): Structure, petrology, and genesis of Cenozoic volcanism, Taupo Volcanic Zone, New Zealand–a review – New Zealand Journal of Geology and Geophysics, Vol. 22, No. 6, pp. 631-657.

Davis, R.A., Jr., Healy, T.R. (1993): Holocene coastal depositional sequences on a tectonically active setting: southeastern Tauranga Harbour, New Zealand – Sedimentary Geology, Vol. 84, pp. 57-69.

Davies-Colley, R.J., Healy, T.R. (1978 a): Sediment and hydrodynamics of the Tauranga Entrance to Tauranga Harbour – New Zealand Journal of Marine and Freshwater Research, Vol. 12, No. 3, pp. 225-36.

Davies-Colley, R.J., Healy, T.R. (1978 b): Sediment transport near the Tauranga Entrance to Tauranga – New Zealand Journal of Marine and Freshwater Research, Vol. 12, No. 5, pp. 237-43.

De Lange, W.P. (1988): Wave Climate and Sediment Transport within Tauranga Harbour, in the Vicinity of the Pilot Bay – University of Waikato, Hamilton, New Zealand. Ph.D. thesis, 189 pp.

DeFalco, G., Budillon, F., Conforti, A., Di Bitetto, M., Di Martino, G., Innangi, S., Simeone, S. Tonielli, R. (2015): Sorted bedforms over transgressive deposits along the continental shelf of western Sardinia (Mediterranean Sea) – Marine Geology, Vol. 359, pp. 75-88.

Dragos, P., Aubrey, D.G. (1990): Atlantic shelf sand ridge study: physical oceanography and sediment dynamics data report – Woods Hole Oceanographic Institute Technical Report, WHOI-90-11, CRC-90-1, Woods Hole, Massachusetts, 1990.

Duane, D.B., Field, M.E., Miesberger, E.P., Swift, D.J.P., Williams, S.J. (1972): Linear shoals on the Atlantic continental shelf, Florida to Long Island – in: Swift, D.J.P., Duane, D.B. Pilkey, O.H. [eds.](1972): Shelf Sediment Transport: Process and Pattern, pp. 447-498, Van Nostrand Reinhold, New York, 1972.

Erdey, M.D., Cochrane, G.R. (2015): Seafloor-Character Map of the Offshore of Point Reyes Map Area (Sheet 5) – in: Watt, J.T., Cochran, S.A. [eds.](2015): California State Waters Map Series - Offshore of Point Reyes, California. U.S. Geological Survey Open-File Report 2015-1114, pamphlet 39 p., 10 sheets, scale 1:24,000, http://dx.doi.org/10.3133/ofr20151114.

Ewart, A. (1965): Review of Mineralogy and Chemistry of the Acidic Volcanic Rocks of Taupo Volcanic Zone, New Zealand – Bulletin Volcanologique, Vol. 29, No. 1, pp. 147-171.

Feldens, P., Diesning, M., Schwarzer, K., Heinrich, C., Schlenz, B. (2015): Occurrence of flow parallel and flow transverse bedforms in Fehmarn Belt (SW Baltic Sea) related to the local palaeomorphology – Geomorphology, Vol. 231, pp 53-62.

Fernlund, J.M.R. (2005): Image analysis method for determining 3-D shape of coarse aggregate – Cement and Concrete Research, Vol. 35, pp. 1629-1637.

Ferrini, V.L., Flood, R.D. (2005): A comparison of Rippled Scour Depressions identified with multibeam sonar: Evidence of sediment transport in inner shelf environments – Continental Shelf Research, Vol. 25, pp. 1979-1995.

Figueiredo, A.G. Sanders, J.E., Swift, D.J.P. (1982): Storm-graded layers on inner continental shelves: Examples from southern Brazil and the Atlantic Coast of the central United States – Sedimentary Geology, Vol. 31, pp. 171-190.

Foster, G.A., Healy, T.R., De Lange, W.P. (1994): Sediment budget and equilibrium for a moderate swell regime, ebb-tidal adjacent beach, Mt. Maunganui, New Zealand – Journal of Coastal Research, Vol. 10, No. 3, pp. 564-575.

Foster, G.A., Healy, T.R., De Lange, W.P. (1996): Presaging Beach Renourishment from a Nearshore Dredge Dump Mound, Mt. Maunganui Beach, New Zealand – Journal of Coastal Research, Vol. 12, No. 2, pp. 395-405.

Frihy, O.E. (1994): Discrimination of accreted and eroded coasts using heavy mineral compositions of the Nile Delta beach sands, Egypt – Sedimentology, Vol. 41, pp. 905-912.

Gao, S., Collins, M.B. (2014): Holocene sedimentary systems on continental shelves – Marine Geology, Vol. 352, pp. 268-294.

Gibb, J.G. (1994): Initial assessment of areas sensitive to coastal hazards for selected parts of the Bay of Plenty coast. Consultancy Report CR94 / I 7 for Bay of Plenty Regional Council, Tauranga, New Zealand, 36pp. + app.

Goff, J.A., Swift, D.J.P., Duncan, C.S., Mayer, L.A., Hughes-Clark, J. (1999): High-resolution swath sonar investigation of sand ridge, dune and ribbon morphology in the offshore environment of the New Jersey margin – Marine Geology, Vol. 161, pp. 307-337.

Goff, J.A., Flood, R.D., Austin, Jr., J.A., Schwab, W., Christensen, B., Browne, C.M., Denny, J.F., Baldwin, W.E. (2015): The impact of Hurricane Sandy on the shoreface and inner shelf of Fire Island, NewYork: Large bedform migration but limited erosion – Continental Shelf Research, Vol. 98, pp. 13-25.

Gorman, R.M., Bryan, K.R., Laing, A.K. (2003): Wave hindcast for the New Zealand region: Nearshore validation and coastal wave climate – New Zealand Journal of Marine and Freshwater Research, Vol. 37, No.3, pp. 567-588, doi: 10.1080/00288330.2003.9517190.

Green, M.O., Vincent, C.E., Trembanis, A.C. (2004): Suspension of coarse and fine sand on a wave-dominated shoreface, with implications for the development of rippled scour depressions – Continental Shelf Research, Vol. 24, pp. 317-335.

Hanquiez, V., Mulder, T., Lecroart, P., Gonthier, E., Marchès, Voisset, M. (2007): High resolution seafloor images in the Gulf of Cadiz, Iberian margin – Marne Geology, Vol. 246, pp. 43-59.

Harray, K.G., Healy, T.R. (1978): Beach erosion at Waihi Beach Bay of Plenty, New Zealand – New Zealand Journal of Marine and Freshwater Research, Vol. 12, No. 2, pp. 99-107.

Healy, T.R. (1977): Progradation at the Entrance, Tauranga Harbour, Bay of Plenty – New Zealand Geographer, Vol. 33, No. 2, pp. 90-92.

Healy, T.R., De Lange, W.P. (2014): Reliability of Geomorphic Indicators of Littoral Drift: Examples from the Bay of Plenty, New Zealand – Journal of Coastal Research, Vol. 30, No 2, pp. 301-318.

Healy, T.R., Kirk, R.M. (1982): Coasts – in: Soons, J.M., Selby, M.J. [eds.] (1982): Landforms of New Zealand, Longman Paul, Auckland. pp. 81-104.

Healy, T.R., Harray, K.G., Richmond, B. (1977): The Bay of Plenty Coastal Erosion Survey – Occasional Report No. 3, Department of Earth Sciences, The University of Waikato, Hamilton, 64 pp.

Healy, T.R., Harms, C., De Lange, W.P. (1991): Dredge spoil and inner shelf investigations off Tauranga Harbour, Bay of Plenty, New Zealand – Coastal Sediments '91, ASCE Seattle, Washongton, pp. 2037-2051.

Healy, T.R., Cole, R., De Lange, W.P. (1996): Geomorphology and ecology of New Zealand shallow estuaries and shorelines – In: Nordstrom, K.F., Roman, C.T. [eds.] (1996): Estuarine Shores, Evolution, Environments and Human Alterations, Wiley & Sons, London, pp. 115-154.

Henry, M.A.C. (1991): The volcanic geology of Motiti Island. Unpublished M.Sc. thesis, lodged in the library of the University of Waikato, Hamilton, New Zealand.

Heward, A.P. (1981): A Review of Wave-Dominated Clastic Shoreline Deposits – Earth-Science Reviews, Vol. 17, pp. 223-276.

Hicks, D.M., Hume, T.M. (1996): Morphology and Size of Ebb Tidal Deltas at Natural Inlets on Open-sea and Pocket-bay Coasts, North Island, New Zealand – Journal of Coastal Research, Vol. 12, No. 1, pp. 47-63.

Hicks, D.M., Hume, T.M. (1997): Determining Sand Volumes and Bathymetric Change on an Ebb-Tidal Delta – Journal of Coastal Research, Vol. 13, No. 2, pp. 407-416.

Hicks, D.M., Hume, T.M., Swales, A., Green. M.O. (1999): Magnitudes, Spatial Extent, Time Scales and Causes of Shoreline Change Adjacent to an Ebb Tidal Delta, Katikati Inlet, New Zealand – Journal of Coastal Research, Vol. 15, No. 1, pp. 220-240.

Iremonger, S. (editor) 2011: NERMN beach profile monitoring 2011 – Bay of Plenty Regional Council Environmental Publication 2011/14.

Kostylev, V.E., Todd, B.J., Fader, G.B.J., Courtney, R.C., Cameron, G.D.M., Pickrill, R.A. (2001): Benthic habitat mapping on the Scotian Shelf based on multibeam bathymetry, surficial geology and sea floor photographs – Marine Ecology Progress Series, Vol. 219, pp. 121-137.

Krüger, J.C., Healy, T.R. (2006): Mapping the morphology of a dredged ebb tidal delta, Tauranga Harbour, New Zealand – Journal of Coastal Research, Vol. 22, No. 3, pp. 720-727.

Leonard, B.S., Begg, J.G., Wilson, C.J.N. (compilers) (2010): Geology of the Rotorua Area – Institute of Geological and Nuclear Sciences 1:250000 geological map 5. 1 sheet + 102 p. Lower Hutt, New Zealand. GNS Science.

Li, G., Yan, W., Zhong, L., Xia, Z., Wang, S. (2015): Provenance of heavy mineral deposits on the northwestern shelf of the South China Sea, evidence from single-mineral chemistry – Marine Geology, Vol. 363, pp. 112-124.

Lobo, F.J., Hernández-Molina, F.J., Somoza, L., Rodero, A., Maldonado, A., Barnolas, A. (2000): Patterns of bottom current flow deduced from dune asymmetries over the Gulf of Cadiz shelf (southwest Spain) – Marine Geology, Vol. 164, pp. 91-117.

Macky, G.H., Latimer, G.J., Smith, K. (1995): Wave climate of the western Bay of Plenty, New Zealand, 1991-93 – New Zealand Journal of Marine and Freshwater Research, Vol. 29, No. 3, pp. 311-327.

Mayer, L.A. (2006): Frontiers in seafloor mapping and visualization – Marine Geophysical Researches, Vol. 27, pp. 7-17, doi:10.1007/s11001-005-0267-x.

McKinney, T.F., Stubblefield, W.F., Swift, D.J.P. (1974): Largescale current lineations on the central New Jersey shelf: investigation by side-scan sonar – Marine Geology, Vol. 17, pp. 79-102.

Michels, K.H., Healy, T.R. (1999): Evaluation of an Inner Shelf Site Off Tauranga Harbour, New Zealand, for Disposal of Muddy-Sandy Dredged Sediments – Journal of Coastal Research, Vol. 13, No. 3, pp. 830-838.

Milkov, A., Vogt, P., Cherkashev, A., Ginsburg, G., Chernova, N., Andriashev, A. (1999): Sea-floor terrains of Haskon Mosby Mud Volcano as surveyed by deep-tow video and still photography – Geo-Marine Letters, Vol. 19, pp. 38-47.

Müller, H., von Dobeneck, T., Hilgenfeldt, C., SanFilipo, B., Rey, D., Rubio, B. (2012): Mapping the magnetic susceptibility and electric conductivity of marine surficial sediments by benthic EM profiling – Geophysics, Vol. 77, No. 1, pp. 1-14.

Murray, A.B., Thieler, E.R. (2004): A new hypothesis and exploratory model for the formation of large-scale inner-shelf sediment sorting and ”rippled scour depressions” – Continental Shelf Research, Vol. 24, pp. 295-315.

Niedoroda, A.W., Swift, D.J.P., Hopkins, T.S. (1984): Shoreface morphodynamics on wave-dominated coasts – Marine Geology, Vol. 60, pp. 331-354.

Niedoroda, A.W. Swift, D.J.P., Hopkins, T.S. (1985): The Shoreface – In: Davis, R.A., Jr. (1985): Coastal Sedimentary Environments, Springer, New York, pp. 533-624.

Pawlowski, G.A. (1985): Quantitative determination of mineral content of geological samples by X-ray diffraction – American Mineralogist, Vol. 70, pp. 663-667.

Pandian, P.K., Ruscoe, J.P., Shields, M., Side, J.C., Harris, R.E., Kerr, S.A., Bullen, C.R. (2009): Seabed habitat mapping techniques: an overview of the performance of various systems – Mediterranean Marine Science, Volume 10/2, pp. 29-43.

Park, S. (2004): Aspects of mangrove distribution and abundance in Tauranga Harbour. Environmental publication 2004/16. Whakatane, New Zealand, Environment Bay of Plenty. 40 p.

Parker, G., Lanfredi, N.W., Swift, D.J.P. (1982): Seafloor response to flow in a southern hemisphere sand-ridge field: Argentine inner shelf – Sedimentary Geology, Vol. 33, pp. 195-216.

Pickrill, R.A., Mitchell, J.S. (1979): Ocean wave characteristics around New Zealand – New Zealand Journal of Marine and Freshwater Research, Vol. 13, No. 4, pp. 501-520.

Rooper, C.N., Zimmermann, M. (2007): A bottom-up methodology for integrating underwater video and acoustic mapping for seafloor substrate classification – Continental Shelf Research, Vol. 27, pp. 947-957.

Schwab, W.C., Baldwin, W.E., Denny, J.F., Hapke, C.J., Gyes, P.T., List, J.H., Warner, J.C. (2014): Modification of the Quaternary stratigraphic framework of the inner-continental shelf by Holocene marine transgression: An example offshore of Fire Island, New York – Marine Geology, Vol. 355, pp. 346-360.

Shepherd, M.J., McFadgen, B.G., Betts, H.D., Sutton, D.G. (1997): Formation, landforms and palaeoenvironment of Matakana Island, Bay of Plenty, and implications for archaeology – Science and Research Series 102. Wellington, New Zealand. Department of Conservation. 100 p.

Shepherd, M.J., Betts, H.D., McFadgen, B.G., Sutton, D.G. (2000): Geomorphological evidence for a Pleistocene barrier at Matakana Island, Bay of Plenty, New Zealand – New Zealand Journal of Geology and Geophysics, Vol. 43, No. 4, pp. 579-586.

Simarro, G., Guilléna, P, Puiga, M., Ribóa, M., Lo Taconob, C., Palanques, A., Muñoz, A., Durána, R., Acosta, J. (2015): Sediment dynamics over sand ridges on a tideless mid-outer continental shelf – Marine Geology, Vol. 361, pp. 25-40.

Spiers, K.C., Healy, T.R. (2007): Investigation of Sorted Bedforms, Tauranga Harbour, New Zealand – Journal of Coastal Research, Special No. 50, pp. 353-357.

Spiers, K.C., Healy, T.R., Winter, C. (2009): Ebb-Jet Dynamics and Transient Eddy Formation at Tauranga Harbour: Implications for Entrance Channel Shoaling – Journal of Coastal Research, Vol. 50, No. 1, pp. 234-247.

Stein, D.L., Tissot, B.N., Hixon, M.A., Barss, W. (1992): Fish-habitat associations on a deep reef at the edge of the Oregon continental shelf – Fishery Bulletin U.S., Vol. 90, pp. 540-551.

Stark, N., Coco, G., Bryan, K.R., Kopf, A. (2012): In-situ geotechnical characterization of mixed-grain size bedforms using a dynamic penetrometer – Journal of Sedimentary Research, Vol. 82, pp. 540-544, doi: 10.2110/jsr.2012.45.

Swift, D.J.P., Field, M.E. (1981): Evolution of a classic sand ridge field: Maryland sector, North American inner shelf – Sedimentology Vol. 28, 461-482.

Swift, D.J.P., Holliday, B., Avignone, N., Shideler, G. (1972): Anatomy of a shoreface ridge system, False Cape, Virginia – Marine Geology, Vol. 12, pp. 59-84.

Thieler, E.R., Foster, D.S., Himmelstoss, E.A., Mallinson, D.J. (2014): Geologic framework of the northern North Carolina, USA inner continental shelf and its influence on coastal evolution – Marine Geology, Vol. 348, pp. 113-130.

Trembanis A.C., Hume, T.M. (2011): Sorted bedforms on the inner shelf off northeastern New Zealand: spatiotemporal relationships and potential paleo-environmental implications – Geo-Marine Letters, Vol. 31, pp. 203-214.

Trowbridge, J.H. (1995): A mechanism for the formation and maintenance of shore-oblique sand ridges on storm-dominated shelves – Journal of Geophysical Research, Vol. 100, No. C8, pp. 16071-16086.

Williams, A., Althaus, F., Schlacher, T.A. (2015): Towed camera imagery and benthic sled catches provide different views of seamount benthic diversity – Limnology and Oceanography: Methods, Vol. 13, pp. 62-73, doi:10.1002/lom3.10007.

Yoklavich, M.M., Greene, H.G., Caillet, G.M., Sullivan, D.E., Lea, R.N., Love, M.S. (2000): Habitat associations of deep-water rockfishes in a submarine canyon: an example of a natural refuge – Fishery Bulletin U.S., Vol. 98, pp. 625-641.

Zevin, L.S, Kimmel, G., Mureinik, I. (editor) (1995): Quantitative X-ray diffractometry – Springer, New York, 372

Chapter 3

Magnetic mineral and sediment porosity distribution on a storm-dominated shelf investigated by benthic electromagnetic profiling (Bay of Plenty, New Zealand)

Tobias Kulgemeyer[a], Tilo von Dobeneck[a], Hendrik Müller[a], Karin Bryan[b], Willem de Lange[b], Christopher Battershill[b]

[a]Faculty of Geosciences and MARUM - Center for Marine Environmental Sciences, University of Bremen, Klagenfurter Straße, 28359 Bremen, Germany

[b]School of Science, University of Waikato, Private Bag 3105, Hamilton, New Zealand

Submitted to Marine Geology on 31/05/2016

Abstract Magnetic susceptibility and electric conductivity within the uppermost meter of the seafloor were measured along 33 coast-normal profiles in the Bay of Plenty, New Zealand. with high resolution using the recently developed electromagnetic benthic profiler MARUM *NERIDIS III*. These parameters are used to determine magnetic mineral concentration and porosity of mostly volcanoclastic sediments between 2-35 m water depth to investigate distribution and formation of magnetic mineral enrichments on a storm-dominated shelf.

In general, magnetic mineral concentration is inversely correlated to porosity. Along profiles, susceptibility maxima and conductivity minima were commonly found on bathy-

metrical elevations such as dune and ripple crests, and on or close to point where the bathymetric gradient is changing. Cores and grab samples show the highest degree of enrichment in the uppermost 20 cm of the seafloor.

Three distinct zones of magnetic mineral enrichment could be identified: a coast-parallel structure with low porosity in fine sand, that stretches along almost the entire coastline between 5-15 m water depth. A highly porous structure was found in older, transgressionally reworked, coarse sand deposits in up to 35 m water depth. This structure is locally confined to an area close to a submarine ridge connecting volcanic island to the main land, sediments of the same lithofacies are usually not enriched in other parts of the study area. A third, cross-shore striking enrichment structure with low porosity was found in medium and coarse sand of similar age. While the fine sand structure is interpreted as the result of an active process, the other two appear to be relics. They are likely a product of the selective entrainment of relatively large light minerals, while smaller heavy minerals remain.

Complementing petromagnetic analysis indicates a spectrum of FeTi-oxides in the sediment, ranging from magnetite and hematite over titanomagnetite (TM40 and TM60) to titanohematite (likely TH80 and TH95). A positive correlation between magnetic and physical grain size of the lithofacies (fine to coarse sand) has been observed. High susceptibilities are clearly a result of enrichment of ferrimagnetic minerals over para- and diamagnetic phases. The enrichment is most effective for all lithofacies in a similar magnetic grain size range.

This study demonstrates how electromagnetic benthic profiling, in combination with environmental magnetic laboratory analysis, provides reliable, highly interpretable data that allow insight into sorting processes within the boundaries of established lithofacies that are difficult to detect using a classical sedimentological approach.

3.1 Introduction

Knowledge of seafloor stability, sediment sources and transport paths are of great importance for coastal protection and management. Common methods for characterizing the seafloor are often based on the analysis of samples, which limits the resolution and is logistically and experimentally expensive. Hydroacoustic surveys can rapidly cover large areas, but mostly focus on topography and

seafloor roughness. The resulting acoustic backscatter values are not unique in terms of grain size and composition and need to be interpreted using samples or other complementary data required for ground truthing. Numerical models likewise need to be empirically calibrated, again based on sample material and long-term measurements of hydrodynamic conditions.

Over the past three decades, electromagnetic (EM) imaging has been increasingly applied for airborne and terrestrial geophysical surveys. The use of EM in a conductive marine environment poses special problems, for which theoretical and practical solutions were laid by Chave & Cox (1982) and Cheesman et al. (1990). Evans (2001) used a towed EM system to investigate sediment porosity on a continental shelf. Müller et al. (2012) developed a system which coevally quantifies electric and magnetic properties of the seafloor using a frequency domain horizontal in-loop sensor in a bottom towed sled.

With this benthic profiler is was possible to locate and quantify freshwater seepage and associated sediment diagenesis, and to classify surficial sediments in coastal and continental shelf environments (Müller et al., 2011, 2012). Baasch et al. (2015) used these multifrequency data for the reconstruction of layering in marine deposits by inversion of sediment conductivity.

The approach described by Müller et al. (2012) provides two distinct physical parameters, that relate two sedimentological properties: the magnetic susceptibility, as a measure of magnetic mineral concentration, and the electric conductivity, which depends on porosity. Measurements are fast, have a high resolution and cover the surface sediment down to ca. one meter depth, where modern transport processes take place. In a multi-sensor survey, EM profile lines can bridge the gap between geological point sampling and hydroacoustic area mapping by reducing the number of samples needed for ground truthing. Furthermore, profile data can be sensibly interpolated to assess the spatial distribution of porosity and magnetic susceptibility to estimate the relative abundance of primarily ferrimagnetic minerals.

Natural ferrimagnetic minerals are iron oxides like magnetite, maghemite and hematite, their respective titanium bearing substitutions, or iron sulfides such as

greigite and pyrrhotite. These are heavy minerals, set apart from light minerals like quartz and feldspars by their much higher density and usually smaller crystal and particle grain size. Due to their different hydrodynamic properties, heavy minerals tend to enrich locally by gravitational and grain-size sorting processes during entrainment, transport, settling and burial (Komar & Wang, 1984; Slingerland & Smith, 1986). Their easy detectability by magnetic methods makes iron oxides an ideal proxy mineral to gain thorough insights into the local dynamics of heavy mineral sorting and enrichment – processes that further differentiate otherwise indistinguishable sediments of a certain lithofacies, and whose scope and magnitude are hard to determine using samples alone. Thereby, (electro)magnetic data provide a relatively easy way to gain information about geological environments that is otherwise difficult to access.

Sediments along the coastline of New Zealand typically contain high concentrations of iron oxides. Magnetite and titanomagnetite enrichments are common, and can form almost pure (90 %) placers (Bryan et al., 2007). In the Bay of Plenty Badesab et al. (2012) investigated the magnetic properties of sediments in and offshore the Tauranga Harbour estuary. Based on sediment susceptibility two coast-parallel belts with relatively high titanomagnetite concentrations of up to 3.3 mass % could be located in water depths of 6-10 m and 10-20 m respectively. This area was chosen for a subsequent survey using various profiling and laboratory techniques.

In this study, we utilize benthic EM profiling in a new coastal mapping and monitoring approach to provide insight into the distribution of light and heavy minerals in a dynamic coastal system. This includes: a) presenting EM and complementing environmental magnetic data from various environments, b) characterizing the magnetic minerals involved as well as the relation between magnetic mineral concentration and the process of enrichment, and c) conceptualize the formation of enrichment structures.

3.2 Geographic and geological setting

The Bay of Plenty (BoP) is located in the north of New Zealand's North Island, bound to the west by the Coromandel Peninsula and to the east by the East Cape region. Our study area stretches 60 km along the coast of the western BoP between Waihi Beach and Okurei Point and 8 km cross-shore from 2 to 35 m water depth (Fig. 3.1). An important feature in this region is the Tauranga Harbour estuary, a mesotidal lagoon with two hydrologically independent basins (De Lange, 1988). The southern basin receives most sediment and fresh water input from the Wairoa River (Park, 2004), which drains source rock from the rhyolitic Taupo Volcanic Zone (TVZ). In contrast, sediment in the northern basin is supplied by the Kaimai Range located in a transitional zone between the TVZ and the older, andesitic to dacitic, Coromandel Volcanic Zone (CVZ) (Briggs et al., 2005).

The estuary is enclosed by Matakana Island and two narrow tombolos (Healy et al., 1996), which both connect to rhyolitic lava domes (Briggs et al., 2005): the 251 m high Mt. Maunganui and the 88 m high Bowentown domes. Tauranga Harbour can be accessed by two entrances: in the north, this is the natural Katikati Entrance, and in the south the larger and artificially-deepened Tauranga Entrance. Material dredged from the ebb tidal delta has been deposited in dumping grounds between 4-7 m, 15-25 m and 28-33 m depths offshore Mt. Maunganui (Healy et al., 1991; Davis & Healy, 1993; Foster et al., 1994, 1996; Michels & Healy, 1999). Sediment transport at the entrances is driven by ebb-tidal currents (Davies-Colley & Healy, 1978a; Hicks & Hume, 1996, 1997) and in part recirculated into the estuary (Davies-Colley & Healy, 1978a,b; Spiers et al., 2009).

Another very large andesitic (Briggs et al., 2005) lava dome ten kilometers offshore is Motiti Island. This island was formed in association with the CVZ (Henry, 1991), and has since been largely eroded so that only a flat remnant remains.

The second major source of terrestrial sediment in the area is the Kaituna River.

This river previously discharged into the Maketu Estuary at the southeastern end of the study area, but was artificially diverted directly into the sea in 1956 (Burton & Healy, 1985). The Kaituna flows from Lake Rotoiti northwards through unwelded rhyolitic ignimbrites of the TVZ (Leonard et al., 2010).
Lithofacies distribution and sediment transport pathways in the study area were described in detail by Kulgemeyer et al. (2016) (*chapter 2, referred to as publication in the following text*). Eight distinct lithofacies, including subtypes, could be distinguished from seafloor photography and sample-based analyses (Fig. 3.2). These are:

- Lithofacies 1: A fine sand mostly comprised of quartz and feldspars, ca. 2.5 % mafic minerals (pyroxene, hornblende, biotite, opaque minerals) and volcanic glass.
- Lithofacies 2a: Medium quartz/feldspar sand with ca. 5 % mafic minerals and a small amount of volcanic glass.
- Lithofacies 2b: Medium sand without volcanic glass.
- Lithofacies 3a: Coarse sand, similar in composition to lithofacies 2b with additional rock fragments.
- Lithofacies 3b: Coarse to very coarse sand variant of lithofacies 3a.
- Lithofacies 4: Medium sand mixture of terrigenous components comparable to lithofacies 2b and bioclastics (shell fragments).
- Lithofacies 5: A coarse sand, composed of siliciclastics comparable to lithofacies 3a and biogenic debris derived from bivalves and sponges. Pebble-sized and larger rock fragments are common.
- Lithofacies 6: A shell detritus layer covering an unidentified substrate.

Sediments were interpreted as Holocene riverine input (lithofacies 1), part of a postglacial transgressive series sourced from reworked pleistocene sands (lithofacies 2a-3b), mixed with local sources such as biogenics (lithofacies 4)

and Motiti Island andesite (lithofacies 5), or are classified as shell detritus on an undetermined substrate (lithofacies 6). This interpretation is in agreement with a model by Bradshaw et al. (1994) for the adjacent Coromandel shelf. Sediment transport is bidirectional and changing depending on the weather. Net transport (littoral drift) direction is to the southwest during fair weather. During stormy weather, a geostrophic current develops that is transporting sediments to the northwest (Bradshaw et al., 1991, 1994).

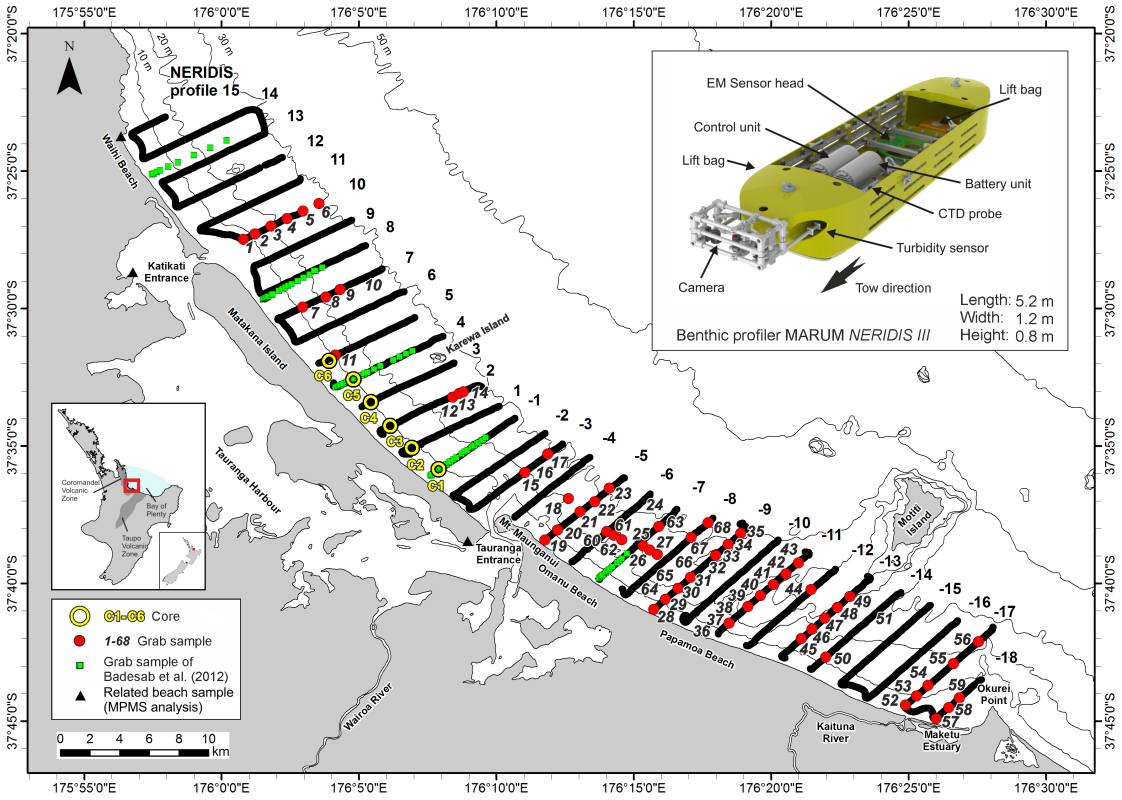

Figure 3.1: Overview of the study area with sample locations and *NERIDIS* survey profiles. The profiler is towed along the seafloor as a sled and is measuring the magnetic susceptibility and electric conductivity of sediments.

3.3 Processes of heavy mineral enrichment

The enrichment of heavy minerals is a complex process that can take place in diverse environments (Slingerland & Smith, 1986), such as rivers (Duk-Rodkin et al., 2001; Burton & Fralick, 2003), tidal channels (Badesab et al., 2012), deltas (Frihy & Komar, 1993; Corbett & Burrell, 2001), beaches (Komar & Wang,

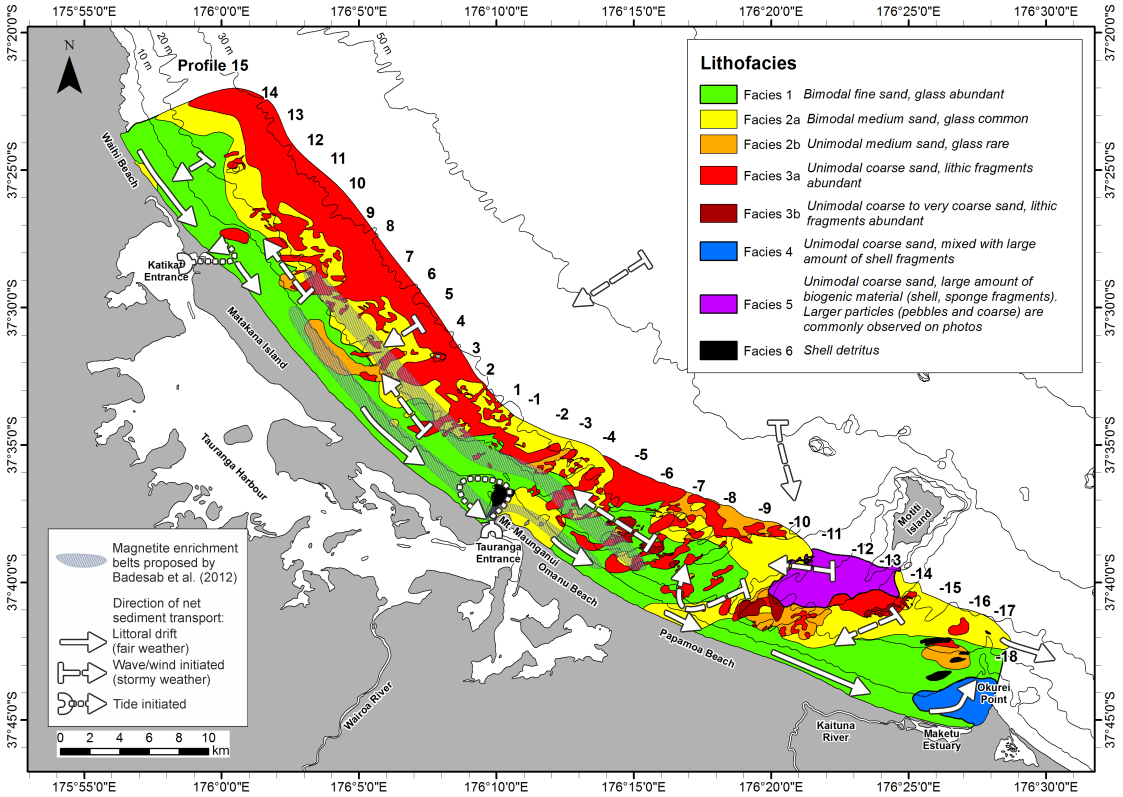

Figure 3.2: Lithofacies of the study area inferred from granulometry, mineralogical composition and photographic appearance. Transport pathways are based on the interpretation lithofacies distribution, bedforms according to acoustic backscatter and turbidity (for details see Kulgemeyer et al. (2016)).

1984; Bryan et al., 2007; Gallaway et al., 2012) and the shoreface (Elsner, 1992; Hamilton & Collins, 1998). Each environment is subject to its unique combination of bathymetry, source rocks, sediment input and wave and current climate, and to date no single model has been developed that can predict the likelihood and degree of heavy mineral enrichment in every environment. High-grade enrichments form placers of economic interest and provide a source for a multitude of materials such as titanium (Corbett & Burrell, 2001; Bryan et al., 2007; Prakash, 2000), iron (McDougall, 1961; Orpin et al., 2009), uranium (Burton & Fralick, 2003), gold (Jones & Davies, 1979; Duk-Rodkin et al., 2001; Burton & Fralick, 2003) and diamonds (Corbett & Burrell, 2001). However, for scientific purposes, low-grade enrichments are also of interest, as they potentially provide information about past and present sediment provenance and dynamics (Frihy, 1994; Zhang et al., 2010; Li et al., 2015).

This study focuses on titanomagnetite enrichments in the nearshore environment.

Often, these types of structures are attributed to the winnowing effect of waves (Hamilton & Collins, 1998) in a process of selective entrainment by grain size. The typically small grain sizes of heavy minerals allow them to be sheltered within the pore space of their surrounding matrix, while larger and lighter mineral grains protrude out of the bed; therefore, they are more exposed to shear stresses and are preferentially entrained (Slingerland, 1977; Komar & Wang, 1984; Li & Komar, 1992; Tomkins et al., 2003). Other effects contributing to the enrichment of heavy minerals are the interplay of size, density and shape with bed roughness, which influence sorting during bedload transport due to variations in the transport rate (Steidtmann, 1982), differing settling velocities that lead to sorting during the deposition of suspended material (Slingerland & Smith, 1986), and the response to current-induced shear stress which leads to burial of finer grains (Sallenger, 1979; Gallaway et al., 2012). All of these processes can play a role in the formation of heavy mineral placers, but to what degree they act and interact in different environments is not yet fully understood (Hughes et al., 2000; Bryan et al., 2007). Overall, the existence of nearshore heavy mineral enrichments appears to be indicative of an erosional environment (Frihy, 1994; Zhang et al., 2010); in a system with very high sediment input, heavy minerals are quickly buried and no sorting can take place (Bryan et al., 2007).

3.4 Materials and methods

3.4.1 Benthic profiling

The magnetic and conductive properties of the BoP seafloor have been investigated with the electromagnetic benthic EM profiler *NERIDIS III* (Fig. 3.1, inlet) in November 2012 using the Western Workboats vessel *MACY GRAY*. This instrument is the latest model of benthic EM profilers developed at MARUM – Center for Marine Environmental Sciences, University of Bremen. It has dimensions of 5.2 $\times$ 1.2 $\times$ 0.8 m, and weighs 900 kg in air, and ca. 250 kg in water. The profiler is equipped with a Controlled Source Electromagnetic (CSEM) induction coil sensor, an Attitude-Heading-Reference-System, a high-resolution camera

for seafloor photography, and an on-board conductivity, temperature and depth probe (CTD) with turbidity sensor. Seafloor photos and turbidity data were used by Kulgemeyer et al. (2016) to analyze sediment facies and dynamics. The profiler towed along the seafloor at 2-4 kn (1-2 m/s) by a ship while skids ensure ground contact and thus a constant altitude of the electromagnetic soundings at 20 cm height. One deployment can cover ca. 50-85 km with power provided for 7-10 h (depending on the number of instruments used) by exchangeable internal 1.4 kWh lithium ion batteries. The position of the profiler is triangulated from the ship's GPS position, cable length and water depth, while heading, pitch, roll and acceleration are used to define the position of the instrument with an accuracy of less than 5 m. The calibrated and drift-corrected raw data were transformed into the appropriate SI units using the half-space inversion method proposed by Müller et al. (2012).

The electric conductivity of the bottom water is a necessary input parameter for the determination of sediment conductivity from the EM signal. Conductivity, temperature and depth were continuously recorded with a Sea & Sun Technology CTD 60M multiparameter probe 0.5 m above the seafloor. Respective accuracies are 0.0001 S/m, 0.001 °C and 0.002 bar ($\approx$ 2 cm; max. 100 bar $\approx$ 1000 m). Simultaneously, the bottom water was monitored with a Seapoint Sensors turbidity sensor. The acquired data range linearly from 0-25 in increments of 0.001 Formazine Turbidity Units (FTU).

The *NERIDIS III* profiler utilizes a horizontal concentric coplanar CSEM-loop sensor design (Won et al., 1997). The 1 m diameter transmitter coil emits alternating magnetic fields that consist of up to 12 combined operation frequencies in the 25 Hz to 20 kHz range with a maximum transmitter moment of up to 2 kAm^2 (48 V, 30 A transmitter, 8 turn loop). A high performance 30 cm diameter receiver coil measures the in-phase and quadrature component (or amplitude and phase) of the secondary magnetic field for all the transmitted frequencies with a sampling rate of 25 Hz. The bucking coil is tuned to create a magnetic cavity in the center of the arrangement. Thus, the receiver virtually does not see the primary transmitter signal and is therefore capable of measuring the minute

secondary electromagnetic subsurface response over a wide dynamic range. The magnetic susceptibility can be derived from the low frequency ($<$ 100 Hz) in-phase signal which is almost a direct measure of the subsurface magnetization. At higher frequencies, field induced eddy currents start to dominate the signal, which allows to measure the electric conductivity of the subsurface with frequency dependent depth penetration and sensitivity. Spectral analysis of the received magnetic fields permits thereby the distinction of two fundamental sediment physical parameters: the magnetic susceptibility and the electric conductivity (Müller et al., 2012; Baasch et al., 2015). The electric conductivity signal is controlled by the seawater contained in pore space which has an almost neglectable magnetic susceptibility. Accordingly, susceptibility is associated with magnetic particles in the solid fraction of the sediment, especially by the concentration of ferrimagnetic particles. Müller et al. (2012) show that a half-space inversion of the right frequency and phase components can be used to receive magnetic and electric signal from comparable depth extends to allow a direct comparison and joint interpretation (characteristics see Table 1).

Table 3.1: Signal characteristics

Parameter	**Susceptibility**	**Conductivity**
Frequency	75 Hz, in-phase	5025 Hz, quadrature
50/90 % signal depth	14/50 cm	21/92 cm
Footprint	1 m	4.5 m
Sensitivity	1×10^{-6} [SI]	1 mS/m
Sediment property	Magnetic mineral content	Porosity

3.4.2 Spatial interpolation of datasets

Datasets obtained with *NERIDIS III* were interpolated in ArcGIS using Universal Kriging. This method was chosen because of underlying trends due to bathymetrical effects and source-to-sink sediment transport. To achieve a greater control over the results, the dataset was not interpolated in one, but divided into 10 overlapping areas of 4-5 profiles each. Thereby, Kriging parameters could be optimized to the local conditions of each area. Input for the interpolation were the extent and type of trend surface (linear or 1st order polynomial, the

trend model that lead to the smallest prediction errors was calculated by trial and error), anisotropy and type of variogram (stable, gaussian or exponential), and the angle and dimensions of the neighborhood search ellipse (2000 m $\times$ 500 m, major axis coast parallel and covering three profiles; ellipse divided into four sectors including 50 points each). The exact parameters were chosen automatically as best fits to minimize mean-square prediction errors. If necessary, the subsets were logarithmically transformed before processing (the datasets are usually right-skewed, but statistical error determination assumes a normal distribution). Datapoints in the original lines are very dense, and so to reduce computing time and minimize some artifacts only every fifth point was included in the interpolation, leaving approximately one point per meter. As a final step to further reduce artifacts, the mosaiced maps were filtered by a moving average filter with a radius of five map cells (1 cell [X, Y] = 29.2 m $\times$ 36.6 m).

3.4.3 EM derived seafloor conductivity and equivalent porosity

Sediment porosity ϕ was derived from electric conductivity of ambient water σ_W and surficial sediment σ_S using the equation of Archie (1942):

$$\sigma_S = a\sigma_W\phi^m \tag{3.1}$$

where a is the pore geometry factor and m the cementation factor. Typical values for a are between 0.5-2.5 (Edwards, 2005) and for m between 1.4 and 3 (Jackson et al., 1978; Edwards, 2005; Evans, 2007). For unconsolidated sediment, a value of $a = 1$ is mostly used (George et al., 2015) and m was set to 1.6 (natural sand according to Jackson et al. (1978)) for all lithofacies. The statistical variance of porosity was only minimally different from that of the electric conductivity of sediment. Both properties will always be discussed together.

3.4.4 EM derived seafloor susceptibility and equivalent magnetite concentration

An equivalent concentration of magnetite can be calculated from the susceptibility as follows: With the simplified assumption that the susceptibility of the matrix κ_{matrix} is determined by pure magnetite, the signal scales linearly to the concentration and, for particles larger than silt, is mostly independent from grain size (Peters & Dekkers, 2003). Susceptibility of natural magnetite κ_{Mt} can span a wide range due to impurities and lattice defects; Peters & Dekkers (2003) provide values of 1.48-6.48 and an average susceptibility for natural magnetite of 3.50 (assuming a density 5.2 g/cm^3). This average value was used to represent a magnetite concentration of 100 % and to calculate the volume concentration C_{Mt} of magnetite from a data point or map cell. After correcting the volume specific magnetic susceptibility for porosity ϕ the apparent portion of magnetite in the total sediment volume is given by:

$$C_{Mt} = \frac{\kappa_S}{\kappa_{Mt}(1-\phi)} \tag{3.2}$$

Obviously, the magnetic mineral assemblages of sediments in the BoP not only contain pure magnetite, but include a range of ferri- and antiferromagnetic FeTi oxides of varying composition and properties. However, even with exact knowledge of magnetic mineralogy, a determination of the concentration for each fraction would need to consider grain size related effects. These can be neglected for multidomain magnetite, but are significant for titanomagnetites and other minerals (Peters & Dekkers, 2003).

3.4.5 Sample material

Grab samples were taken at 68 stations during a survey in December 2013 and complemented by samples collected in early 2010 by Badesab et al. (2012). All grab samples were collected with a small Van Veen grab sampler and represent the uppermost ca. 5 cm of seafloor. Six short sediment cores were taken by divers in 6-8 m water depth offshore Matakana Island (Fig. 3.2) in April 2014

using plastic tubes 10 cm in diameter with fitted caps. All cores were taken from a fine sand deposit that has been designated as ”inner magnetite enrichment belt” by Badesab et al. (2012). The core barrels were pressed into the seafloor by stacking weights on top, excavated by hand and quickly sealed to prevent material loss.

3.4.6 Magnetic susceptibility of samples

Bulk magnetic susceptibility measurements were applied to all cores at 2 cm intervals and to the surface samples on with a Geofyzika Brno Kappabridge KLY-2 susceptometer. Sample material was prepared in plastic cubes with dimensions of $2 \times 2 \times 1.6$ cm.

3.4.7 Thermal demagnetization of samples

Triaxial thermal demagnetization after Lowrie (1990) has been conducted to identify magnetic minerals based on their characteristic unblocking temperature (approximated by the Curie temperature) and coercivity ranges. A total of 23 cubic samples from all lithofacies were prepared with water glass (sodium silicate) to fixate the grains during heating. At first, isothermal remanent magnetization (IRM) curves were acquired by stepwise magnetization of the samples up to 2 T. Thereafter, the samples were re-magnetized along perpendicular axes in 120 and 40 mT pulse fields. This aligns mineral-specific remanences along any of the three axis according to their coercivity of remanence B_{CR}. The magnetized samples were heated stepwise to a maximum temperature of 680 °C. After each heating step, remanent magnetization was measured along each axis at room temperature with a 2G Enterprises Cryogenic Magnetometer. In parallel to this, the susceptibility of the samples was recorded on the Kappabridge to keep track of chemical transformations.

Existing low-temperature saturated isothermal remanent magnetization (SIRM) curves of three related BoP sediment samples are included. These measurement were done on a Quantum Design Magnetic Property Measurement System (MPMS).

3.4.8 Magnetic hysteresis of samples

Magnetic hysteresis loops were measured on surficial samples with a Princeton Measurements Corporation MicroMag 2900 Alternating Gradient Field Magnetometer. Specimen of ca. 20-30 mg of dry sediment were prepared in small cylindrical plastic containers and fixated with glue. Two hysteresis loops were recorded for each sample, up to a maximum applied field of 300 mT in 2 mT increments, and up to 1 T in 5 mT increments. The resulting curves were analyzed with the program Hystear using the method described by von Dobeneck (1996). Magnetization and coercivity parameters were calculated on 300 mT hysteresis loops, total mass-specific susceptibility as well as the contributions of ferrimagnetic and paramagnetic components were derived from 1 T loops.

3.5 Results

3.5.1 Electromagnetic lithofacies characterization

Boxplots in Fig. 3.3 show the statistical parameters for every lithofacies identified by Kulgemeyer et al. (2016) along coast-normal profiles. As a general trend, the coarser deposits (facies 2a-6) have a slightly higher average susceptibility, but also larger variability. Coarser sediments tend to have a smaller average conductivity and a higher variability than finer ones. As the coarser sediments in the BoP are older deposits reworked from Pleistocene sands during the Holocene transgression (Bradshaw et al., 1994), the smaller conductivity (porosity) is possibly a result of better grain sorting over time. The differences are not large enough to identify and distinguish these lithofacies on a regional scale, but as the next sections will show, there are local effects that control the EM characterization both between and within lithofacies.

3.5.2 Electromagnetic profile characterization

Apart from the SE-NW gradient of susceptibility, some further general observations can be made. Magnetic minerals tend to accumulate on top of dune and

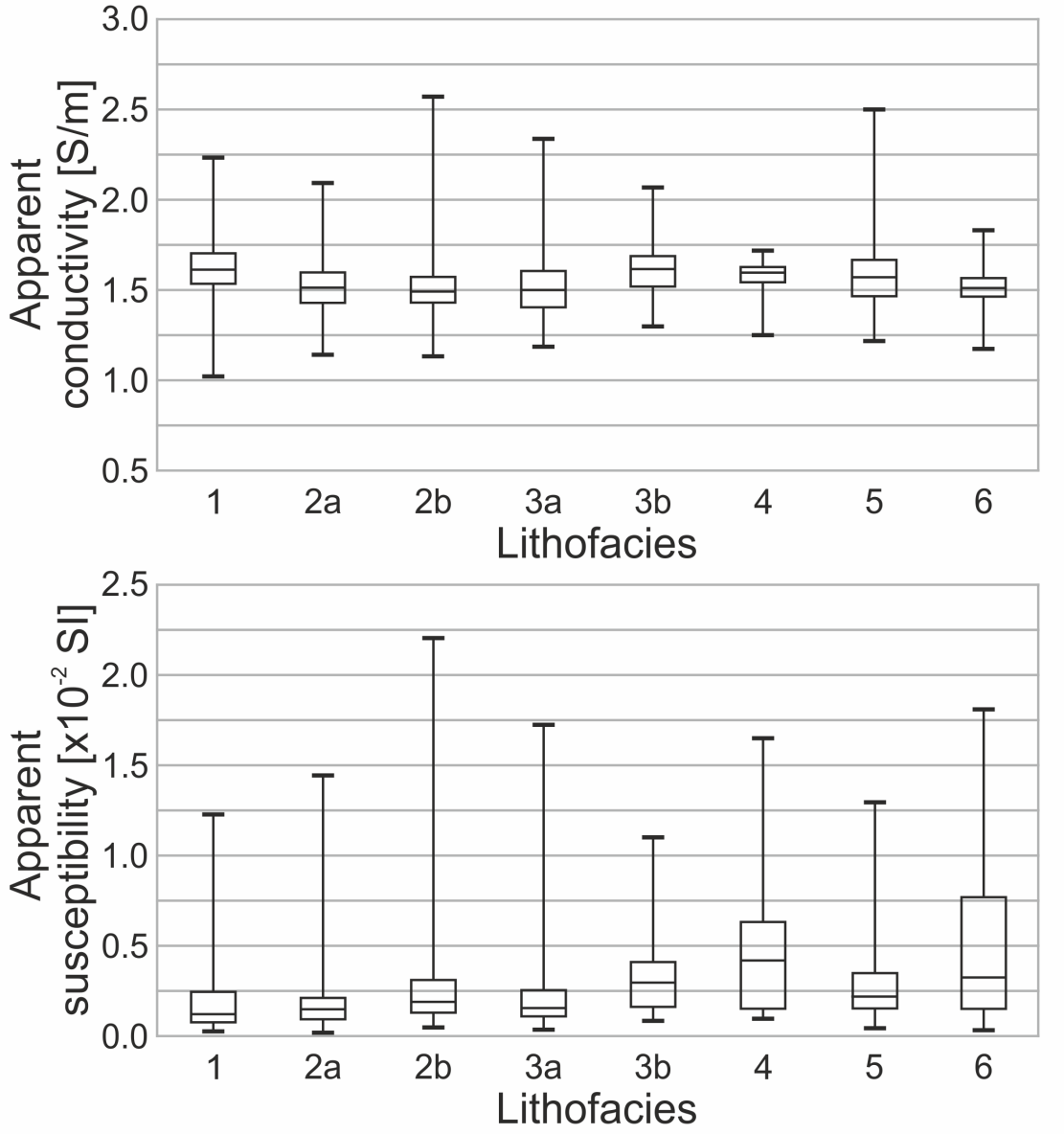

Figure 3.3: Boxplots of conductivity and susceptibility for every lithofacies.

ripple crests, as well as slope breaks; these point often coincide with a porosity minimum. A closer look at the profiles shows distinctive features or combinations of features on both curves that appear to be typical for certain environments.

The southeastern end of the study area (Fig. 3.4, profile -17) is characterized by the proximity to the mouth of the Kaituna River and a low bathymetric gradient. Susceptibility is very high, while conductivity is is low and has little variation. Magnetic minerals appear to accumulate especially in places were they are shielded by large grains or shell detritus.

At the Motiti Island ridge (profile -12), the susceptibility curve has some very

distinct peaks aligned with small elevations of the seafloor. Conductivity first decreases with water depth, but increases again in lithofacies 5, a coarse sand characterized by the presence of pebbles and diverse biota (bivalves, sea lettuce).

Profile -7 crosses a sorted bedform in 10-20 m water depth with high magnetite concentration and low porosity. The symmetrical shape of the curves may indicate local hydrodynamics, a longshore current that is responsible for the preservation of the bedform. The surrounding fine sand is very low in susceptibility, but increases again in the deeper section of this profile over a coarse sand deposit. Porosity here is relatively high compared to other profiles, although the maximum porosity is still measured in the fine sand deposits. Below 30 m the change from fine to coarse sand goes along with an increased susceptibility.

Along profile -5, susceptibility is very low down to a water depth of 30 m where magnetically enriched coarse sand with high porosity is observed. Additionally two peaks are present at around 20 and 25 m depth, where this coarse sand facies is exposed.

Further north is the ebb tidal delta of Tauranga Entrance (Fig. 3.5, profile -2). Within the delta, conductivity is high with little variation, while susceptibility is low and only has a few sharp peaks on the tidal upcurrent side of bathymetric highs (probably sandbars).

High susceptibility was also measured all along profile 2, and a greater number of distinct peaks are seen at small elevations or slope breaks. Conductivity slightly decreases seawards, but then remains relatively stable.

On profile 6 the long-shore enrichment structure is very distinct in medium between 5-15 m, an underlying deposit excavated by erosion (Kulgemeyer et al., 2016). In contrast to the sorted bedform on profile -7, where coarse sand has been excavated, the curve on profile 6 has an asymmetrical shape with a much steeper gradient towards the coast. This might be an indication that this erosion is more related to the action of waves approaching from the sea than a strong long-shore current exposing the substrata.

The tidal delta of the northern entrance (profile -9) has again a high and stable

conductivity, while susceptibility is extremely low. Only in greater water depth, where coarser and older sediments are deposited, does it increase slightly, while conductivity decreases. A prominent feature is the slope break in 25 m depth, susceptibility drastically drops over a short distance while conductivity curve has a sharp peak. On this slope break both heavy and fine light minerals seem to be depleted, leading to a higher porosity. This distinguishes this place from most other slope breaks in the study area.

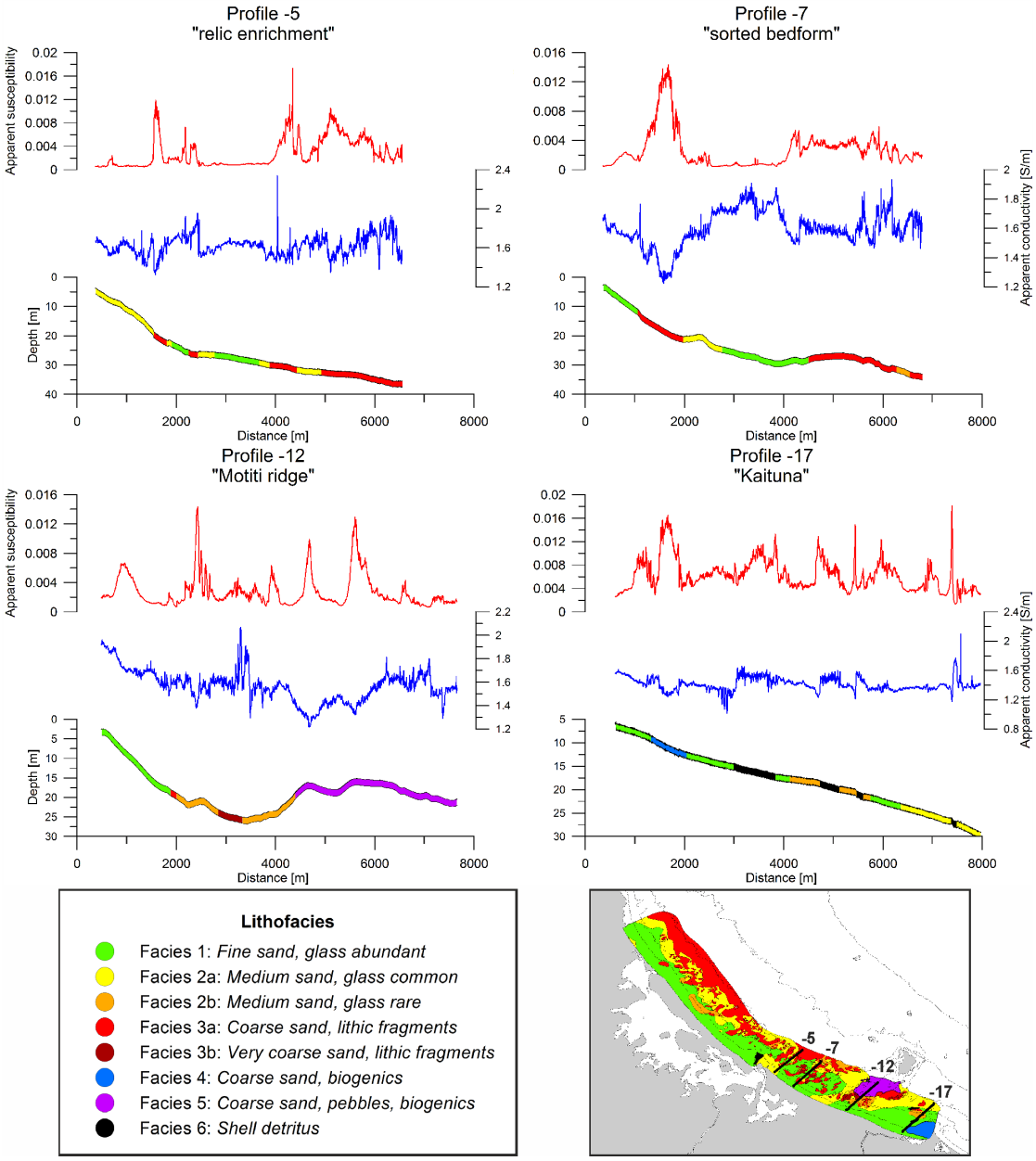

Figure 3.4: Examples of selected profiles along Papamoa and Omanu Beach showing the apparent susceptibility and conductivity, bathymetry and lithofacies with distance from the shore. Thickness of lithofacies is purely schematic and does not represent physical stratigraphy.

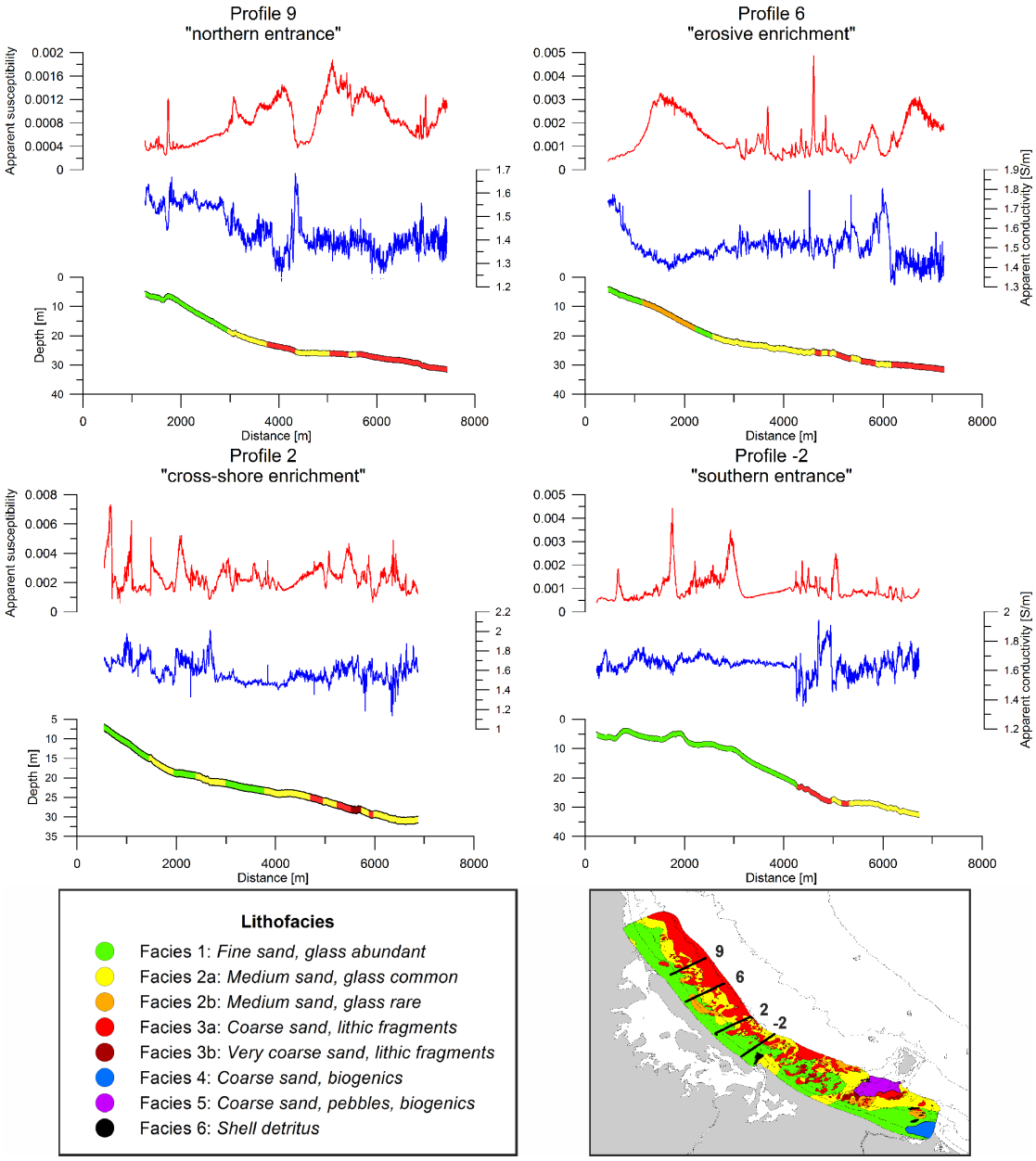

Figure 3.5: Examples of selected profiles along Matakana Island showing the apparent susceptibility and conductivity, bathymetry and lithofacies with distance from the shore. Thickness of lithofacies is purely schematic and does not represent physical stratigraphy.

3.5.3 Spatial distribution of susceptibility/magnetic mineral enrichments

While individual profiles show the cross-shore variation of EM parameters, the distance between profiles (ca. 2 km) makes it hard to intuitively draw connections between observed features. Interpolated maps are better suited for an overview.

The highest susceptibility (Fig. 3.6) was measured at the southeastern end of the study area (Maketu Estuary) and a general decrease towards the northwest (Waihi Beach) was observed. Values drop to a medium range at the Tauranga Entrance, but increase again over a short distance to the NW. From there, they continue to decrease along the 10-15 m isobath where the (inner) enrichment belt as described by Badesab et al. (2012) is clearly developed. Further areas with high susceptibility are observed northwest of the Tauranga Entrance ebb tidal delta, at the seaward end of profiles -5 to -9 and south of Motiti Island. Very low values characterize the environment of the Kaituna Entrance.

The interpolation reveals certain regional structures. Connected to the area of susceptibility offshore the Maketu Estuary this is a smaller area of high susceptibility between profiles -14 and -13 at a depth of 10 m to 20 m, which stretches parallel to the 10 m isobath and shows a decreasing susceptibility with a minimal value also at profile -10. From there, values increase again while the structure shifts towards deeper regions until another maximum is reached in 15 m depth at profile -7. From here, susceptibility decreases and, apart from a small area at profile -5, remains at mid-range values while the structure is in close proximity to Mt. Maunganui and Tauranga Entrance at a constant depth of 15 m. Northwest of this location, susceptibility increases again towards profile -1 and continues to be elevated between 5-15 m depth over 14 km along Matakana Island, only shortly disrupted at profile 5, until it ends at a very low susceptibility at the ebb tidal delta of Katikati Entrance (ocean outfall of the Katikati sewage treatment plant discharges at profile 5, although it is unclear if this has any influence on the sediment). This structure aligns perfectly with the inner magnetite enrichment belt described by Badesab et al. (2012). The outer, less well defined, belt proposed by these authors is only observed as a series of disconnected patches.

A similar, although unconnected, structure exists at 25 m depth south of Motiti Island. Extending from these two features towards the northwest are four elongated structures in 20-25 m depth. The three outermost ones are relatively short and end at profile -10. However, the rugged bathymetry of the Motiti Island ridge

is not taken into consideration by the interpolation. As such, it is unclear if these structures are actually connected with each other or instead consist of a number of smaller, localized enrichments.

Apart from the coast-parallel structures, two cross-shore oriented regions of high susceptibility exist offshore Matakana Island and Omanu Beach. The structure at Matakana Island strikes eastwards and covers a large area between profiles -1 and 4, and merges with the elongated structure at profile 2 and 3. The entire region northwest of this area, along northern Matakana Island and Waihi Beach (profile 5 to 15) in a depth below 20 m, is characterized by very low to average susceptibility. Some additional elongated structures are visible that form two more series of unconnected patches in 20 m and 25 m respectively. Very small patches of higher susceptibility are present at the seaward ends of profiles 6 and 4.

The feature at Omanu Beach, starting at profile -10, strikes in NNW direction until it reaches the 30 m mark at profile -7. Here it merges with a larger coast-parallel structure. The deepest part of the study area is characterized by a very high susceptibility not only in profiles -6 and -5 adjacent to the described feature, but also at the seaward ends of profiles -8 and -9. The exact nature of the cross-shore structure is not clear, lithofacies in this region is variable (see Fig. 3.2), and in any case, the interpolated data offshore Omanu Beach should are uncertain. Therefore, the patterns determined from surficial samples were used to obtain more insights, as discussed in the next section.

The physical meaning of magnetic susceptibility is somewhat abstract in sedimentological terms, an equivalent magnetite concentration is more intuitively comprehensible. Concentrations range from 0.0023 % to 0.58 % (mean: 0.12 %), so even the local enrichments are apparently rather low in magnetic mineral content and not comparable to the black sand beaches at the west coast. For a statistical examination of the dataset, only the cross-shore profiles were used; as the few connecting lines are not evenly distributed throughout the area their inclusion would have biased the statistics. A histogram of the susceptibility (Fig. 3.6, inlet) shows a strongly right-skewed distribution; the statistics of the

magnetite concentration are almost equal.
This estimate is only valid if the sediment composition is homogenous over the penetration depth of the EM signal. This is probably not the case in the outer parts of the study area. An examination of seafloor photos shows a change in sedimentology below approximately 20 m water depth. The sediment below this point is an older transgressive deposit that underlies the highstand the deposits closer to the beach (Kulgemeyer et al., 2016). This should gain influence on the EM signal with increasing distance to the coast, but as a fundamental relation between lithofacies and susceptibility has not been observed this effect can not be accounted for with the data at hand.

3.5.4 Spatial distribution of conductivity/porosity

Conductivity profiles (Fig. 3.7) usually have their highest values close to the beach and decrease slightly with offshore distance. Values on profile -11 were significantly higher (up to 2.7 S/m) than the rest of the profiles. Due to corrupted CTD data these values are considered unreliable and were excluded from the dataset. The camera installed on the profiler showed the presence of sheets of *Ulva* (sea lettuce), that may have influenced the signal by restricting water flow through the profiler. Sea lettuce also covered the profiler on part of profile -3, and these data have also excluded. Susceptibility, measured at lower frequencies, appears to be largely unaffected.
In contrast to susceptibility, conductivity does not have a longshore trend; both the southeastern and northwestern ends of the study area have low values. An area of very high conductivity stretches from central Papamoa Beach to southern Matakana (profiles -10 to -1), for the most part located at depths below 20 m. Enclosed between this feature and the stretch of high conductivity along the beach is an area with average to very low values located between 10 m and 20 m depth at Omanu Beach. This coincides with the observed coast-parallel zone of high susceptibility. Here, the sorting of sediment has resulted in both a relatively high concentration of magnetic minerals and a low porosity. A local anomaly is observed at the shoreward end of profile 7 where an unusually high

electric conductivity was measured.

The porosity of a sediment is dependent on a number of variables like packing, sphericity and, most prominently, sorting (Rogers & Head, 1961). EM porosity values in the study area are between 40 and 72 %. Based on surficial sediment samples, no strong differences in sorting were observed between sediments from the highly porous region offshore from Omanu Beach and less porous sediments of the same lithofacies and water depth at Matakana Island. However, these samples only represent the modern seafloor, and sorting might be different over the sediment column imaged by the EM system. The sediments off Omanu Beach might also be more loosely packed than further up the coastline. For comparison, the consistently high porosity close to the shore is likely to be a result of loose packing due to frequent remobilization by wave action.

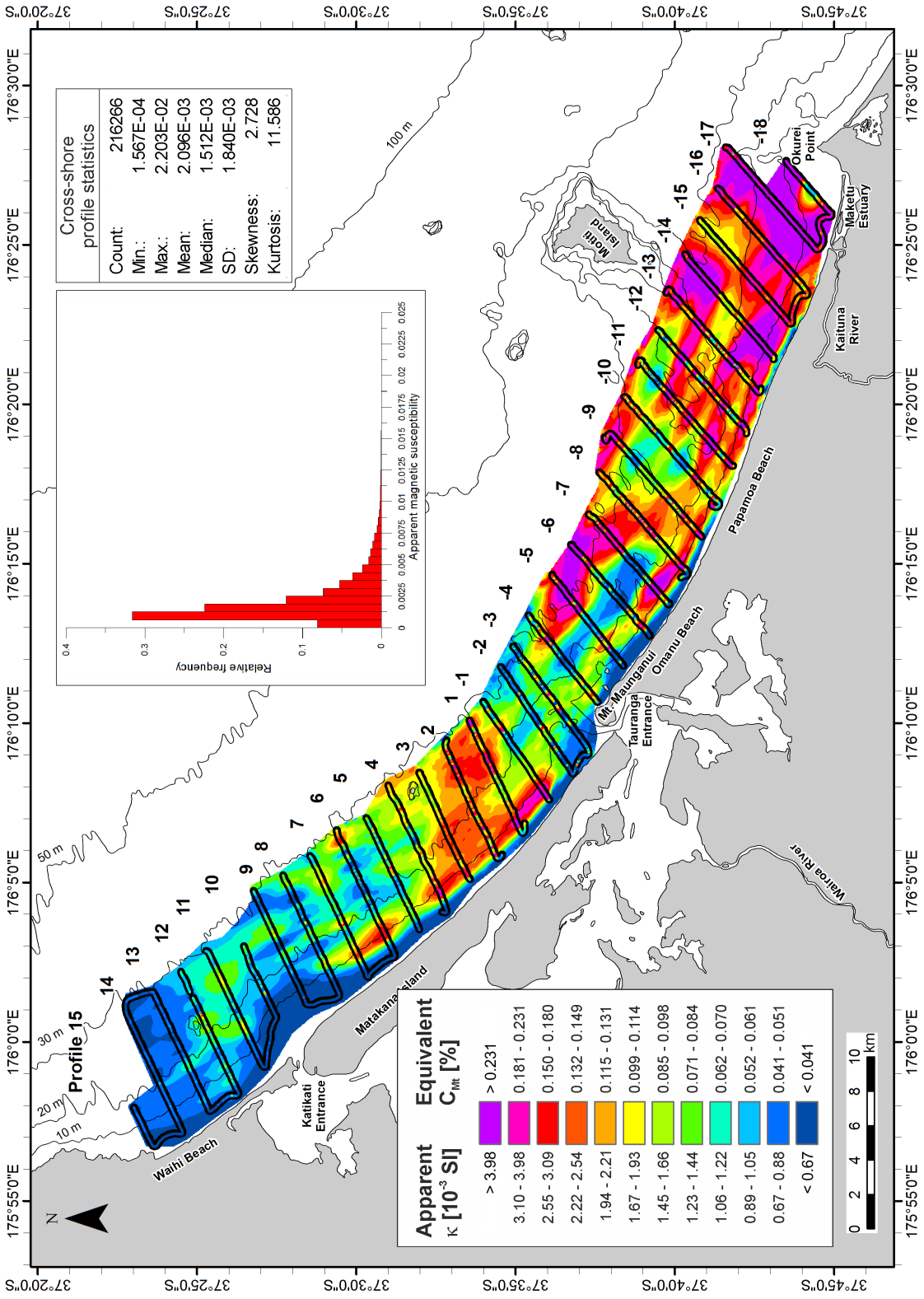

Figure 3.6: Apparent magnetic susceptibility κ with equivalent concentration of magnetite C_{Mt} of the seafloor, displayed on a quantile color scale. Profiles show the original data (width exaggerated). The histograms show the statistical distribution for the cross-shore profiles.

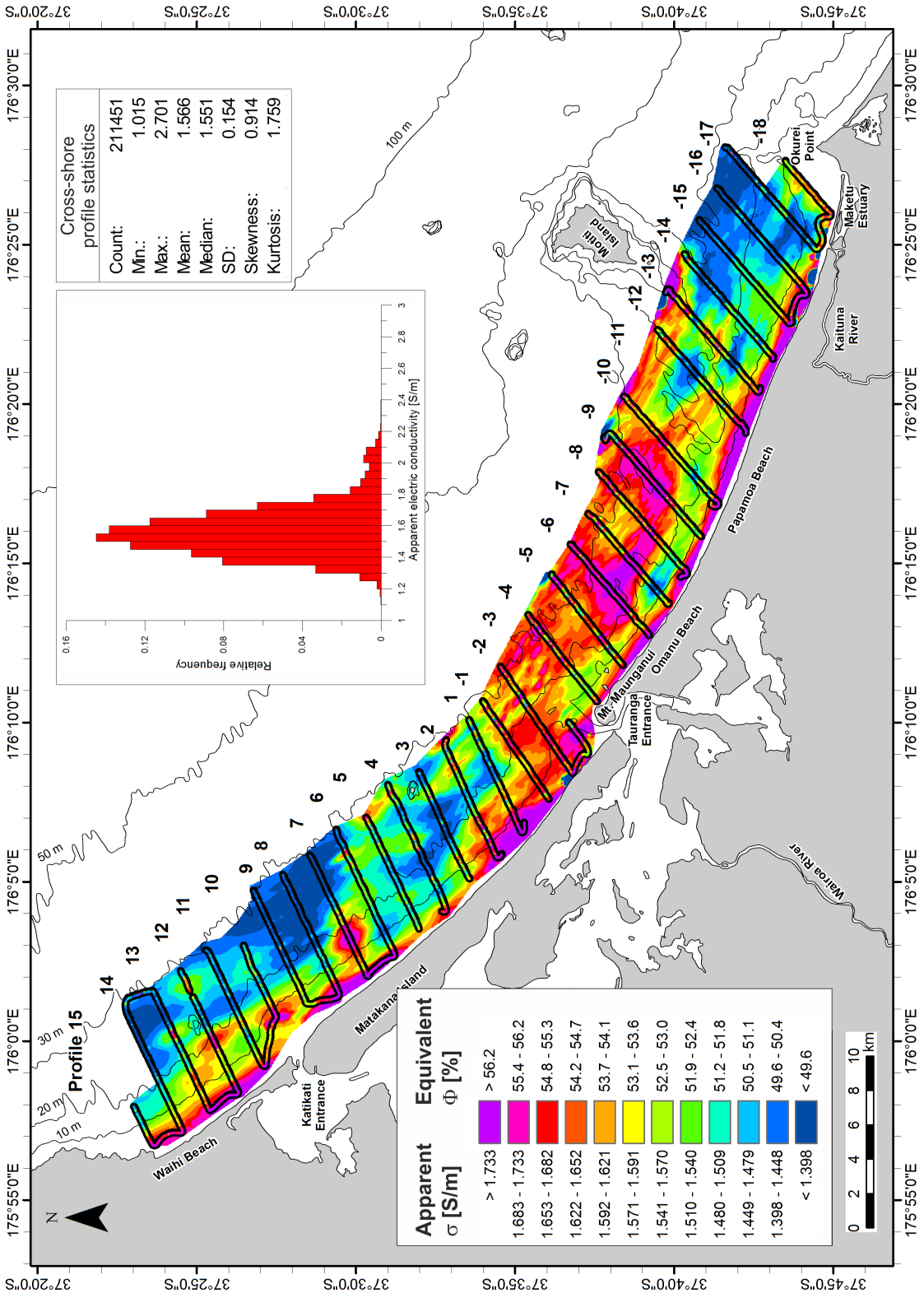

Figure 3.7: Apparent electric conductivity σ and porosity ϕ of the seafloor, displayed on a quantile color scale. Profiles show the original data (width exaggerated). The histograms show the statistical distribution for the cross-shore profiles.

3.6 Discussion

3.6.1 Internal structure and composition of magnetic mineral enrichments

Before the described structures are discussed, some details about the nature of the observed magnetic mineral enrichments should be examined closer. These include a comparison of EM data to sample material, a validation of the hypothesis that increased concentrations of magnetic minerals are a result of grain sorting, and a brief overview of the magnetic mineralogy.

Susceptibility of sample material

In a comparison of the measured 68 surficial samples to the *in situ* measurements of the uppermost 0.5 m of seafloor, two observations can be made (Fig. 3.8): First, an *in situ* enrichment relates to an increased amount of ferrimagnetic minerals on the surface, and second, the concentration of ferrimagnetic minerals close to the surface material is almost always higher than the depth-integrated concentration. Overall, core and grab sample values show a heterogeneous distribution of magnetic minerals in the sediment, which typically form an enriched layer close to the surface. This kind of layering is common in placers (Tomkins et al., 2003; Bryan et al., 2007; Gallaway et al., 2012).

While the spatial distribution in Fig. 3.8 follows the same basic patterns, surficial sediment in some locations where no EM data is available was found to be enriched in magnetite. Especially noteworthy in this regard are the sorted bedforms offshore from Omanu Beach. Some of these bedforms are covered by EM profiles, and the coarse sand of the central regions of the bedforms falls within the interpolated zone of cross-shore enrichment. Coarse sand classified as lithofacies 3a by Kulgemeyer et al. (2016) in a large bedform between profile -6 and -7 is enriched in magnetic minerals, whereas very coarse sand (lithofacies 3b) is not necessarily enriched. While coarse sand in deeper regions that is not part of sorted bedforms is likewise enriched, there is no continuous enrichment

in the fine sand between these bedforms. This enrichment sets these coarse sands apart from deposits of the same lithofacies in the northern part of the study area.

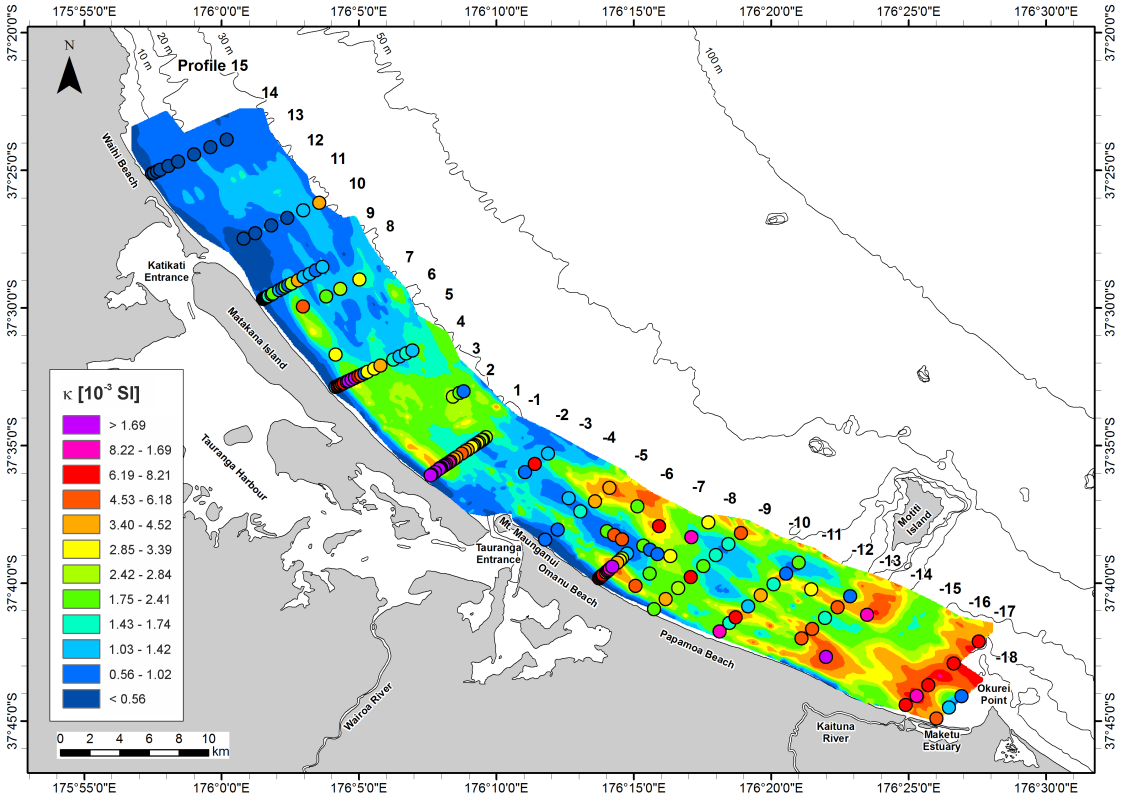

Figure 3.8: Susceptibility of sample material (dots) compared to *in situ* data of the uppermost 0.5 m of the seafloor. Samples taken directly from the surface tend to be more enriched in magnetite. The spatial distribution is following the same observed patterns. Deviations exist where no EM data is available, e.g. a sorted bedform between profiles -6 and -7.

To examine the internal structure of magnetic mineral enrichments, sediment cores have been analyzed. All sediment six cores consist of homogeneous fine sand from lithofacies 1 (Fig. 3.2), from the magnetite enrichment belt of Badesab et al. (2012) offshore Matakana Island. The increase in susceptibility close to the seafloor suggested by the surficial sample material is confirmed by the reference cores. Dotted lines in Fig. 3.9 show the expected depth-integrated susceptibility of the cores calculated using the depth-related weighting function of Müller et al. (2012). These values are compared to the respective values taken from interpolated maps (discussed in section 3.5.3). While cores 1, 3 and 6 are in good agreement, the interpolated values for the positions of cores

2, 4 and 5 are lower than expected. There are numerous factors that have an influence on this value: inevitable inaccuracies of the interpolation, the calibration of the instrument based on regional rather than specific local conditions, the relatively large volume represented by an EM data point, compression of core material before the were opened in the laboratory, and even sedimentological changes like erosion and deposition in the two years between the profiling and the core sampling. Despite these factors, each of which could potentially result in a mismatch on a scale of orders of magnitude, the interpolated susceptibility is in a realistic range.

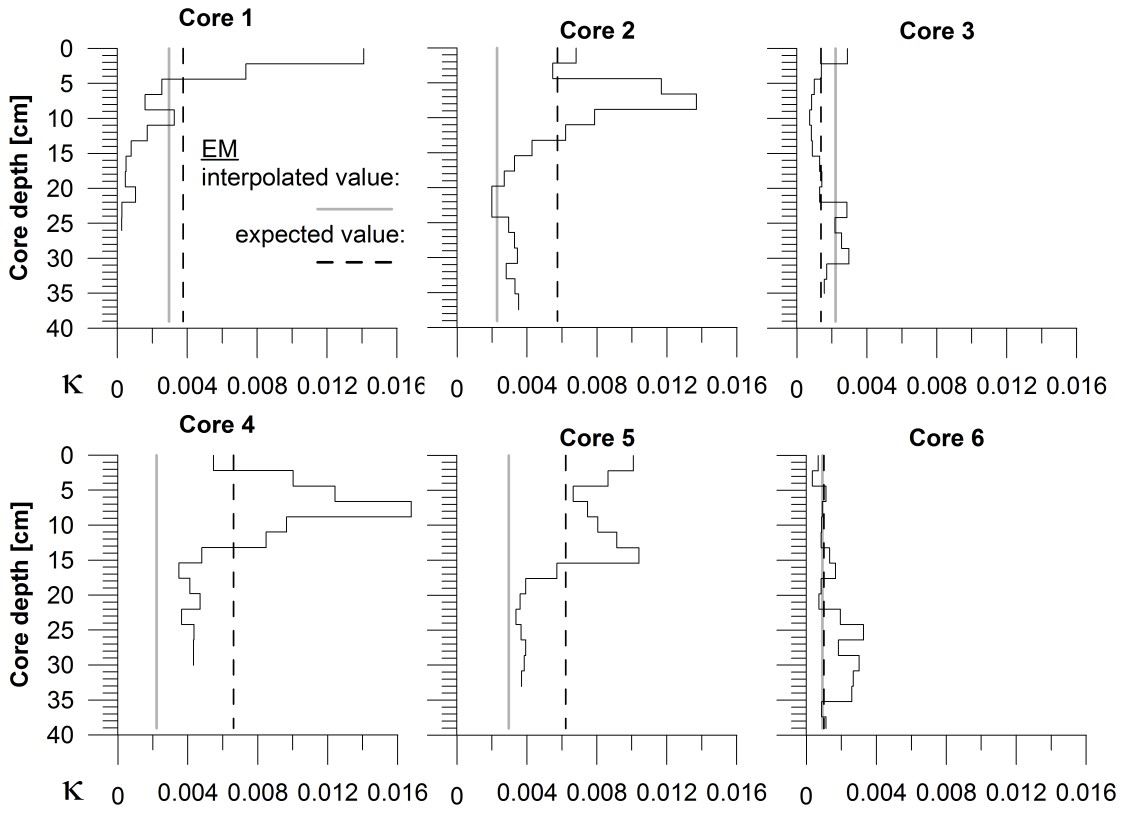

Figure 3.9: Susceptibility of sediment cores collected from 10 m water depth offshore Matakana Island, compared with the expected depth-integrated value and the corresponding interpolated value based on EM measurements.

Lithofacies-specific correlation of EM parameters

Crossplots of susceptibility and conductivity for all lithofacies (Fig. 3.10) reveal no distinct facies-specific correlation. These facies differ mainly in grain size, mineralogically they are dominated by quartz, feldspar and occasionally car-

bonates (Kulgemeyer et al., 2016). To better visualize the processes involved, susceptibility isolines were drawn using the equation (Müller et al., 2011):

$$\kappa_S = \kappa_M(1 - \frac{\sigma_S}{\sigma_W})^{1/m} \tag{3.3}$$

where κ_S is the susceptibility of the seafloor, κ_M the susceptibility of the pure matrix, σ_S the conductivity of the seafloor, σ_W the conductivity of pore water and m the cementation factor. σ_W is held constant at 4.3 S/m, and likewise m at a value of 1.6. According to this equation, sediment susceptibility with κ_M would follow a hyperbolic curve with increasing pore water conductivity, resp. porosity. The three hyperbolae shown correspond to sediments with κ_M = 0.004, 0.008 and 0.012. Most measured data follows these lines, but the highest susceptibilities always go along with low porosity. This is most prominent in lithofacies 2b, 4 and 6. While the distribution within lithofacies 2a and 3a is broader, the maximum susceptibility (mostly small isolated areas) is still related to low porosity values. This indicates that low-grade susceptibility changes indeed partly result from magnetic mineral enrichment by sorting processes, which affects both susceptibility and porosity. Alternative interpretations, like a change of sediment susceptibility primarily controlled by source rock composition, or by post-depositional diagenetic processes, would have little to no effect on porosity.

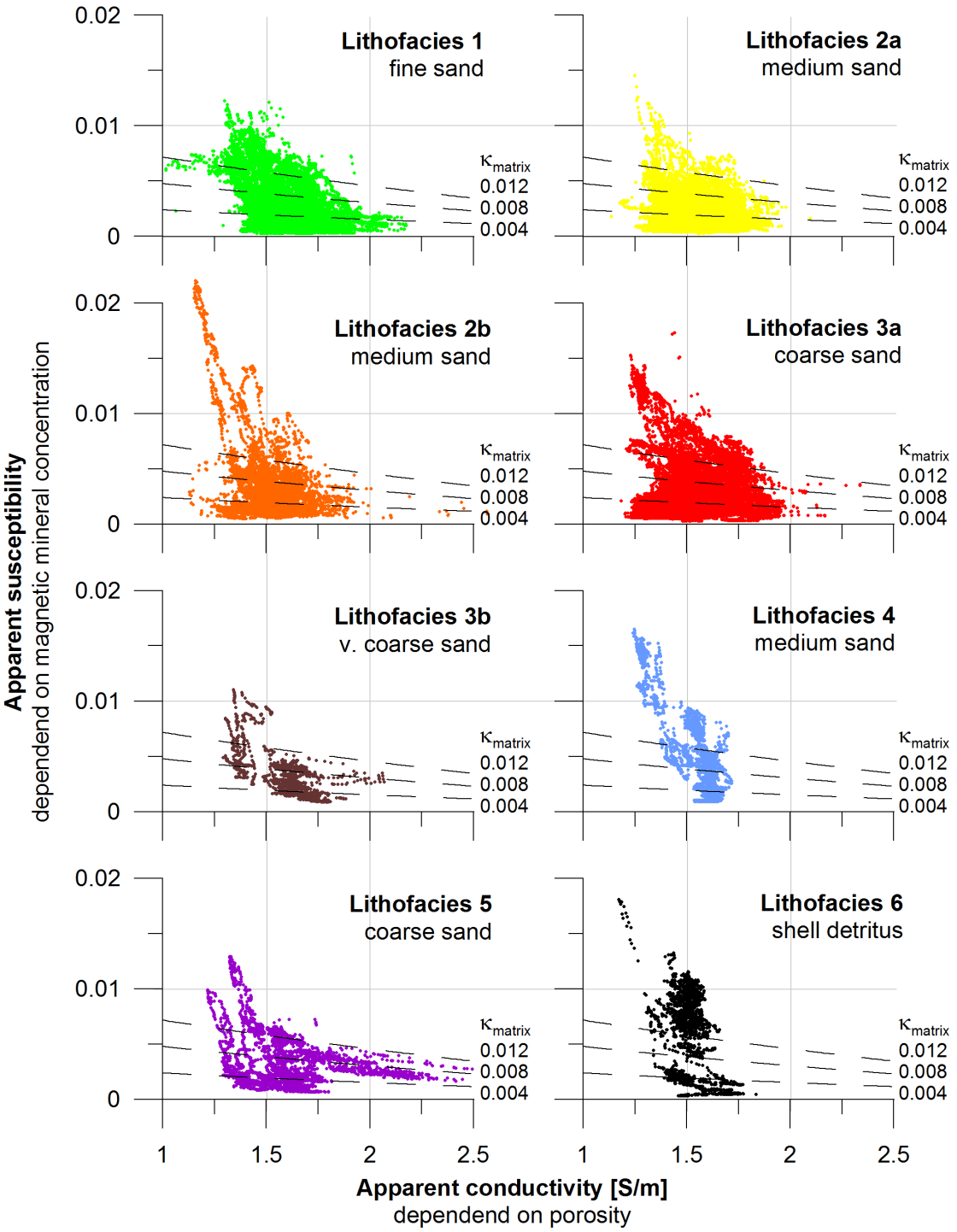

Figure 3.10: Crossplots of susceptibility vs. conductivity for every lithofacies identified by Kulgemeyer et al. (2016). Isolines show the change of susceptibility for three different theoretical sediment compositions with increasing porosity according to equation 3.3. Increasing porosity shifts data points along these lines to the right, while enrichment of magnetic minerals shifts data upwards.

Petromagnetic analysis of enrichments

For an insight into the grain size distribution of the magnetic fraction within a lithofacies, a modified Day plot (Day et al., 1977) has been prepared (Fig. 3.11 a). The plot shows the ratio of remanent magnetization M_{rs} to saturation magnetization M_s in relation to the ratio of the coercivity of remanence H_{cr} to the coercive force H_c. Instead of H_{cr} this modified plot uses the "median remanent hysteretic magnetization" H_{rh} by von Dobeneck (1996), which approximates H_{cr} with an accuracy of ca. 5 mT from hysteresis parameters alone without the need of a separate backfield measurement. According to this, the magnetic grain size is related to the physical grain size of the respective lithofacies.

Fig. 3.11 b shows the ratio of ferrimagnetic (χ_{ferri}) to paramagnetic (χ_{para}) susceptibility components compared to the total mass-specific susceptibility χ. As iron-bearing silicate minerals (other than iron oxides) are among the most strongly paramagnetic natural minerals (Hunt et al., 1995), this parameter can be used as an indicator for the content of iron not bound by iron oxides. The data shows that, across all lithofacies, a higher susceptibility directly results from a higher iron oxide concentration. If the χ_{ferri}/χ_{para} ratio was predetermined by source material, a facies-specific, more or less constant, factor would be expected. This is clearly not the case. This again indicates that these high concentrations are likely the result of an enrichment process based on the hydrodynamic properties (grain size and density) of the respective fractions. Furthermore, an especially low total susceptibility could be a result of iron oxide depletion, while the total iron content in a sample remains relatively stable. This could be caused by diagenetic processes, in anoxic conditions magnetite is dissolved an the available iron can be bound in newly formed iron sulfides (Rowan et al., 2009). Known anoxic environments in the area exist e.g. within Tauranga Harbour in places where mangrove forests have been mulched (Pratt et al., 2013).

The data in Fig. 3.11 c shows how the concentration of magnetic minerals related to the magnetic grain sizes. The smallest grain sizes are found in sediment with a very low concentration. There also appears to be a trend for the largest magnetic

grain sizes to occur in relatively low concentrations. The highest concentrations are connected to grain slightly smaller than the limit for multidomain magnetite. Interestingly, the most effective enrichment for all lithofacies is achieved with similar magnetic grain sizes.

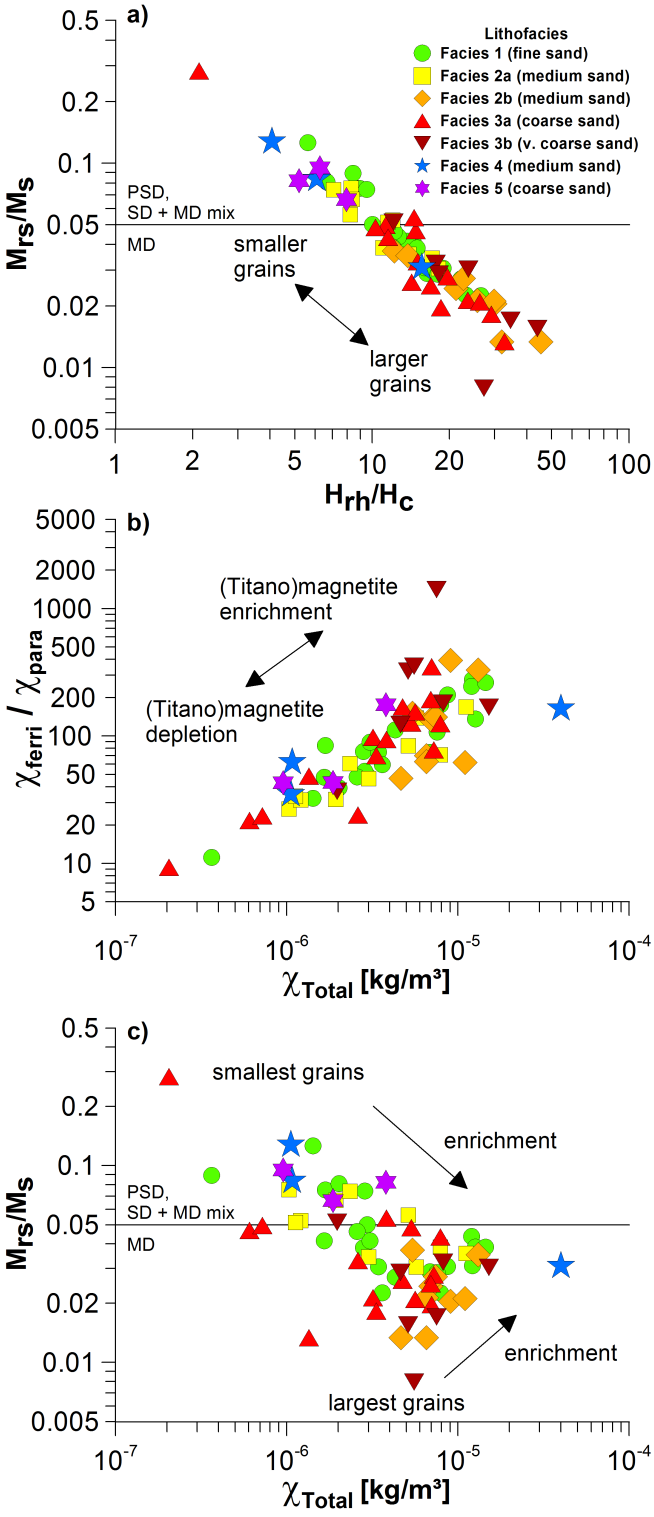

Figure 3.11: a) modified Day plot showing the magnetic grain sizes (domain states) for surficial samples of all lithofacies (SD = single-domain, PSD = pseudo-single-domain, MD = multidomain grains). b) ratio of ferrimagnetic to paramagnetic mass-specific susceptibility χ (indicative of magnetite to total iron content) in relation to total χ. c) magnetic grain size in relation total mass-specific susceptibility.

Petromagnetic mineralogy

So far, the results have shown where enrichment of magnetic minerals occurs, but the minerals that are contributing to the measured sediment susceptibility have yet to be characterized.

Based on IRM the acquisition curves (Fig. 3.12 a), three mineralogical groups can be distinguished, which also show similar thermal demagnetization curves (Fig. 3.12 b-d). The main difference between these groups is the contribution of the soft magnetic fraction ($B_{cr} < 40$mT). Samples 6, 7, 11, 12, 44 and 57 belong to the group with a large soft magnetic fraction, samples 13, 15, 23, 28 and 58 have a medium soft magnetic fraction and sample 1 a small one.

In all groups, magnetization is lost at the same temperature steps: the soft magnetic fraction demagnetizes between 150 and 220, at 300 and around 580 °C, which is interpreted as two different titanomagnetites with Ti mole fraction of x=0.6 (TM60) and x=0.4 (TM40), and a very low Ti titanomagnetite or magnetite. The intermediate fraction demagnetizes at 300 and 580 °C, these should be the same minerals with a smaller grain size. The hard magnetic fraction demagnetizes around 580 and 680 °C. The latter temperature is indicative of hematite, but a contribution of magnetite to this fraction is unusual. The reason might be partly oxidized grains, either as lamellae or surficial oxidization. Partial oxidization of magnetite to maghemite and hematite might also explain the difference between the three groups: the larger the soft magnetic fraction, the fewer oxidized magnetite crystals are present.

For a basic understanding of the rest of the FeTi-oxides in the region, existing low temperature SIRM measurements from three additional samples (Waihi Beach, Tanners Point in the northern basin of Tauranga Harbour, and the south-eastern cost of Matakana Island in the southern basin) are included (Fig. 3.12 e-g). These samples were magnetically enriched prior to the measurement. After magnetic saturation at room temperature (RT-SIRM), these samples were cooled down to a temperature of 5 K, while the remanent magnetization was continuously measured. They all show a loss in magnetization around -66 °C, which is interpreted as the Curie temperature of titanohematite with Ti-

mole fraction of x=0.8 (Nagata, 1961). Paramagnetic at room temperature, the mineral becomes ferrimagnetic below this temperature. The magnetic moments are magnetostatically aligned anti-parallel to the remanent magnetization of surrounding (titano)magnetite, thus reducing the total magnetization (Garming et al., 2007). The Waihi Beach and Tanners Point samples show an increase of SIRM after this point, with a maximum around -230 °C. This effect does not have an obvious explanation. We suggest another titanohematite phase with x=0.92: upon cooling, the mineral changes from a paramagnetic to a superparamagnetic state at -97 °C, aligns its magnetic domains to surrounding remanent fields and increases the global magnetization of the sample. At -230 °C, it changes its magnetic order again to an antiferromagnetic state and at -240 °Cto a spin glass structure were the magnetic moments are randomly oriented, causing a decrease in total magnetization (Burton et al., 2008).

An alternative interpretation could be a grain size related effect (Day et al., 1977). However, the presence of paramagnetic iron oxide phases in the magnetic extract used for the low temperature measurements supports the hypothesis of partial oxidation, and a correlation between either magnetic grain size or lithofacies to the magnetic mineralogy has not been observed. A better predictor for the magnetic mineralogy across all lithofacies is the geographic location: The sample with the small soft magnetic fraction is located at the northern entrance to Tauranga Harbour, while the ”medium” group is mostly found in the center of the study area (Fig. 3.12 h). While the differences in magnetic mineral concentrations within a lithofacies are evidently a result of sorting instead of source rock composition, this might well be different for the magnetic mineralogy. Potential source rocks include e.g. formations in the TVZ, Kaimai Range, Papamoa Range, Mt. Maunganui, Okurei Point, and Motiti Island. All of these sources contain andesitic to rhyolithic material (Leonard et al., 2010), which must have entered the western BoP system at various point in time. While the basic composition is similar and forms otherwise indistinguishable lithofacies, subtle differences in the accessory minerals can be preserved. However, more measurements, especially electron microscopy, would be required to determine if partial oxidation is actually

causing the observed behavior, and to determine the provenance of sediments additional samples from potential source material needs to be included. This is beyond the scope of this paper.

3.6.2 Formation of magnetic mineral enrichments

All available evidence indicates that the hypothesis of high magnetic mineral concentration being caused by grain sorting is applicable to all lithofacies in the study area. Next, the sorting process needs to be conceptualized.

Implications of EM parameter combinations for grain sorting

Before any attempt at an interpretation of enrichment formation mechanisms can be made, the implications of different combinations of susceptibility and conductivity should be discussed. Different combinations of high or low magnetomineral content and porosity do not appear to be useful for identifying the lithofacies described earlier by Kulgemeyer et al. (2016) in the BoP. Instead, they appear to be more useful for recognizing sorting mechanisms in specific environments in modern and relic sediments. There are four basic cases:

- Case 1: The combination of a **high** magnetic mineral concentration and a **low** porosity suggests sorting by the selective entrainment of a larger grain size, while finer particles (including heavy minerals) remain. Porosity remains low, whether these particles simply fit well into the pore space of the coarser matrix, or they are buried and can thus quickly enter the pore space. This fits to results from laboratory experiments by Li & Komar (1992), which demonstrated how the intermediate fraction of a sediment was the most easily entrained.

- Case 2: The combination of **high** concentration of magnetic minerals coupled with a **high** porosity either requires a mechanism that primarily sorts out most of the fine light minerals, or indicates a frequent remobilization of an already enriched bed.

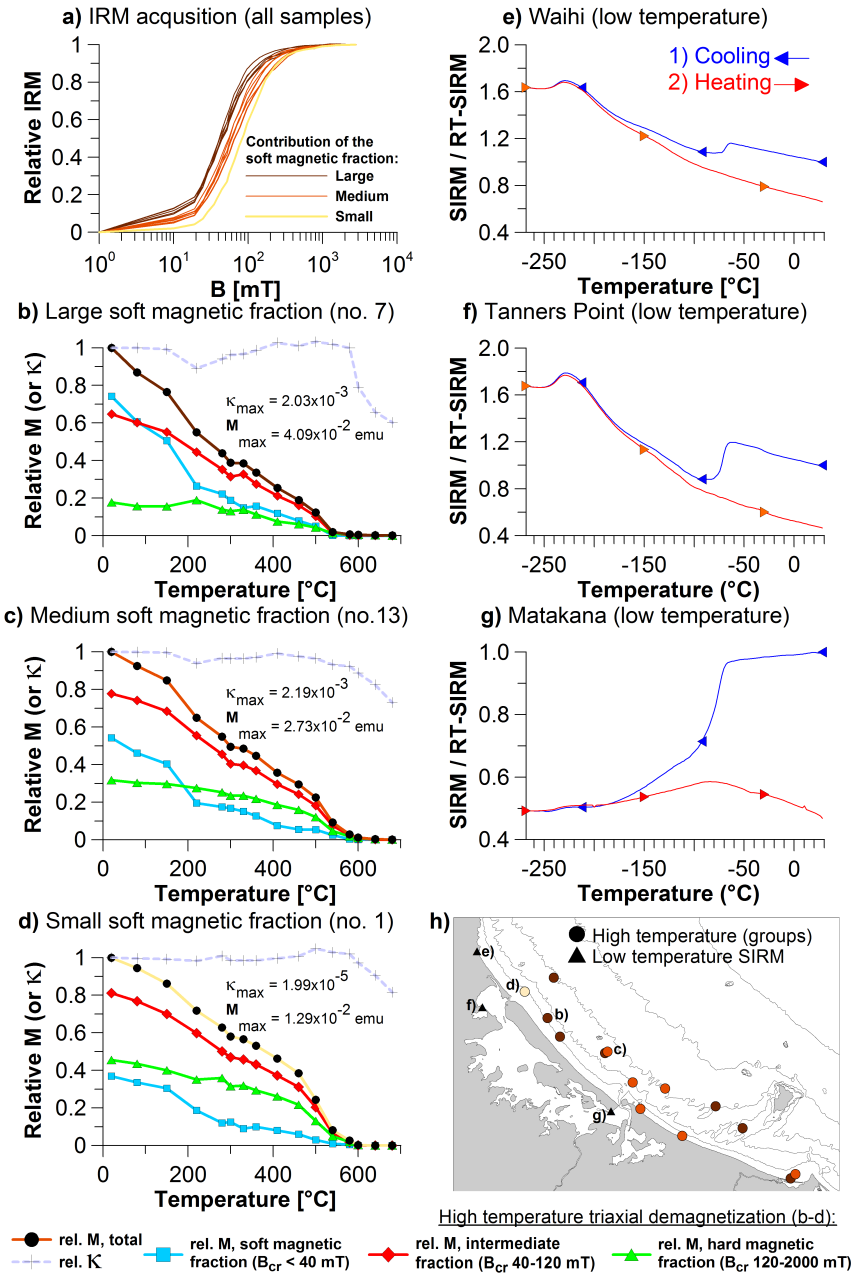

Figure 3.12: a) isothermal remanent magnetization (IRM) acquisition of all samples. Three groups are apparent, by comparison to thermal demagnetization curves these can be linked to the contribution of the soft magnetic within a sample. b-d) thermal demagnetization curves of selected samples from each of the three groups; the curves show the relative magnetization M of soft, intermediate and hard magnetic fractions, the total magnetization and volume susceptibility κ after each heating step. e-g) SIRM to room-temperature SIRM during cooling and heating of related samples. h) locations of thermal demagnetization groups and related samples.

- Case 3: Several scenarios can lead to a **low** concentration of titanomagnetite with a **high** porosity: heavy minerals have either been sorted out

along with the rest of the fine fraction, or a recently deposited sediment has not yet been subjected to enrichment processes, or the initial titanomagnetite concentration was too low for an effective enrichment.

- Case 4: Regions with **low** magnetic mineral concentration and **low** porosity do not appear to have experienced any sorting. This could be due to energetical conditions, or because sediment supply balanced out non-magnetic grains that were transported away.

Evidence for cross-shore and lonsghore grain sorting

Numerous studies, like the aforementioned Slingerland (1977); Komar & Wang (1984); Li & Komar (1992); Hamilton & Collins (1998); Tomkins et al. (2003), ascribe a large influence on heavy mineral enrichment to the effect of grain size selective entrainment. It mostly depends on the bed shear stress created by wave action, which is a function of water depth (Soulsby, 1997) and is thus much more variable in cross-shore than longshore direction. For a first test, samples of fine and coarse sand (d_{50} of 160 and 630 µm) were sieved and the susceptibility of the sieve fractions was measured to determine the typical size of magnetic particles (63 and 200 µm). A comparison of critical shear stresses of these fractions (Soulsby, 1997) to the bed shear stress produced by the average BoP wave climate given by Gorman et al. (2003) (wave height 0.86 m, period 5.75 s) shows that in fine sand quartz should be mobilized around 17 m water depth while magnetite remains immobile until a depth of 8 m. For coarse sand, the critical depths are 15 and 7 m, this sediment is mostly found below 20 m it should not undergo sorting under modern conditions.

The observed SE-NW susceptibility gradient of the seafloor points in direction of net the sediment transport driven by storm induced geostrophic currents (Kulgemeyer et al., 2016). Apparently some form of sorting occurs during this process. This is likely a result of the diffusive transport of sediment, and is commonly observed in enrichments spreading out from a point source both in natural environments (Li & Komar, 1992; Hamilton & Collins, 1998; Gallaway et al., 2012) and experiments (Li & Komar, 1992). Mechanisms at work can be the

selective entrainment of grains by size and density, but also differential transport of bedload and suspended material.

Longshore transport is controlling the distribution of sediment, for recently deposited sediments it can be assumed that points in proximity to sources have a higher magnetomineral concentration. However, susceptibility in the study area is much more variable over relatively short distances cross-shore than it is longshore. This and the clearly defined boundaries of this coast-parallel enrichment in 5-15 m water depth indicate that longshore sorting is less important to the degree of enrichment.

Interpretation of enrichment structures

Three distinct structures with high concentration of magnetic minerals can be distinguished based on susceptibility, conductivity and the lithofacies defined by Kulgemeyer et al. (2016) (Fig. 3.13):

Structure A: Coast-parallel fine sand enrichment, low porosity. This structure extends through almost the entire study area along the 10 m isoline (Fig. 3.13). While the southeastern area is relatively shallow and has a very flat gradient, for the most part the longshore enrichments coincide with slope breaks, and the structure is confined between depths of 5-15 m. Data from Badesab et al. (2012) suggests that the greatest degree of titanomagnetite enrichment in the structure occurs in more poorly sorted samples with a larger than usual amount of medium sand. The likely enrichment mechanism is turbulence generated by shoaling waves that selectively entrains of light fine sand particles, while smaller heavy minerals remain as lag (case 1). The low porosity can be a result of the particular mixture left behind by entrainment sorting (Fig. 3.14 a).

This structure is interrupted by the ebb-tidal delta between Mt. Maunganui and Tauranga Entrance. One factor that will affect the enrichment is the increased competence of the flow due to the tidal currents over the delta and particularly in the channel. Another is the presence of some small islands, which could focus approaching waves, whose increased energy could be sufficient to entrain heavy minerals. Structure A includes mostly late Holocene fine sand (lithofacies

1), but also covers some erosive environments such as the sorted bedforms offshore from Omanu Beach. The SE-NW decreasing concentration gradient suggests that the Kaituna River and Tauranga Entrance were the main sources of magnetic minerals in the past (nowadays, sediments are circulated in and out of Tauranga Entrance by tidal currents (Davies-Colley & Healy, 1978a,b; Spiers et al., 2009). Close to these sources, a large volume of sediment can be sorted for a relatively long time under average wave conditions. Most of the time, the light minerals entrained by wave action are transported in SE direction. When strong onshore winds induce a NW geostrophic current, light minerals are transported longshore. Where they settle, they bury the previous enrichment, as observed in sediment cores (Fig. 3.9). More severe storms will enable the transport of the bulk sediment without further sorting, thereby contributing to the spreading of the enrichment in NW direction. After redeposition, active enrichment will continue during fair weather conditions.

Structure B: Coarse sand enrichment, high porosity. This enrichment structure consists of the coarse sand (lithofacies 3a) between Motiti Island and Mt. Maunganui, which includes: the coast parallel enrichment below 30 m; the (apparent) cross-shore enrichment offshore Omanu Beach, where the underlying sediment is exposed inside sorted bedforms; and the sorted bedforms between profile -6 and -7, where enriched sample material was collected (Fig. 3.13). Very coarse sand (lithofacies 3b) is not necessarily enriched. During fair weather, the sediment of this structure is not transported. The sorting mechanisms that keeps the bedforms free from fine sand is based on turbulence that prevents the settling of fine sand in the first place (Murray & Thieler, 2004; Coco et al., 2007); but this does not sort separate particles within the coarse sand bed. Storm wave and induced currents transport sediment to the northwest (see Fig. 3.2), but these are short-term, highly energetic events that affect the entire coastline. It is highly questionable if these are the means to initiate a delicate process like grain sorting and does not explain the enrichment in greater water depths, where no sorted bedforms have been observed.

Rather, it is more likely that these enrichments are a facies-specific relic related to

the reworking of Pleistocene sand during the Holocene transgression. What sets this area apart from other, non-enriched deposits of the same lithofacies is the proximity to Motiti Island. Before the stabilization of the sea level to the modern elevation, Motiti Island (including the submarine ridge) would have formed a peninsula which was cutting off this area from longshore sediment transport. Without much supply of sediment to replaces transported quartz, a wide-spread enrichment formed; at the same time, transport of non-magnetic material to the northwest may have prevented enrichment further up the coastline. The basic sorting mechanism probably was similar to the process forming recent fine sand deposits (shallow water process in Fig. 3.14 b).

Structure C: Coarse sand enrichment, high porosity. This very small structure (Fig. 3.13) only contains the deepest observed enrichment (30-35 m water depth on profile -6). Thus it is likely the oldest of the observed structures and is an advanced form of structure B. Due to the rising sea level, sorting took place under varying energy regimes that over time have affected a wide range of grain sizes. After a sufficient amount of larger grains have been removed, previously shielded small grains can be entrained even as the bed shear stress decreases with increasing water depth. Very large grains remain along with small heavy minerals in a loosely packed grain structure. As a result this relic structure has a relatively high porosity. While sorting started out as the process defined as case 1, by removing a large part of the former median grain size and providing the opportunity to entrain a wider range of grain sizes it has over time shifted to case 2 (deep water process in Fig. 3.14 b).

3.7 Conclusions

The use of benthic electromagnetic profiling has revealed the distribution of ferrimagnetic minerals and the apparent porosity of sediments in the study area with great detail. Both are the result of sediment sorting that occurs within established lithofacies (ranging from fine to very coarse sand) and would have been very difficult to detect with other methods. Along with complementing

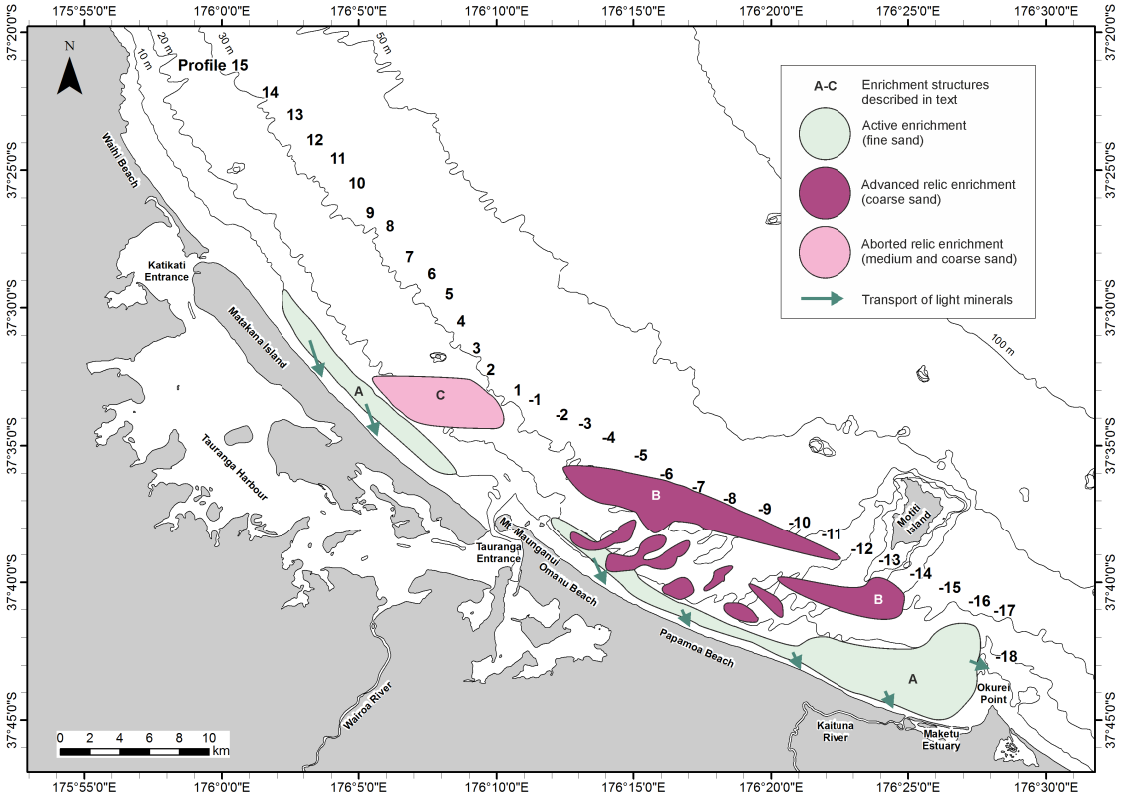

Figure 3.13: Titanomagnetite enrichment structures interpreted as lag deposits with high or low porosity, and inferred transport paths of light minerals that contributes to the enrichment.

sedimentological and environmental magnetic evidence, the use of benthic EM profiling allows a more detailed understanding of the processes at work and is a clear benefit to the research of heterogeneous and highly dynamic coastal systems.

Laboratory analyses indicate a suite of FeTi-oxides in the sediment ranging from magnetite to TM40 and TM60, likely with corresponding titanomaghemites, and from hematite to TH80 and TH92. Ferrimagnetic minerals are preferentially enriched both compared to the diamagnetic quartz-feldspar matrix, and to paramagnetic minerals. Enrichment is most effective in a similar grain size range for all lithofacies. These result strongly suggest sorting based on grain size and mineral density.

The EM profiling method provides insights into the depositional history of an area from the degree and variability of porosity. In the study area, recently deposited sediments in ebb tidal deltas have a characteristic high porosity and

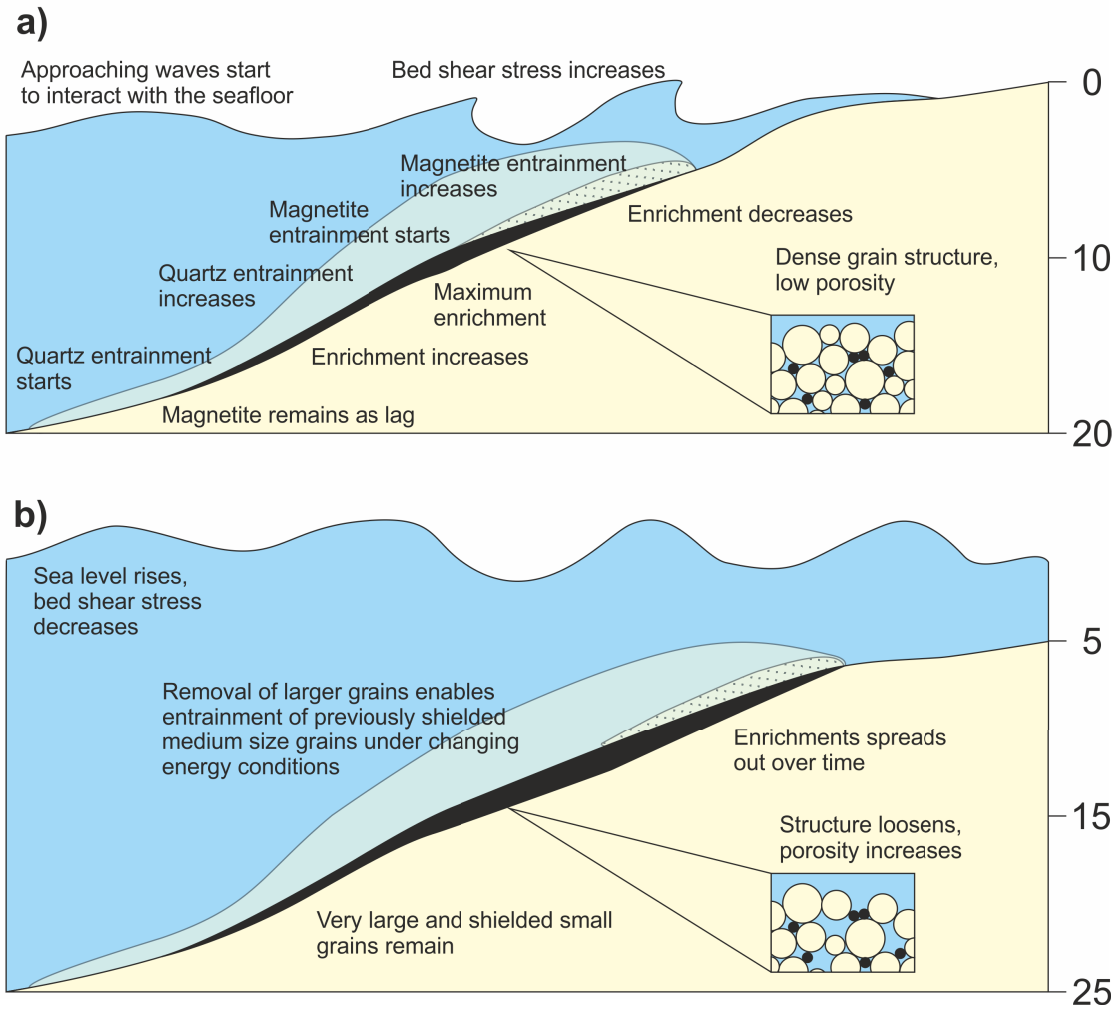

Figure 3.14: Conceptual model of coast-parallel magnetite enrichment formation producing the observed structures.

(depending on the source material) low to very low magnetomineral content. If sorting has taken place, it is constrained to the upcurrent side of elevations on the seafloor like sandbars. Effective sorting of light and heavy minerals takes place outside the ebb tidal deltas, were waves can work the seafloor without the regular interruption by tidal currents and freshly supplied sediment. Here, the highest concentrations are often found on or very close to slope breaks. On a smaller scale, ripple crests are prone to titanomagnetite accumulation.

Three main structures of titanomagnetite enrichments were distinguished in the western BoP and formation mechanisms proposed. One of these structures was first described in 10 m depth offshore Matakana Island as ”inner magnetite enrichment belt” by Badesab et al. (2012). It is confined to late Holocene fine

sand and stretches coast-parallel between the Maketu Estuary and the northern end of Matakana Island. The ”outer belt” they also proposed consists partly as a segment of a cross-shore oriented enrichment northwest of Tauranga Entrance, and several unconnected patches of local enrichments further up the coastline. The third structure is an enriched coarse sand offshore from Omanu and Papamoa Beach. At depths less than 30 m it is largely covered by fine sand, but is exposed in sorted bedforms.

Enrichments in older lithofacies tend to have an increased average porosity relative to younger deposits. The likely explanation is that the due to the rising sea level during the Holocene, these sediments have been subjected to varying energy regimes that favored the sorting of different grain sizes. In younger sediment that was deposited after sea level stabilization this process is still going on, and the available evidence indicates selective entrainment being the most likely sorting mechanism.

3.8 Acknowledgments

We thank Dirk Immenga, Chris Morcom, Chris Eager and Brice Blossier for their guidance and assistance in the sampling campaign and Christian Hilgenfeldt and Benjamin Baasch for their participation in the 2012 *NERIDIS* survey. That survey took place using the Western Workboats vessel *MACY GRAY* with great support by Henry Wolfenden and Sean Kelly. At the University of Bremen, we thank Thomas Frederichs and Liane Brück for their guidance in the implementation and interpretation of various magnetic laboratory techniques, and Konstantin Reeck for the processing of diverse datasets. The deployment of *NERIDIS* was financed by the *RENA* Long Term Environmental Recovery Monitoring Program. This study is a project of the collaborative graduate school INTERCOAST of the Universities of Bremen and Waikato, with financing provided by the German Research Foundation (Deutsche Forschungsgesellschaft, DFG). Data will be made available on www.pangaea.de.

Bibliography

Archie, G.E. (1942): The electrical resistivity log as an aid in determining some reservoir characteristics – Journal of Petroleum Technology, Vol. 5, pp. 1-8.

Baasch, B., Müller, H., Oberle, F.K.J., von Dobeneck, T. (2015): Inversion of marine multifrequency electromagnetic profiling data: a new approach to resolve surficial sediment stratification – Geophysical Journal International, Vol. 200, pp. 439-451.

Badesab, F., von Dobeneck T., Bryan, K.R., Müller, H., Briggs, R.M., Frederichs, T., Kwoll, E. (2012): Formation of magnetite-enriched zones in and offshore of a mesotidal estuarine lagoon: An environmental magnetic study of Tauranga Harbour and Bay of Plenty, New Zealand – Geochemistry, Geophysics, Geosystems, Vol. 13, Q06012, doi:10.1029/2012GC004125.

Bradshaw, B.E., Healy, T.R., Dell, P.M., Bolstad, W.M. (1991): Inner shelf dynamics on a storm-dominated coast, East Coromandel, New Zealand – Journal of Coastal Research, Vol. 7, No. 1, pp. 11-30.

Bradshaw, B.E., Healy, T.R., Campbell, S.N., Dell, P.M., de Lange, W.P. (1994): Holocene sediment lithofacies and dispersal systems on a storm-dominated, back-arc shelf margin: the east Coromandel coast, New Zealand – Marine Geology, Vol. 119, pp. 75-98.

Briggs, R.M., Houghton, B.F., McWilliams, M., Wilson, C.J.N. (2005): $^{40}\mathrm{Ar}/^{39}\mathrm{Ar}$ ages of silicic volcanic rocks in the Tauranga-Kaimai area, New Zealand: dating the transition between volcanism in the Coromandel Arc and the Taupo Volcanic Zone – New Zealand Journal of Geology and Geophysics, Vol. 48, pp. 459-469.

Bryan, K.R., Robinson, A., Briggs, R.M. (2007): Spatial and temporal variability of titanomagnetite placer deposits on a predominantly black sand beach – Marine Geology, Vol. 236, pp. 45-59.

Burton, J.H ., Healy, T.R. (1985): Tidal Hydraulics and Stability of the Maketu Inlet, Bay of Plenty – in: 1985 Australasian Conference on Coastal and Ocean Engineering. Barton, A.C.T.: Institution of Engineers, Australia, 1985, pp. 697-702.

Burton, J.P., Fralick, P. (2003): Depositional Placer Accumulations in Coarse-Grained Alluvial Braided River Systems – Economic Geology, Vol. 98, pp. 985-1001.

Burton, B.P., Robinson, P., McEnroe, S.A., Boffa-Balaran, T. (2008): A Low-temperature phase diagram for ilmenite-rich compositions in the system Fe_2O_3-$FeTiO_3$ – American Mineralogist, Vol. 93, pp. 1260-1272, doi:10.2138/am.2008.2690.

Chave, A.D., Cox, C.S. (1982): Controlled Electromagnetic Sources for Measuring Electrical Conductivity Beneath the Oceans 1. Forward Problem and Model Study – Journal of Geophysical Research, Vol. 87, No. B7, pp. 5327-5338.

Cheesman, S.J., Edwards, R.N., Law, L.K. (1990): A test of a short-baseline sea-floor transient electromagnetic system – Geophysical Journal International, Vol. 103, pp. 431-437.

Coco, G., Murray, A.B., Green, M.O. (2007): Sorted bed forms as self-organized patterns: 1. Model development – Journal of Geophysical Research, Vol. 112, F03015, doi:10.1029/2006JF000665.

Corbett, I., Burrell, B. (2001): The earliest Pleistocene(?) Orange River fan-delta: an example of succesful exploration delivery aided by applied Quaternary research in diamond placer sedimentology and plaeontology – Quaternary International, Vol. 82, pp. 63-73.

De Lange, W.P. (1988): Wave Climate and Sediment Transport within Tauranga Harbour, in the Vicinity of the Pilot Bay – Ph.D. thesis, 189 pp. University of Waikato, Hamilton, New Zealand.

Davis, R.A., Healy, T.R. (1993): Holocene coastal depositional sequences on a tectonically active setting: southeastern Tauranga Harbour, New Zealand – Sedimentary Geology, Vol. 84, pp. 57-69.

Davies-Colley, R.J., Healy, T.R. (1978 a): Sediment and hydrodynamics of the Tauranga Entrance to Tauranga Harbour – New Zealand Journal of Marine and Freshwater Research, Vol. 12, No. 3, pp. 225-36.

Davies-Colley, R.J., Healy, T.R. (1978 b): Sediment transport near the Tauranga Entrance to Tauranga – New Zealand Journal of Marine and Freshwater Research, Vol. 12, No. 5, pp. 237-43.

Day, R., Fuller, M., Schmidt, V.A. (1977): Hysteresis properties of titanomagnetites: Grain size and compositional dependence – Physics of the Earth and Planetary Interiors, Vol. 13, pp. 260-267.

Duk-Rodkin, A., Barendregtb, R.W., Whitea, J.M., Singhrey, V.H. (2001): Geologic evolution of the Yukon River: implications for placer gold – Quaternary International, Vol. 82, pp. 5-31.

Edwards, N. (2005): Marine controlled source electromagnetics : Principles, methodologies, future commercial applications – Surveys in Geophysics, Vol. 26, pp. 675-700, doi 10.1007/s10712-005-1830-3.

Elsner, H. (1992): Granulometry and mineralogy of some northeastern Florida placers: a consequence of heavy mineral concentration in nearshore bars – Sedimentary Geology, Vol. 76, pp. 233-255.

Evans, R.L. (2001): Measuring the shallow porosity structure of sediments on the continental shelf: A comparison of an electromagnetic approach with cores and acoustic backscatter – Journal of Geophysical Research, Vol. 106, No. C11, pp. 27047-27060.

Evans, R.L. (2007): Using CSEM techniques to map the shallow section of seafloor: From the coastline to the edges of the continental slope – Geophysics, Vol. 72, No. 2, WA105-WA116, doi: 10.1190/1.2434798.

Foster, G.A., Healy, T.R., De Lange, W.P. (1994): Sediment budget and equilibrium for a moderate swell regime, ebb-tidal adjacent beach, Mt. Maunganui, New Zealand – Journal of Coastal Research, Vol. 10, No. 3, pp. 564-575.

Foster, G.A., Healy, T.R., De Lange, W.P. (1996): Presaging Beach Renourishment from a Nearshore Dredge Dump Mound, Mt. Maunganui Beach, New Zealand – Journal of Coastal Research, Vol. 12, No. 2, pp. 395-405.

Frihy, O.E. (1994): Discrimination of accreted and eroded coasts using heavy mineral compositions of the Nile Delta beach sands, Egypt – Sedimentology, Vol. 41, pp. 905-912.

Frihy, O.E., Komar, P.D. (1993): Long-term shoreline changes and the concentration of heavy minerals in beach sands of the Nile Delta, Egypt – Marine Geology, Vol. 115, pp. 253-262.

Gallaway, E., Trenhaile, A.S., Cioppa, M.T., Hatfield, R.G. (2012): Magnetic mineral transport and sorting in the swash-zone: northern Lake Erie, Canada – Sedimentology, Vol. 59, pp. 1718-1734.

Garming, J.F.L., von Dobeneck, T., Franke, C., Bleil, U. (2007): Low-temperature partial magnetic self-reversal in marine sediments by magnetostatic interaction of titanomagnetite and titanohematite intergrowths – Geophysical Journal International, Vol. 170, pp. 1067-1075.

George, N.J., Emah, J.B., Ekong, U.N. (2015): Geohydrodynamic properties of hydrogeological units in parts of Niger Delta, southern Nigeria – Journal of African Earth Sciences, Vol. 105, pp. 55-63.

Gorman, R.M., Bryan, K.R., Laing, A.K. (2003): Wave hindcast for the New Zealand region: Nearshore validation and coastal wave climate – New Zealand Journal of Marine and Freshwater Research, Vol. 37, No.3, pp. 567-588, doi: 10.1080/00288330.2003.9517190.

Hamilton, N.T.M., Collins, L.B. (2001): Placer Formation in a Holocene Barrier System, Southwestern Australia – Journal of Coastal Research, Vol. 14, No. 1, pp. 240-255.

Healy, T.R., Harms, C., De Lange, W.P. (1991): Dredge spoil and inner shelf investigations off Tauranga Harbour, Bay of Plenty, New Zealand – Coastal Sediments '91, ASCE Seattle, Washongton, pp. 2037-2051.

Healy, T.R., Cole, R., De Lange, W.P. (1996): Geomorphology and ecology of New Zealand shallow estuaries and shorelines – in: Nordstrom, K.F., Roman, C.T. [eds.] (1996): Estuarine Shores, Evolution, Environments and Human Alterations, Wiley & Sons, London, pp. 115-154.

Henry, M.A.C. (1991): The volcanic geology of Motiti Island. Unpublished M.Sc. thesis, lodged in the library of the University of Waikato, Hamilton, New Zealand.

Hicks, D.M., Hume, T.M. (1996): Morphology and Size of Ebb Tidal Deltas at Natural Inlets on Open-sea and Pocket-bay Coasts, North Island, New Zealand – Journal of Coastal Research, Vol. 12, No. 1, pp. 47-63.

Hicks, D.M., Hume, T.M. (1997): Determining Sand Volumes and Bathymetric Change on an Ebb-Tidal Delta – Journal of Coastal Research, Vol. 13, No. 2, pp. 407-416.

Hjulström, F. (1939): Transport of detritus by moving water recent marine sediments – in: Trask, P.D. [ed.](1939): Recent Marine Sediments: a symposium, Tulsa Oklakoma, American Association of Petroleum Geologists, New York, London, T. Murby & Co., Reprinted 1968 by Dover Publications p. 3-31.

Hughes, M.G., Keene, J.B., Joseph, R.G. (2000): Hydraulic sorting of heavy-mineral grains by swash on a medium-sand beach – Journal of Sedimentary Research, Vol. 70, No. 5, pp. 994-1004.

Hunt, C.P., Moskowitz, B.M., Banerjee, S.K. (1995): Magnetic properties of rocks and minerals – in: Ahrens, T.J. [ed.](1995): Rock Physics and Phase Relations. A Handbook of Physical Constants, American Geophysical Union, pp. 189-204.

Jackson, P., Smith, D.T., Stanford, P.N. (1978): Resistivity-porosity-particle shape relationships for marine sands – Geophysics, Vol. 43, No. b, pp. 1250-1268.

Jones, H.A., Davies, P.J. (1979): Preliminary studies of offshore placer deposits, eastern Australia – Marine Geology, Vol. 30, pp. 243-268.

Komar, P.D., Wang, C. (1984): Processes of selective grain transport and the formation of placers on beaches – Journal of Geology, Vol. 92, pp. 637-655.

Kulgemeyer, T., von Dobeneck, T., Bryan, K.R., Müller, H., de Lange, W., Battershill, C. (2016): Lithofacies distribution and sediment dynamics in the western Bay of Plenty (New Zealand) from combined photographic, acoustic and sedimentological methods – Marine Geology, Vol. 376, pp. 158-174, doi:10.1016/j.margeo.2016.03.005.

Leonard, B.S., Begg, J.G., Wilson, C.J.N. (compilers) (2010): Geology of the Rotorua Area – Institute of Geological and Nuclear Sciences 1:250000 geological map 5. 1 sheet + 102 p., GNS Science, Lower Hutt, New Zealand.

Li, M.Z., Komar, P.D. (1992 a): Longshore grain sorting and beach placer formation adjcanet to the Columbia River – Journal of Sedimentary Petrology, Vol. 62, No. 3, pp. 429-441.

Li, M.Z., Komar, P.D. (1992 b): Selective entrainment and transport of mixed size and density sands: Flume experiments simulating the formation of black-sand placers – Journal of Sedimentary Petrology, Vol. 62, No. 4, pp. 584-590.

Li, G., Yan, W., Zhong, L., Xia, Z., Wang, S. (2015): Provenance of heavy mineral deposits on the northwestern shelf of the South China Sea, evidence from single-mineral chemistry – Marine Geology, Vol. 263, pp. 112-124.

Lowrie, W.L. (1990): Identification of ferromagnetic minerals in a rock by coercivity and unblocking temperature – Geophysical Research Letters, Vol. 17, No. 2, pp. 159-162.

McDougall, J.C. (1961): Ironsand deposits offshore from the west coast, North Island, New Zealand – New Zealand Journal of Geology and Geophysics, Vol. 3, pp. 283-300.

Michels, K.H., Healy, T.R. (1999): Evaluation of an inner Shelf Site Off Tauranga Harbour, New Zealand, for Disposal of Muddy-Sandy Dredged Sediments – Journal of Coastal Research, Vol. 13, No. 3, pp. 830-838.

Müller, H., von Dobeneck, T., Nehmiz, W., Hamer, K. (2010): Near-surface electromagnetic, rock magnetic, and geochemical fingerprinting of submarine freshwater seepage at Eckernförde Bay (SW Baltic Sea) – Geo-Marine Letters, Vol. 31, No. 2, pp. 123-140, doi: 10.1007/s00367-010-0220-0.

Müller, H., von Dobeneck, T., Hilgenfeldt, C., SanFilipo, B., Rey, D., Rubio, B. (2012): Mapping the magnetic susceptibility and electric conductivity of marine surficial sediments by benthic EM profiling – Geophysics, Vol. 77, No. 1, pp. 1-14.

Murray, A.B., Thieler, E.R. (2004): A new hypothesis and exploratory model for the formation of large-scale inner-shelf sediment sorting and ”rippled scour depressions” – Continental Shelf Research, Vol. 24, pp. 295-315.

Nagata, T. (1961): Rock Magnetism, 2nd edn – Maruzen, Tokyo, 350 pp.

Orpin, A., Bostock, H., Nodder, S., Barnes, P., Lamarche, G. (2009): Resource evaluation, exploration and current prospecting interests of west coast ironsands, North Island, New Zealand – in: Coasts and Ports 2009: In a Dynamic Environment. Wellington, N.Z.: Engineers Australia 2009, pp. 98-104.

Park, S. (2004): Aspects of mangrove distribution and abundance in Tauranga Harbour. Environmental publication 2004/16. Whakatane, New Zealand, Environment Bay of Plenty. 40 p.

Peters, C., Dekkers, M.J. (2003): Selected room temperature magnetic parameters as a function of mineralogy, concentration and grain size – Physics and Chemistry of the Earth, Vol. 28, pp. 659-667.

Prakash, T.N. (2000): Sediment distribution and placer mineral enrichment in the inenr shelf of Quilon, SW coast of India – Indian Journal of Marine Sciences, Vol. 29, pp. 120-127.

Pratt, S.J., Lundquist, C.J., Nelson, W., Gemmill, C.E.C. (2013): A new record of Percursaria percursa (Ulvaceae, Ulvales) on the North Island, New Zealand – New Zealand Journal of Botany, Vol, 51, No. 1, pp. 71-74, DOI: 10.1080/0028825X.2012.728137.

Rogers, J.J.W., Head, W.B. (1961): Relationships between porosity, median size, and sorting coefficients of synthetic sands – Journal of Sedimentary Petrology, Vol. 31, No. 3, pp. 467-470.

Rowan, C.J., Roberts, A.P., Broadbent, T. (2009): Reductive diagenesis, magnetite dissolution, greigite growth and paleomagnetic smoothing in marine sediments: A new view – Earth and Planetary Science Letters, Vol. 277, pp. 223-235.

Sallenger, A.H. (1979): Inverse grading and hydraulic equivalence in grain flow deposits – Journal of Sedimentary Petrology, Vol. 49, pp. 553-562.

Shepherd, M.J., McFadgen, B.G., Betts, H.D., Sutton, D.G. (1997): Formation, landforms and palaeoenvironment of Matakana Island, Bay of Plenty, and implications for archaeology – Science and Research Series 102. Wellington, New Zealand. Department of Conservation. 100 p.

Slingerland, R. (1977): The effects of entrainment on the hydraulic equivalence relationships of light and heavy minerals in sands – Journal of Sedimentary Petrology, Vol. 47, No. 2, pp. 753-770.

Slingerland, R., Smith, N.D. (1986): Occurence and formation of water-laid placers – Annual Review of Earth and Planetary Sciences, Vol 14, pp. 113-47.

Soulsby, R. (1997): Dynamics of Marine Sand – Thomas Telford Publishing, London, 272 pp.

Spiers, K.C., Healy, T.R., Winter, C. (2009): Ebb-Jet Dynamics and Transient Eddy Formation at Tauranga Harbour: Implications for Entrance Channel Shoaling – Journal of Coastal Research, Vol. 50, No. 1, pp. 234-247.

Steidtmann, J.R. (1982): Size-density sorting of sand-size spheres during deposition from bedload transport and implications concerning hydraulic equivalence – Sedimentology, Vol. 29, pp. 877-883.

Tomkins, M.R., Nielsen, P., Hughes, M. (2003): Selective entrainment of sediment graded by size and density under waves – Journal of Sedimentary Research, Vol. 73, No. 6, pp. 906-911.

von Dobeneck, T. (1996): A systematic analysis of natural magnetic mineral assemblages based on modelling hysteresis loops with coercivity-related hyperbolic basis functions – Geophysical Journal International, Vol. 124, pp. 675-694.

Won, I.J., Keiswetter, D.A., Hanson, D.R., Novikova, E., Hall, T.M. (1997): GEM-3: A monostatic broadband electromagnetic induction sensor – Journal of Environmental and Engineering Geophysics, Vol. 2, No. 1, pp. 53-64.

Zhang, S., Cioppa, M., Zhang, S. (2010): Spatial Variations in Particle Size and Magnetite Concentration on Cedar Beach: Implications for Grain-Sorting Processes, Western Lake Erie, Canada – Acta Geologica Sinica (English Edition), Vol. 84, No. 6, pp. 1520-1532.

Chapter 4

Formation process of coast-parallel heavy mineral enrichments investigated by exploratory numerical modelling

Tobias Kulgemeyer[a], Karin Bryan[b]

[a]Faculty of Geosciences and MARUM - Center for Marine Environmental Sciences, University of Bremen, Klagenfurter Straße, 28359 Bremen, Germany

[b]School of Science, University of Waikato, Private Bag 3105, Hamilton, New Zealand

To be submitted

Abstract A numerical model is developed to investigate the formation process of coast-parallel magnetite enrichments in the western Bay of Plenty (New Zealand). The model is based on the work of Murray & Thieler (2004) and Coco et al. (2007 a) for differential transport of fractions in a graded bed with two different grain sizes. It has been modified for use on an inclined surface and takes the effect of differing grain densities into account. An updated set of equations is adopted which produces results comparable to field observations. Using the average hydrodynamic conditions of the study area as forcing conditions for the model, a coast-parallel structure develops from an initially homogeneous fine sand bed consisting of 160 µm quartz grains and 62 µm magnetite concentrated at a volume ratio of 0.001. Starting from the water depth in which wave- and current-induced bed shear stress first overcomes the critical shear stress of quartz

grains, magnetite concentrations increase coastwards until the critical shear stress of magnetite is surpassed. After this point, the concentration decreases. This highlights the role of selective entrainment as the dominant process initializing the formation of this type of structure. The degree of enrichment is further controlled by the differential transport rate of the quartz and magnetite fraction. Additional tests demonstrate the influence of variations in the hydrodynamic (wave height and period, current velocities) and geological conditions (grain size and density ratio, bed slope, initial concentration). Parameters that change the bed shear stress consequently shift the enrichment into deeper or shallower water depths. For an effective enrichment, sediment needs to be transported cross-shore. As bottom currents get stronger in shallower water, enrichment higher up the slope occurs more easily than in deep water with the same wave and current conditions. On more inclined beds, the greater spatial rate of increase in bed shear stress and transport rates likewise enables more effective enrichment. This model demonstrates the mechanisms for the formation of this type of structure, and should be able to predict the location of enrichment zones in other coastal environments for a variety of heavy mineral types.

4.1 Introduction

Heavy mineral enrichments, or placers, form under the influence of waves and currents in various environments between source and sink (Slingerland & Smith, 1986), such as rivers (Duk-Rodkin et al., 2001; Burton & Fralick, 2003), tidal channels (Badesab et al., 2012), deltas (Frihy & Komar, 1993; Corbett & Burrell, 2001), beaches (Komar & Wang, 1984; Bryan et al., 2007; Gallaway et al., 2012) and the inner shelf (Elsner, 1992; Hamilton & Collins, 1998). Accessory heavy minerals are often used as a proxy to research transport paths and mechanisms (May, 1973; Gallaway et al., 2012; Razik et al., 2013), sediment provenance (Li et al., 2015; Razik et al., 2015; Krippner et al., 2016; Pan et al., 2016) and regions of accretion and erosion (Frihy, 1994; Frihy et al., 1995; Zhang et al., 2010). Highly concentrated placers are of economic interest and provide a valuable source of of materials like titanium (Corbett & Burrell, 2001; Bryan et al., 2007;

Prakash, 2000), iron (McDougall, 1961; Orpin et al., 2009), uranium (Burton & Fralick, 2003), gold (Jones & Davies, 1979; Duk-Rodkin et al., 2001; Burton & Fralick, 2003) and diamonds (Corbett & Burrell, 2001). Potentially, enrichments of very fine heavy minerals can also have a stabilizing effect on the seafloor if they block the pore space of the matrix and decrease pore water inflow, as was demonstrated for silt by Bartzke et al. (2013) and Bartzke & Huhn (2015).

The formation of heavy mineral enrichments results from unique combinations of bathymetry, source rock, sediment supply and wave and current climate. Set apart from the bulk of rock-building minerals, such as quartz and feldspars, by their high density and often small grain size, heavy minerals possess different hydrodynamic properties that subjects them sorting processes during entrainment, transport, settling and burial (Komar & Wang, 1984; Slingerland & Smith, 1986). An important process is that of selective entrainment of different sizes grains (Slingerland, 1977; Slingerland & Smith, 1986; Komar & Wang, 1984; ReidFrostick, 1985; Li & Komar, 1992; Hamilton & Collins, 1998; Tomkins et al., 2003). In a graded sediment, smaller grains are sheltered in the pore space of the matrix, have a higher pivoting angle, are less exposed to shear stress and are therefore harder to entrain than in a unimodal bed. Likewise, the larger grains are more exposed and can be entrained more easily than in a bed with homogeneous grain sizes (Slingerland, 1977; Slingerland & Smith, 1986). Apart from selective entrainment, the combination of grain size, density, shape and resulting bed roughness leads to sorting during sediment transport by inducing differential transport rates of the respective sediment fractions (Slingerland & Smith, 1986; Steidtmann, 1982). Different settling velocities allow sorting during the deposition of suspended material (Rubey, 1933), while current-induced shear stress can initiate the burial of finer grains after deposition (Sallenger, 1979; Gallaway et al., 2012). Ultimately, all of these processes can have an influence on placer formation, although in variable degrees. Their interaction is complex and not yet fully understood (Hughes et al., 2000; Bryan et al., 2007), and the complexity of environmental conditions and sorting processes means that no single model for heavy mineral enrichment valid for every environment has yet

been developed.

The complexity of sediment transport in nature is reflected by the numerous different approaches used in numerical modelling of the phenomenon. Examples include approaches that aim for detailed simulations on a regional scale like Delft3D (Deltares Systems, 2014) and SEDTRANS (Li & Amos, 1995, 2001; Neumaier et al., 2008), models simulating the behavior of individual grains like Bartzke & Huhn (2015), or exploratory models that reduce the included variables to the simplest feasible representation of the system so that key processes can be determined without being buried in details (Murray, 2002, 2003). While more detailed models potentially yield better quantitative results, they can be risky as a large number of variables also increases the uncertainty in the calibration. Simpler models are more robust in that regard, and the reduced uncertainty of calibrated variables may even lead to more realistic results; a review on this issue is given e.g. by (Merritt et al., 2003).

In this study we use an exploratory model simulating the transport of two separate grain fraction to examine the processes responsible for the formation of coast parallel titanomagnetite enrichments. The boundary conditions are based on structures first observed by Badesab et al. (2012) in 5-15 m water depth on the inner shelf of the Bay of Plenty, New Zealand. Kulgemeyer et al. (2016 b) described these structures in detail and presented a conceptual model for their formation based on the selective entrainment of quartz grains, while titanomagnetite remains as a lag deposit. Its concentration within the seabed therefore increases until a certain water depth, when the bed shear stress applied to the seafloor is sufficient to overcome the critical shear stress of magnetite. Beyond this critical depth, it becomes entrained and the concentration within the seabed decreases coastwards.

Here, this conceptual model is tested using a numerical sediment transport model based on the work of Murray & Thieler (2004) and (Coco et al., 2007 a,b), and reference data from samples taken in the study area. This allows us to expand the original concept based solely on selective entrainment to include the effect of differential transport, to test the response of the model to varying

hydrodynamic conditions, estimate the relative time it takes to reach the observed enrichment and make predictions for differently-composed sediments in similar settings.

4.2 Study area

4.2.1 Geographic and geological setting

The study area is in the western part of the Bay of Plenty (BoP). Details to the sedimentology of the region are found in Kulgemeyer et al. (2016 a). This embayment on the North Island of New Zealand is sedimentologically characterized by late Holocene volcanoclastic fine sand deposited between the beach and 20-25 m water depth (facies 1 in Fig. 4.1), which is overlaying a transgressional series of medium to coarse sands (facies 2a-3b); additional facies are mixtures with sediment from local and biogenic sources (Kulgemeyer et al., 2016 a). Sediment transport frequently changes with weather conditions. In fair weather, the net transport (littoral drift) is directed towards the southwest. Evidence suggests that during storm conditions, a geostrophic current develops which transports sediments to the northwest (Bradshaw et al., 1991, 1994; Kulgemeyer et al., 2016 a). Important regional features are the Tauranga Harbour estuary, bound by the barrier island of Matakana which leaves two entrances on the northern (Katikati) and southern (Tauranga) end of the harbor. Offshore are Motiti Island and the small Karewa Island, both volcanic in origin (Briggs et al., 2005).

Titanomagnetite-enriched areas are present both in fine and coarse sand. Fine sand enrichments form a coast-parallel belt between 5-15 m water depth, while coarse sand enrichments are concentrated in the center of the study area between Tauranga Entrance and a submarine ridge connecting Motiti Island to the main land (Fig. 4.2). This coarse sand is mostly found below 25 m water depth, but is also exposed in sorted bedforms closer to the beach. The fine sand structures have been attributed to an active sorting process caused by selective entrainment (Badesab et al., 2012; Kulgemeyer et al., 2016 b). Enrichments in coarse sand are likely relics that formed by a similar process before or during

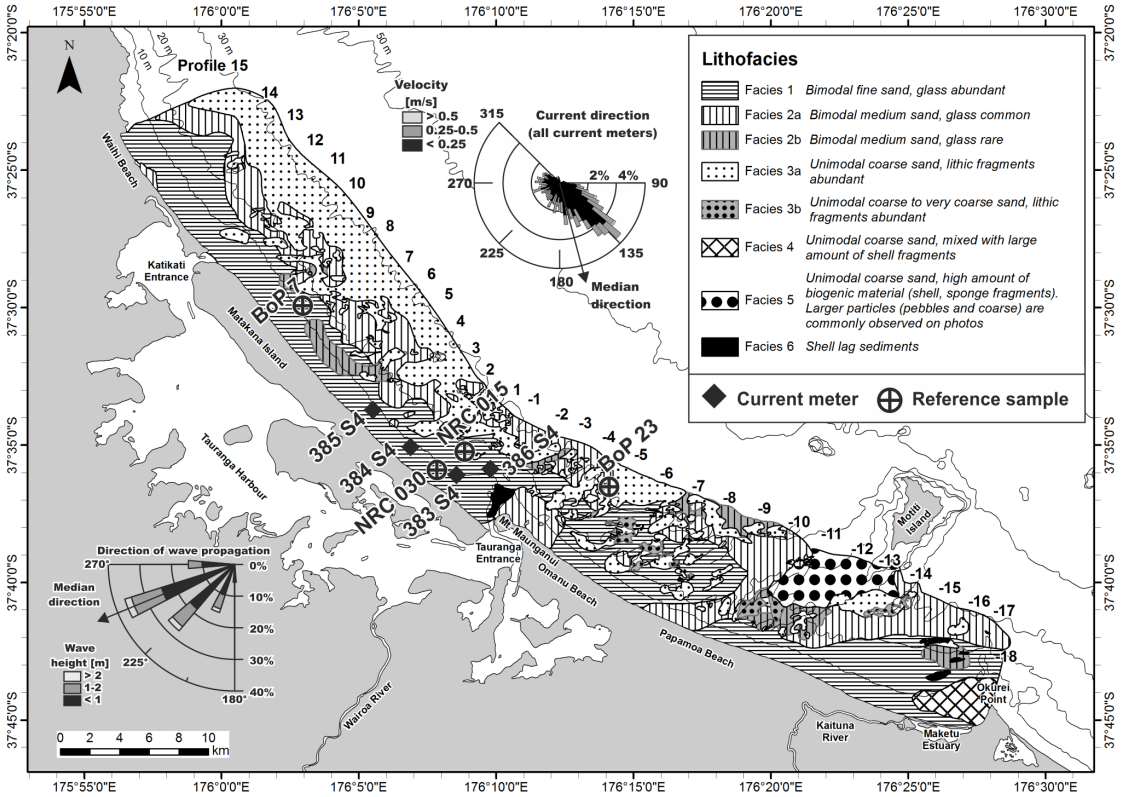

Figure 4.1: Study area in the Bay of Plenty with local lithofacies according to Kulgemeyer et al. (2016 a), wave climate of Gorman et al. (2003), current climate and location of reference samples.

the Holocene transgression, when the local medium and coarse sands were reworked from older Pleistocene deposits (Bradshaw et al., 1994; Kulgemeyer et al., 2016 b). Some of the enrichments in proximity to Motiti Island were apparently active during the transgression, resulting in a characteristically high porosity.

4.3 Methods and materials

4.3.1 Benthic profiling

The magnetic susceptibility and electric conductivity of the uppermost 0.5-1 m of seafloor were measured using the electromagnetic benthic profiler MARUM *NERIDIS III*. This instrument operates as a ship-towed sled and is equipped with a is equipped with a Controlled Source Electromagnetic (CSEM) induction coil sensor based on (Won et al., 1997). It consists of three concentric and coplanar coils. The outermost coil (diameter 1 m) transmits an alternating magnetic field

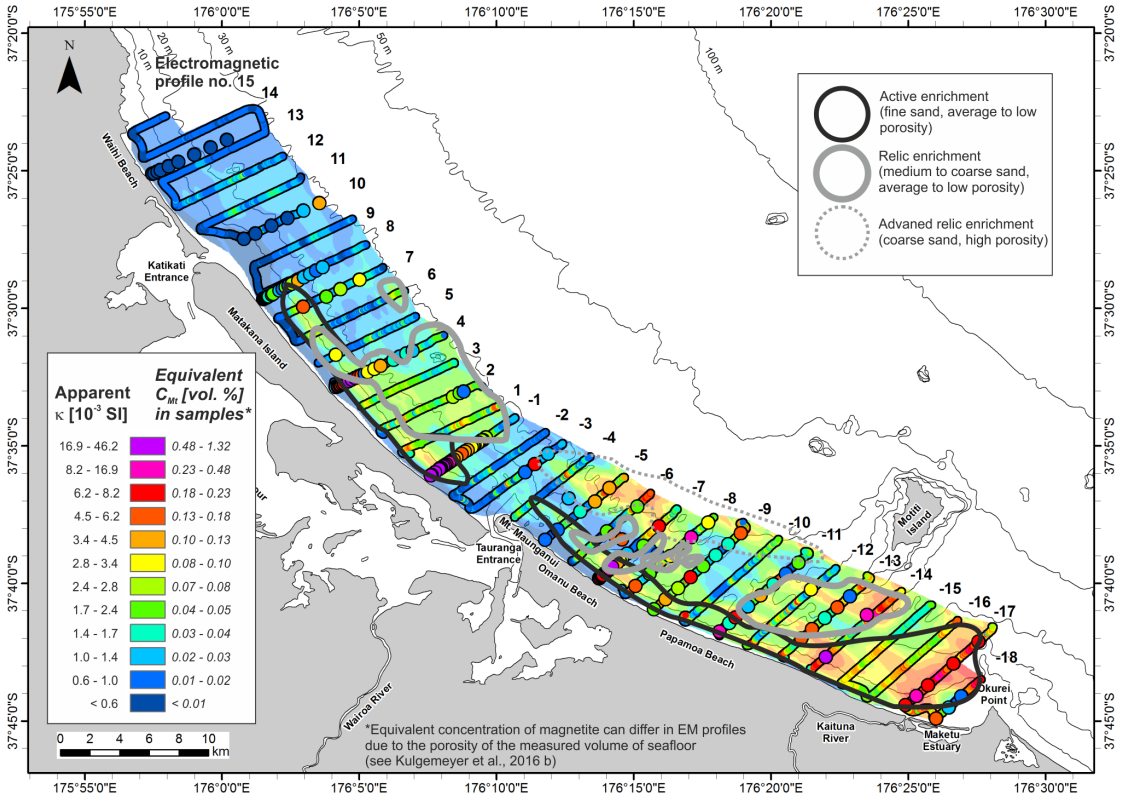

Figure 4.2: Enrichment structures interpreted according to Kulgemeyer et al. (2016 b) with (volumetric) susceptibility κ of sample material and interpolated susceptibility of the uppermost ca. 0.5 m of the seafloor.

with up to 12 combined frequencies between 25 Hz and 20 kHz, which induces a secondary magnetic field in the sediment and pore water of the seafloor. The receiver coil (diameter 30 cm) measures in-phase and quadrature components of the secondary field. Between transmitter and receiver is a bucking coil which creates a magnetic cavity that allows the receiver to see the secondary magnetic field while not being directly influenced by the transmitter signal.

The magnetic susceptibility is controlled by the amount of magnetic particles in the sediment. Susceptibility and magnetic mineral concentrations scale linear with each other. This parameter is picked from low frequency ($<$ 100 Hz) components of the in-phase signal. In contrast, the electric conductivity is almost exclusively controlled by the amount of conductive pore water and can be used as a measure of porosity. It is determined from high frequencies (5000 kHz) of the quadrature component. Details to the survey and the magnetic properties of sediments in the Bay of Plenty are found in Kulgemeyer et al. (2016 b). The

instrument is described in detail in Müller et al. (2012).

4.3.2 Reference samples

All reference samples were obtained using a Van Veen grab sampler and represent the uppermost ca. 5 cm of the seafloor. The magnetic fraction in the BoP sediment consists mainly of a mixture of magnetite and titanomagnetite (Kulgemeyer et al., 2016 b). For the sake of simplicity, and because the susceptibility of the titanomagnetite is strongly dependent both on Ti content and on grain size, all concentrations shown in this paper refer to a concentration of stochiometric magnetite equivalent to the measured susceptibility.

According to sediment cores from Kulgemeyer et al. (2016 b), the highest susceptibility is usually measured either directly at the seafloor, or in a layer 5-10 cm below, and decreases sharply with depth. Surficial concentrations follow the same trends, but are usually larger than the depth-integrated EM value. Because of this, reference concentrations for enriched and non-enriched sediment are better taken from surficial sample material. Two grab samples (NRC 015 and NRC 030 from Badesab et al. (2012)) were chosen for this. NRC 015 is located in 17 m water depth near Tauranga Entrance; presumably this sediment is close to its original composition and has not been subjected to extensive sorting processes. NRC 030 is located in 10 m water depth in within coast-parallel enrichment structure stretching along Matakana Island. The mass-specific susceptibility (NRC 015: $1.502 \cdot 10^{-6}$ m^3/kg, NRC 030: $1.657 \cdot 10^{-5}$ m^3/kg) of this material was converted into volumetric susceptibility using an approximate sediment density of 2700 kg/m^3, and the equivalent concentration of magnetite determined by dividing by the susceptibility of magnetite (Peters & Dekkers, 2003). This gave a volumetric concentration of 0.001 for the non-enriched and 0.013 for the enriched sediment.

Two more samples (BoP 7 and BoP 23 from Kulgemeyer et al. (2016 a)) were used to provide a measure for the typical grain sizes of the magnetic and non-magnetic fraction in the local fine (facies 1) and coarse sand (facies 3a) deposits. As magnetite makes up only a small fraction even in the enriched sediment, the

d_{50} grain sizes of (Kulgemeyer et al., 2016 a), obtained from laser diffractometry, are used as typical sizes for the non-magnetic fraction, which consists primarily of quartz: 160 µm(BoP 7), and 630 µm(BoP 23). These samples were prepared prior to the analysis by dissolving organic components by using 10 % H_2O_2.
To have a measure for the typical magnetite grain sizes, ca. 100 g of these samples were wet sieved in 1/2 ϕ increments. These samples were not treated with H_2O_2, as this can potentially oxidize or dissolve magnetic components. For every sieve fraction, as much material as possible was filled into a $2 \times 2 \times 1.6$ cm plastic cube and the (volumetric) susceptibility measured on a Geofyzika Brno Kappabridge KLY-2 susceptometer. Following Razik et al. (2014), the results were transformed into the mass-specific susceptibility values of each fraction χ_f and then mass weighted $\chi_{f,w}$ by multiplying with the proportion of the mass of the size fraction m_f to the total sample mass m_t: $\chi_{f,w} = \chi_f \frac{m_f}{m_t}$ (Fig. 4.3). While χ_f shows the concentration of magnetite within a grain size fraction, but high values might not contribute much to the overall number of magnetite grains if the respective grain size fraction is small. By multiplying with the proportion of the grain size fraction, $\chi_{f,w}$ corresponds to the abundance of a certain magnetite grain size within the entire sample. Thereby, the resulting curve gives a measure of the magnetic mineral grain size distribution. The data were analyzed using GRADISTAT from Blott & Pye (2001). Based on this, a typical magnetite grain size in fine sand is 62 µm and in coarse sand 238 µm.
Note that because of the different treatment, the overall grain size distribution of the sieve fractions deviates slightly from the data of Kulgemeyer et al. (2016 a). For the purpose of modelling the regional conditions, the latter is seen as a better representation of the non-magnetic components of the respective lithofacies. The small error in the grain sizes used to determine the magnetic fraction should be negligible after multiplication with the susceptibility.

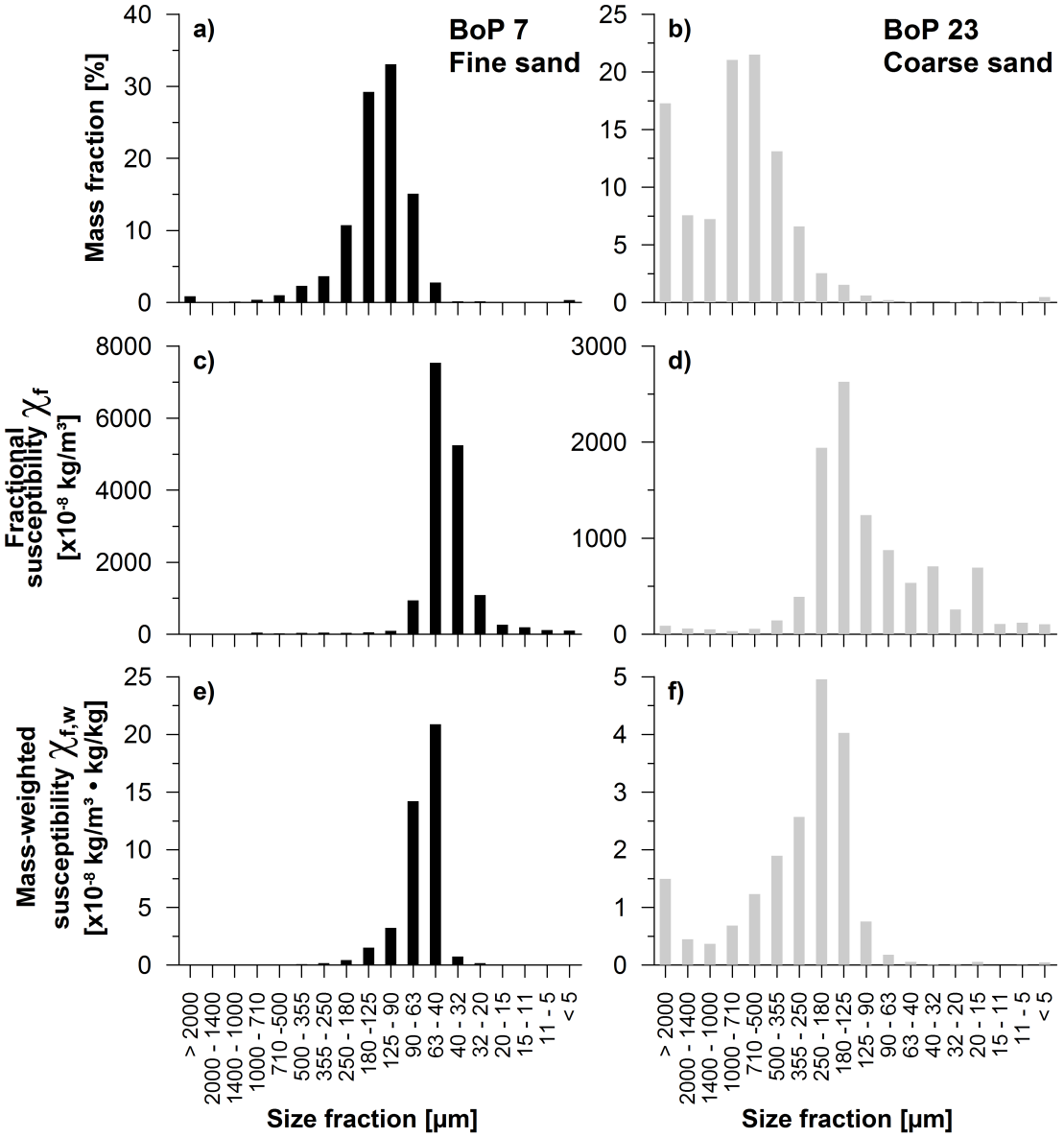

Figure 4.3: a, b) Grain size distribution of a fine sand (BoP 7) and coarse sand sample (BoP 23) by wet sieving. c, d) Mass-specific susceptibility of grain size fractions χ_f for both samples. e, f) Mass-weighted, mass-specific susceptibility of grain size fractions $\chi_{f,w}$ for both samples.

4.4 Modelling approach

4.4.1 Numerical model

The numerical model used here builds on an existing model first developed by Murray & Thieler (2004), and later extended and modified by Coco et al. (2007 a,b) and Goldstein et al. (2014) to explore the formation of sorted bedforms.

The version used in this study is based on that of Coco et al. (2007 a), and is written in C++. This model has been modified to address the requirements for a coastal environment. Rather than looking at a section of the seafloor with a constant depth, sediment transport takes place over a sloping bathymetry. While the original model used periodic boundaries, on a sloping seabed this setup is no longer realistic in cross-shore direction and this option was disabled. However, this also means that sediment that is transported out of the coastward boundary is permanently removed from the system, and the model looses mass through time.

4.4.2 Assessment of selective entrainment potential

Selective entrainment is a major sorting mechanism in the formation of heavy mineral enrichments (Slingerland & Smith, 1986; Li & Komar, 1992; Tomkins et al., 2003). Badesab et al. (2012) suggested this as being the dominant fractionation mechanism active in the Bay of Plenty (at least in fine sand). To support the interpretation of the observed structures, this assumption is tested.

Hydrodynamic conditions

The model is forced using the local hydrodynamic conditions in the region of interest. The availability of wave data is not optimal, with the only active wave buoy in the Bay of Plenty being located several kilometers away from the study area, offshore Pukehina Beach in 62 m water depth. Gorman et al. (2003) have modeled general wave conditions for locations around New Zealand, and used data from a buoy at Katikati Beach in 34 m that was active between 1991-1993 for validation. This is considered to be the best available data. Based on this, significant wave height H was set to 0.86 m and wave period T to 5.75 s, and the median direction of wave propagation to 247.5°. Current data was from four current meters that were deployed between April and May 2013 offshore southern Matakana island (see Fig. 4.1). For a regional average, the data of these instruments were combined. Current direction was mostly longshore in SW direction, but frequently changes direction to NE. To reflect this, the median

direction and flow velocity U_c of the current used as an input was 0.16 m/s, with a direction of 165 $^\circ$ azimuth (SW, slightly onshore). In the model, all current related parameters were evaluated separately for the longshore and cross-shore current component, and the respective flow velocities are 0.138 m/s (longshore) 0.08 m/s (onshore).

From Soulsby & Smallman (1986), the root mean square orbital velocity U_{rms} at the seafloor was calculated by an algebraic approximation on the JONSWAP dataset for natural wave spectra by

$$U_{rms} = \frac{0.25H}{(1 + B(T_n/T)^2)^3}/T_n \tag{4.1}$$

with $T_n = (h/g)^{1/2}$, h is the water depth, g gravity, and $B = (6500 + (0.56 + 15.54(T_n/T)^6)^{1/6}$. Following Soulsby (1997), this is transformed into the orbital velocity U_w, period T_p and orbital excursion (amplitude) A of an equivalent monochromatic wave with the same velocity variance as the full spectrum using the relationships:

$$U_w = \sqrt{2}U_{rms} \tag{4.2}$$

$$T_p = 1.281T \tag{4.3}$$

$$A = \frac{U_w T_p}{2\pi} \tag{4.4}$$

Using the viscosity of sea water $\nu = 1.210^-{-6}$, the Reynold's number $R = U_w A/\nu$ and the skin friction factor $z_{0,s} = d_{50}/12$ for a bed with median grain size d_{50} were determined. With this, a rough bed friction factor $f_{wr} = 1.39(A/z_{0,s})^{-0.52}$ is calculated with the Soulsby method (Soulsby et al., 1993; Soulsby & Clark, 2005), and a smooth bed friction factor $f_{ws} = bR^{-N}$ is given by Soulsby (1997), where $b = 2$, $N = 0.5$ for $R \leq 5 \times 10^5$ (laminar flow) and $b = 0.0521$, $N = 0.187$ for greater R (turbulent flow). The greater of f_{wr} and f_{ws} is chosen as the friction factor f_w, and used along with the density of water ρ_w and the orbital velocity to

calculate the wave related bed shear stress in $\tau_{b,w}$ with a unit of N/m^2

$$\tau_{b,w} = 0.5\rho_w f_w U_w^2 \tag{4.5}$$

Another bed shear component is that related to current friction. For this, the drag coefficient resulting from skin friction $C_{D,s}$ is calculated as (Soulsby, 1997):

$$C_{D,s} = (\frac{\kappa}{1 + log(z_{0,s}/h)})^2 \tag{4.6}$$

with von Karman constant $\kappa = 0.4$. With the current velocity U_c this gives the current related bed shear stress $\tau_{b,c}$ as

$$\tau_{b,c} = C_{D,s} U_c^2 \tag{4.7}$$

The two bed shear stresses combine according to Soulsby (1995) to a mean bed shear stress over a wave cycle $\tau_{b,mean}$ and a maximum $\tau_{b,max}$, the latter of which is relevant for the entrainment of particles:

$$\tau_{b,mean} = \tau_{b,c}(1 + 1.2(\frac{\tau_{b,w}}{\tau_{b,w} + \tau_{b,c}})^{1.5}) \tag{4.8}$$

$$\tau_{b,max} = \sqrt{(\tau_{b,mean} + \tau_{b,w} cos(\alpha))^2 + (\tau_{b,w} sin(\alpha))^2} \tag{4.9}$$

where α is the angle between wave and current direction (ca. 82 °). Where longshore and cross-shore components are evaluated in the model, the respective angle of these components relative to the waves is used.

Critical shear stress

Selective entrainment depends on differing critical shear stresses of particles. For testing if the conditions for selective entrainment are given, typical grain sizes for the quartz and magnetite fractions in fine sand (160 µm, resp. 62 µm) and in coarse sand (630 µm, resp. 238 µm) are used.

Based on procedures outlined in Soulsby (1997), the critical shear stress for each individual fraction i is calculated as follows:

First, the dimensionless grain size D_i is calculated by

$$D_i = d_i(\frac{g((\rho_i/\rho_w)-1)}{\nu^2})^{1/3} \tag{4.10}$$

with d_i grain size of fraction i, gravity g = 9.81 m/s^2, ρ_i density of sediment fraction (5200 kg/m^3 for magnetite, 2650 kg/m^3 for quartz), ρ_w density of sea water (1027 kg/m^3, at salinity 35 ppt and 15 °C), ν kinematic viscosity of sea water (1.2×10^{-6} m^2/s).

The dimensionless Shields parameter for critical shear stress $\theta_{i,cr}$ is taken from an algebraic approximation of the Shields (1936) curve from Soulsby & Whitehouse (1997)

$$\theta_{i,cr,Shields} = \frac{0.3}{1+1.2*D_i} + 0.055(1-exp(-0.020D_i) \tag{4.11}$$

This gives a critical bed shear stress $\tau_{i,cr}$ in N/m^2 as

$$\tau_{i,cr,Shields} = \theta_{i,cr,Shields} g(\rho_i - \rho_w) d_i \tag{4.12}$$

The Shields curve applies to uniform beds. To take the effect of grain shielding in a mixed bed into account, it has should be modified by a hiding/exposure factor ξ_i. This is usually a function of d_i/d_{50}, and various approaches to determine this factor are possible. According to Kleinhans & van Rijn (2002) and van Rijn (2007), the most realistic result should be given by the hiding/exposure factor of Egiazaroff (1965)

$$\xi_i = [\frac{(\log(19)}{\log(19 d_i/d_{50}))}]^2 \tag{4.13}$$

This modifies the critical shear stress to (van Rijn, 2007)

$$\tau_{i,cr} = \xi_i \frac{d_i}{d_{50}} \tau_{d_{50},cr,Shields} \tag{4.14}$$

An important notion here is that ξ_i only depends on the grain size ratio; it changes the critical shear stress of the fraction i relative to the d_{50} grain size in a bed *of the same properties*. The Shields parameter from Eq. 4.11 changes not only

with size but also with density. To solve Eq. 4.14 for a small magnetite particle in a mixed bed, $\tau_{d_{50},cr,Shields}$ has to be calculated from Eq. 4.10-4.12 for a bed of magnetite of the size d_{50}.

Using the above equations results in a clear difference in critical shear stress for magnetite and quartz in both sediments. In fine sand, it is ca. 0.27 N/m^2 for magnetite and 0.16 N/m^2 for quartz. In coarse sand, magnetite requires 0.65 N/m^2 and quartz 0.30 N/m^2.

When these results are compared to the bed shear stress conditions given by equation 4.9, the onset of quartz mobilization in fine sand can be expected in 18.7 m depth, and that of magnetite at 9.7 m (Fig. 4.4). For coarse sand, the limits are 13.6 m for quartz and 6.9 m for magnetite. Coarse sand is rare in this water depth, most deposits are unaffected by average wave conditions. The expected maximum of the coast-parallel enrichment in fine sand should be around 10 m when quartz is fully mobilized and magnetite is still immobile. This comes close to the observation made on most EM profiles (maximum at 8-10 m, examples in Fig. 4.5), with some shifts caused by the exact local sediment composition and hydrodynamic conditions. Additional sorting during transport may also influence the position and degree of the enrichment, but selective entrainment appears to be the major factor.

4.4.3 Sediment transport

The model by Coco et al. (2007 a) predicts sediment transport for two different grain sizes, this aspect has further been modified to take the different densities of each fraction into account. Further modifications were made to implement various sediment transport equations, that were more recent formulations, or that compared will with the observations made in the BoP environment. Bed shear stresses and critical shear stresses of each fraction were determined using the approach described in section 4.4.2. For more details about the technical implementation see Murray & Thieler (2004); Coco et al. (2007 a). The basic principle of the model is to compare the time it takes for advected sediment of the fraction i to cross through a cell ($T_{i,advec}$) to the time it takes to settle to

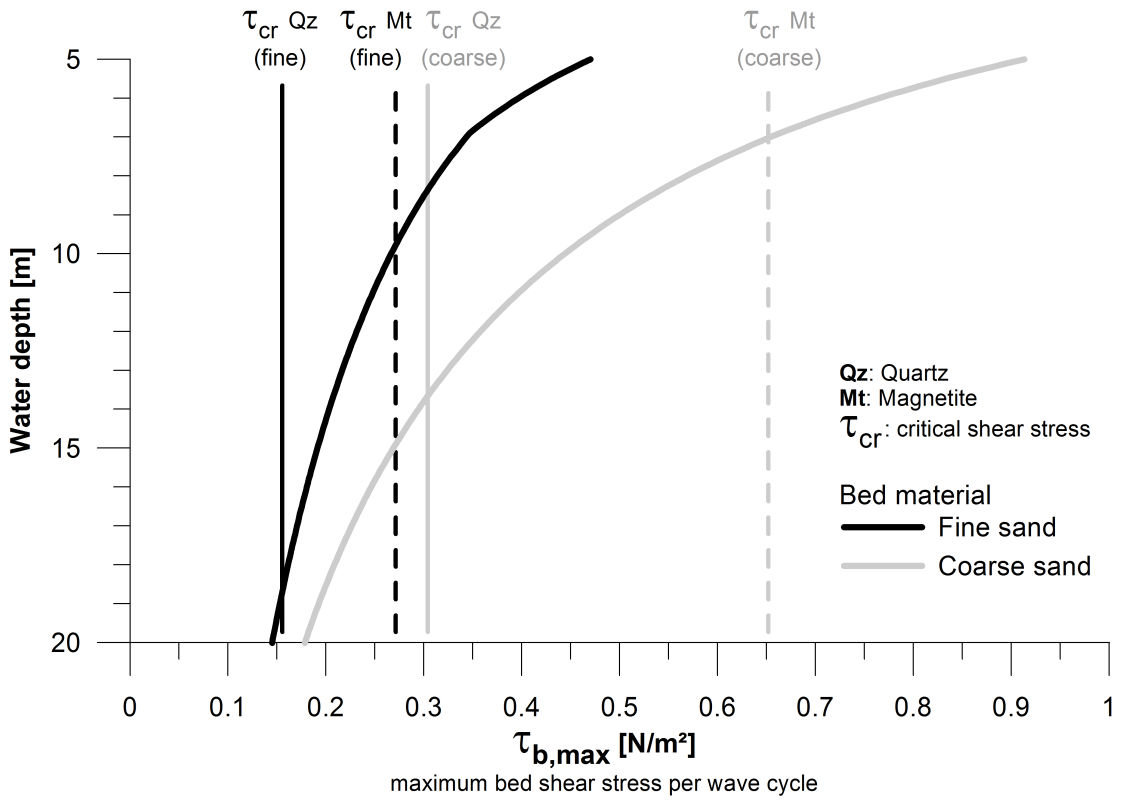

Figure 4.4: Bed shear stress depending on water depth under average wave conditions for local fine and coarse sand (lithofacies 1 and 3). Vertical bars show critical shear stresses τ_{cr} necessary to entrain quartz or magnetite of a grain size typical for the sediment. Selective entrainment in fine sand occurs between 7-22 m, in coarse sand potentially between 5-18 m; however; this facies is usually only observed below 20 m.

the seabed ($T_{i,settle}$). This gives a ratio $P_i = T_{advec}/T_{settle} = Xw_i/U_cH_{i,eff}$; with cell size X, settling velocity W_i, current velocity U_c and effective profile height $H_{i,eff}$. P_i determines whether sediment moves to the next cell, or settles to the seabed and causes accretion and changes to the bed composition. W_i of natural, irregularly shaped sand can be calculated as (Soulsby, 1997)

$$W_i = \frac{\nu}{d_i}(\sqrt{10.36^2 + 1.049D_i^3} - 10.36) \tag{4.15}$$

With this, W_i of the fine sand quartz fraction is 0.0153 m/s, that of magnetite 0.0064 m/s. In coarse sand, these values are 0.0835 m/s and 0.0604 m/s, respectively.

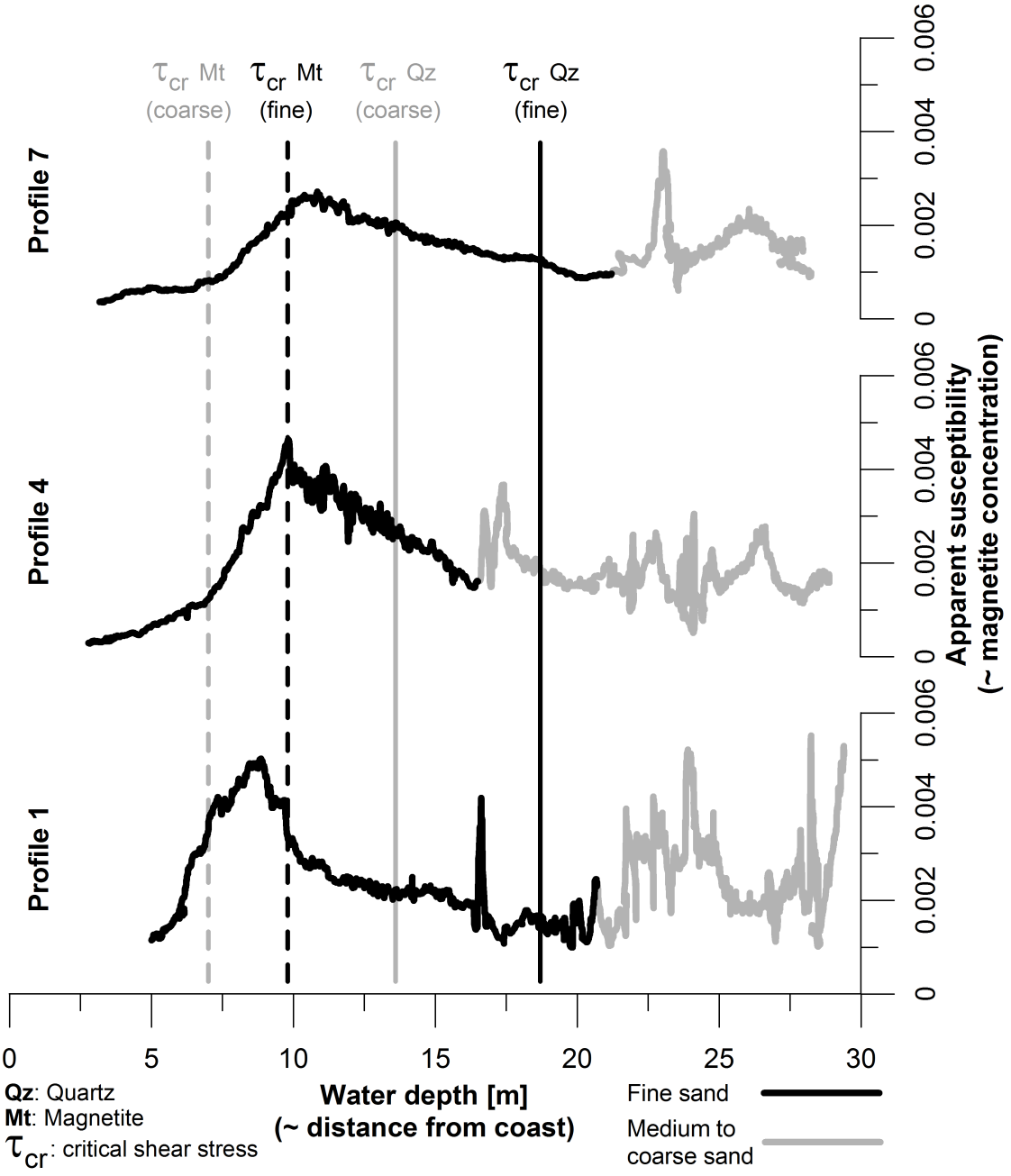

Figure 4.5: Examples of EM profiles with magnetite enrichment in Holocene fine sand (water depth corresponds to distance from the shore). Thick horizontal lines denote the depth where the bed shear stress under average wave conditions exceeds the critical shear stresses τ_{cr} of quartz and magnetite in fine sand.

Coco et al. (2007 a) use $H_{i,eff} = \epsilon_i / W_i$, where the diffusion coefficient ϵ is defined as (Fredso & Deigaard, 1992)

$$\epsilon_i = \lambda A \omega \exp(1.5 - 4500 d_i - 1.2 \ln \frac{U_w}{W_i}) \tag{4.16}$$

Here, λ is the ripple wave length as determined by the method of Styles & Glenn (2002).

The local sediment flux for each fraction $\vec{q_i}$ is the sum of suspended load $\vec{q}_{i,susp}$ and bedload $\vec{q}_{i,bed}$. The latter is calculated using van Rijn (2007)

$$\vec{q}_{i,bed} = 0.5 \rho_w d_i D_i^{-0.3} T_i \sqrt{\tau_{b,max} / \rho_w} \tag{4.17}$$

Suspended sediment flux is given by Coco et al. (2007 a), based on Bailard (1981), as

$$\vec{q}_{i,susp} = \int C_i \vec{V} dz - \gamma_i \frac{1}{5 W_i} U_w^5 \vec{\nabla} z \tag{4.18}$$

z is the vertical coordinate (origin at the sea floor), suspended sediment C_i the concentration and $\vec{V}$ the depth related current velocity. $\vec{\nabla} z$ is a bedslope term indicating the spatial gradient of the bottom perturbation in relation to the undisturbed sediment. γ is a coefficient defined as

$$\gamma = \gamma_c C_{D,r} \frac{16 E \rho_w}{3 \pi W_i} \tag{4.19}$$

, with efficiency factor $E = 0.035$ and a correction factor γ_c. Goldstein et al. (2014) notes that this factor should be chosen to maintain ca. one order of magnitude difference between the two terms on the right hand side of equation 4.18. Goldstein et al. (2014) used a value of 0.07, although this often overestimated the term in the magnetite fraction while underestimating it for quartz. As a compromise, a value of 0.03 was chosen and is used unless otherwise indicated. As the diffusion process is greatly influenced by ripples, the drag coefficient in equation 4.19 is not only based in skin friction (as in eq. 4.6, but is now given by

$C_{D,r}$ (Soulsby, 1997):

$$C_{D,r} = \frac{\kappa}{1 + log(z_0/h)} \tag{4.20}$$

The parameter z_0 is the roughness related to ripples $z_0 = \frac{1}{30}(2d_{50} + 28\frac{\eta^2}{\lambda})$ (van Rijn, 1993), with ripple height η again based on the method of Styles & Glenn (2002).

C_i is determined using from the concentration profile $C_i(z)$ (Nielsen, 1979; Fredso & Deigaard, 1992) describing the distribution of the suspended load over a wave period along ripples

$$C_i(z) = C_{i,0}\exp(-W_i z/\epsilon_i) \tag{4.21}$$

with the bottom concentration of suspended sediment $C_{i,0}$ is calculated based on van Rijn (2007) as:

$$C_{i,0} = \frac{d_i}{0.01} D_i^{-0.3} T_i^{1.5} \tag{4.22}$$

where T_i is a dimensionless bed shear stress parameter

$$T_i = \frac{\tau_b - \tau_{i,cr}}{\frac{d_i}{d_{50}}\tau_{d_{50},cr,Shields}} \tag{4.23}$$

The horizontal current velocity $\vec{V}$, Coco et al. (2007 a) use a logarithmic current profile with the form

$$\vec{V}(z) = \frac{1}{\kappa} U_* \log\frac{z}{z_0} \tag{4.24}$$

with the current related shear velocity $U_* = \sqrt{\tau_{b,c}/\rho_w}$. Note that ripple-generated turbulence has an influence both on $\vec{V}$ and U_* (Soulsby, 1997). To reflect this, and in accordance with the method used by Coco et al. (2007 a), $\tau_{b,c}$ has been calculated by substituting $C_{D,r}$ for $C_{D,s}$ in equation 4.7 for the determination of U_* (although if this is not done, the outcomes differ only slightly).

4.5 Modeling results

4.5.1 General outcomes

Unless otherwise indicated, all model runs started with a homogeneous distribution of 62 µm magnetite with a concentration of 0.001 in a 160 µm quartz matrix in $5 \times 5 \times 0.05$ m cells with a slope of 0.02 between a water depth of 3-30 m for a coastline striking 135° azimuth, and use the average hydrodynamic conditions of the Bay of Plenty (0.86 m wave height, 5.75 s wave period in direction 247.5 °, longshore current 0.138 m/s onshore current 0.08 m/s). To reduce artifacts, the output was filtered with a 3-cell median filter. Above a water depth of 5 m, the model tends to develop extreme magnetite concentrations which can be several orders of magnitude larger than the actual enrichment structure. This is considered an artifact of incorrectly representing hydrodynamic condition in such shallow water (e.g. no drift or wave skewness) and is not shown in the following diagrams. The cross-shore distribution of the BoP standard conditions is provided as a reference in figures, to the effect of variations in the hydrodynamic and geological setup described in the following sections.

The results of the numerical model show the development of a coast parallel magnetite enrichment, with a pattern comparable to the field observations. Enrichment of magnetite starts shortly after the initiation of sediment transport at the entrainment depth of quartz and increases coastwards until the entrainment depth of magnetite is reached (Fig. 4.6 a). It remains relatively stable until the transport rate of magnetite is great enough to surpass the modelled redeposition. From there, the concentration decreases again. The growth rate of the enrichment, observed at the peak of the curve, is linear with time (Fig. 4.6 b). At this rate, it would take 4000 days (10.9 years) of constant forcing to reach the peak enrichment of 0.013 observed in the reference sample. This is likely to be a minimum timeframe, as conditions that are greater than the mean waves would be much more effective at processing bed sediments.

A second, smaller enrichment peak is observed between 7-5 m water depth. This is a depth where the gradient of the theoretical bed shear stress curve

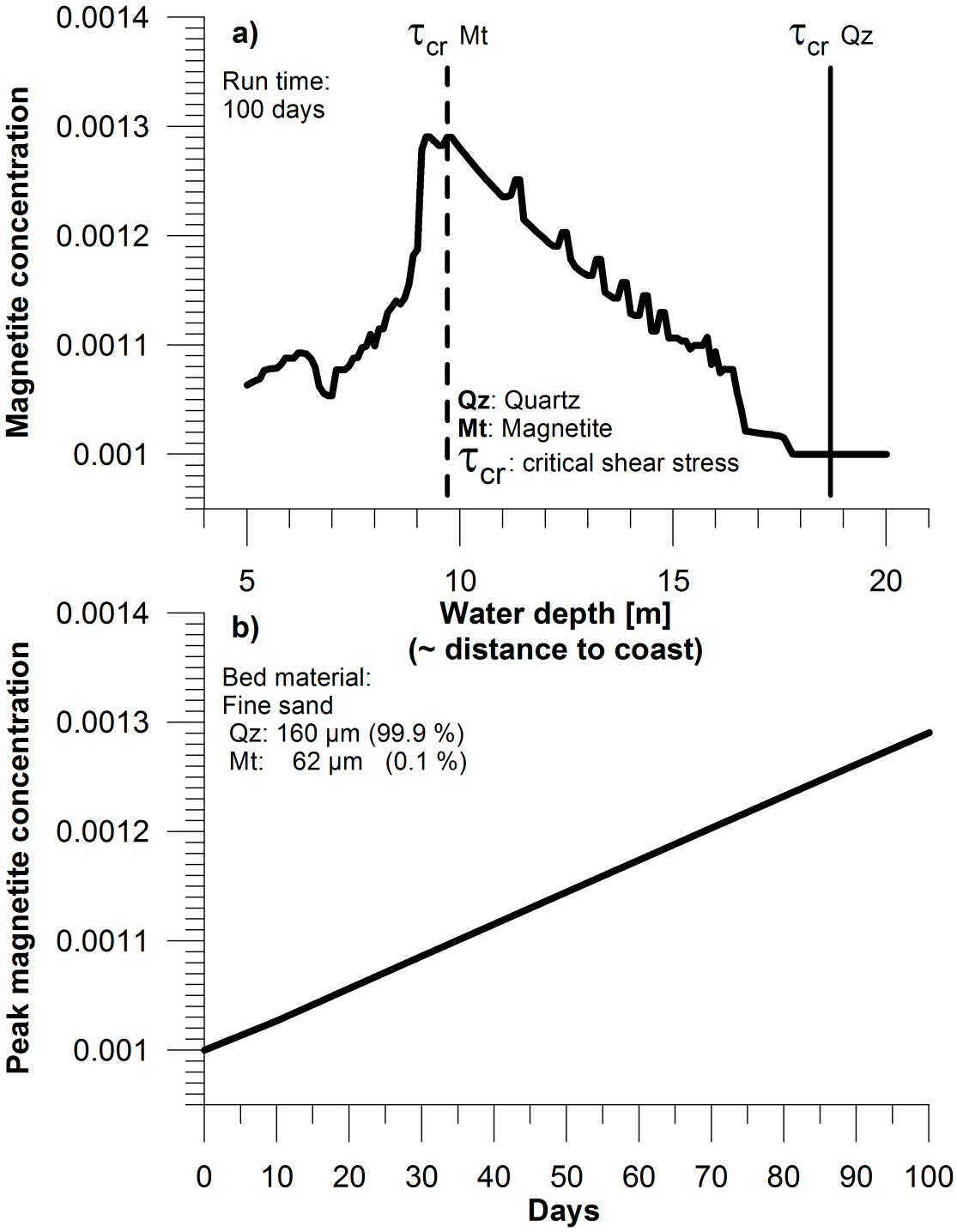

Figure 4.6: a) Cross-shore profile of the model results after 100 days of constant forcing conditions with lines indicating the entrainment depth of quartz and magnetite grains. b) Development of the peak enrichment over 100 days.

becomes much steeper, which apparently affects the balance between the fractional transport rates. This second peak is not consistent with observations, thus might be an artifact that arises from applying the equations in very shallow

water. Smaller, likewise artificial, undulations of the concentration profile are likely a result of the stepwise, thus discontinuous, bathymetry.

4.5.2 Response to hydrodynamic variations

Variations in the wave height (Fig. 4.7 a) affect the bed shear stress, which results in shifting the entrainment depths coastwards (decreasing wave height) or seawards (increasing wave height). As the bed shear stress of waves is strongly dependent on water depth this is an expected outcome. The wave period has a similar, although less marked effect (Fig. 4.7 b).

Increasing the longshore current component also increases the bed shear stress, shifting the enrichment considerably towards deeper water where the wave related shear stress is still relatively small (Fig. 4.7 c). Conversely, decreasing the longshore current is little effect on the position of the entrainment depths, as it is mostly controlled by wave action in more shallow water. Variations in the onshore component of the current have almost no effect on the position of the enrichment structure, even when it is doubled this component remains small relative to the energy provided by the longshore current and wave action. However, it also increases the transport rate of mobilized sediments towards the shore, and through this greatly affects the degree of enrichment (Fig. 4.7 d).

For comparison, the model was tested using waves and either only the longshore or only the onshore current component. Using only the longshore current results in a very small enrichment structure (Fig. 4.7 e). The onshore-only case produces an enrichment similar to the standard case, although again shifted towards the coast due to the lower bed shear stress (Fig. 4.7 f). This shows that the onshore transport of sediments is critical for the development of this type of enrichment structure. Interestingly, enrichments in shallower water depths generally reach a higher value. This is caused by the vertical current velocity profile; as it is influenced by the water depth via through parameter U_*, bottom currents are slightly stronger in shallower water.

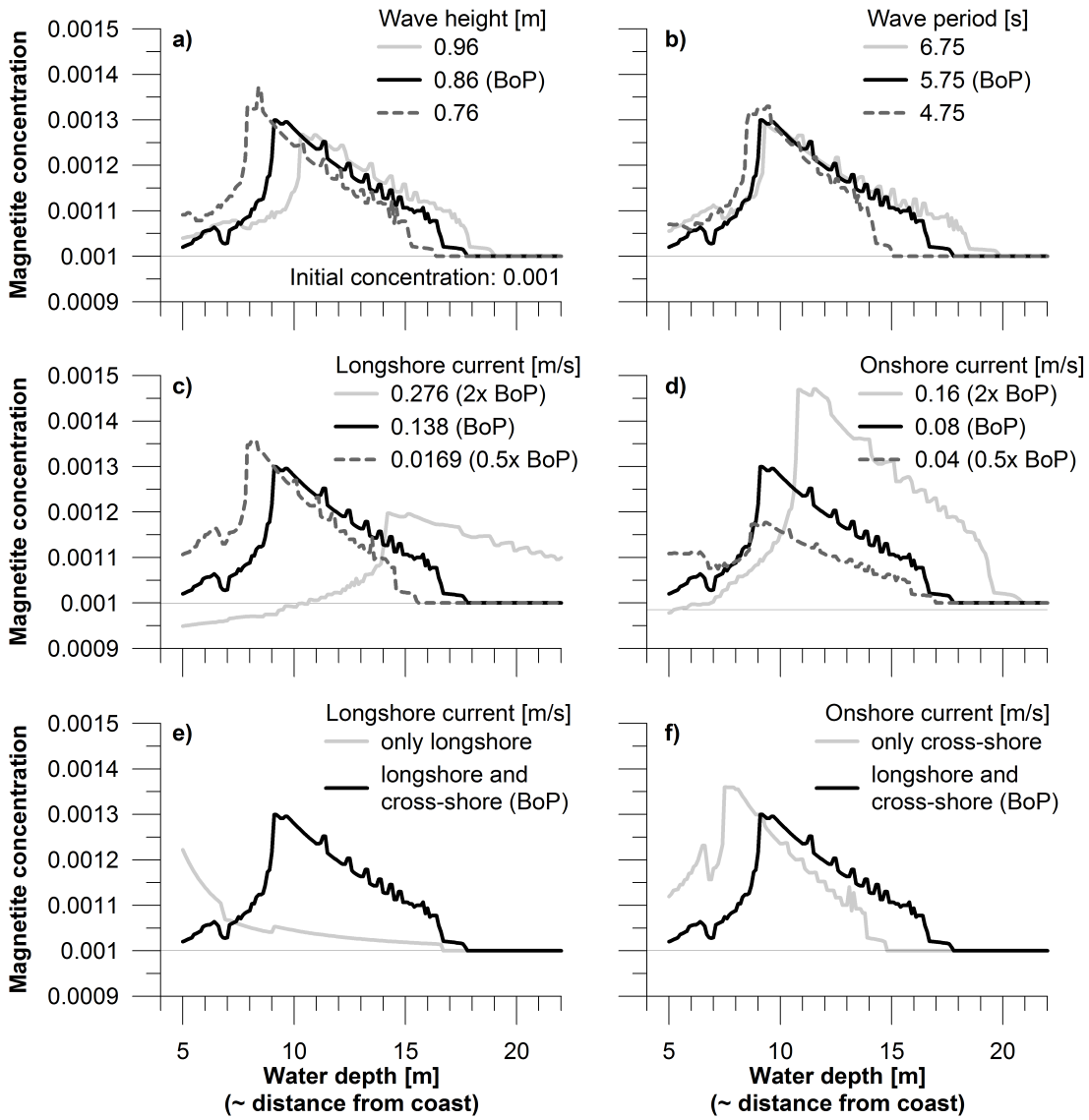

Figure 4.7: Model response after 100 days of constant forcing to variations in the hydrodynamic conditions. Reference conditions that apply to the bay of Plenty are denoted as (BoP). a) Changes in wave height, b) changes in wave period, c) changes in longshore current velocity, d) changes in cross-shore (onshore) current velocity, e) model outcome without cross-shore current, f) model outcome without longshore current.

4.5.3 Response to geological variations

Increasing the initial concentration of magnetite by a factor of 5 or 10 (Fig. 4.8 a) produces a profile very similar in shape to the tested BoP standard case; apart from some minor variations in artifacts the result is the same as multiplying the standard curve by the respective factor. Consequently, the additional magnetite

in the system leads to a proportionally higher rate of enrichment (Fig. 4.8 b). Although coarse sand in the BoP is generally found below the entrainment depths of its components, for a comparison, the model has been run with the respective grain size configurations (quartz 630 µm, magnetite 200 µm). The resulting enrichment is far surpasses the enrichment on fine sand (Fig. 4.8 c). It appears that the much higher grain roughness results in higher rates of entrainment and sediment transport, which far outweighs the greater mass of the particles.

Adjusting the bathymetry to a steeper or flatter slope angle likewise greatly influences the degree of the enrichment (Fig. 4.8 d). This is likely caused by the greater difference in wave energy and current velocity between neighboring cells for steeper bed slopes. At first, a greater volume of sediment is mobilized in a cell relative to an adjacent, more seaward cell than is the case on a less inclined slope. As the difference is cross-shore current velocities in these adjacent cells is likewise greater than on more flat surface, the horizontal transport rate is increased. A physical interpretation would be the focusing of wave and current energy on a smaller surface area of the seabed.

Fig 4.8 e) shows the result of adjusting the size of the magnetite fraction. Increasing the grain size to be equal to the surrounding quartz matrix (160 µm) does not result in an enrichment structure with a pronounced peak like it is observed in the natural environment of the BoP. The concentration of magnetite first increases coastwards just like it does in the standard case. Judging by the critical shear stress alone, the 160 µm magnetite should be entrained close to this depth, an effect of its greater grain size and mass. A decrease in concentration should be expected. However, instead the enrichment increases at a much higher rate between 7-6 m, then increases further with a similar rate as in deep water. This is caused by a change in the gradient of the bed shear stress curve (Fig. 4.4), which leads to much larger volume of sediment being entrained. The transport rate quartz in shallow water becomes so high that it can not balanced out by magnetite within the boundaries of the model. Interestingly, decreasing the magnetite grain size also increases the critical shear stress, which is caused by the hiding effect.

If the density is decreased from that of magnetite (5200 kg/m^3) to that of ilmenite (4720 kg/m^3), the critical shear stress decreases and the peak of the enrichments shifts towards deeper water. Decreasing the density further so that the model operates with two different-sized quartz fractions (2650 kg/m^3), the minor fraction does not become enriched at all. At this grain size, the critical shear stress of the fine quartz fraction of 0.13 N/m^2 is still lower than that of the larger fraction. At any depth, the minor fraction is mobilized and transported at a higher rate, which results its depletion and the enrichment of the major fraction. Enrichment of the fine quartz fraction can only take place at even smaller grain sizes, when the shielding effect is large enough to put its critical shear stress above that of the coarser fraction.

4.5.4 Alternative sorting mechanisms

Apart from selective entrainment and differential transport, a number of other sorting mechanisms can play a role in the formation of enrichments. One such mechanism, discussed e.g. by Wilson (1989); Hughes et al. (2000), is shear sorting. This can occur in sheet flow conditions and will result in larger grains being moved vertically upwards while smaller grains are buried beneath. According to Wilson (1989), sheet flow conditions for a quartz sand bed are fulfilled when

$$A > 0.65 d_{50}^{0.417} (g((\rho_{50}/\rho_w) - 1) T^2)^{0.583} \tag{4.25}$$

Again T_p has been used as substitute for T in the a monochromatic wave spectrum. The above condition is never fulfilled for fine or coarse sand in the enriched areas in 10 m or 30 m. Therefore, shear sorting can be ruled out as a major sorting mechanism in the Bay of Plenty.

Sorting could further be achieved by the settling of fractions with differing settling velocity. The role of this mechanism is often seen as small compared to other, more effective means of enrichment based on entrainment and

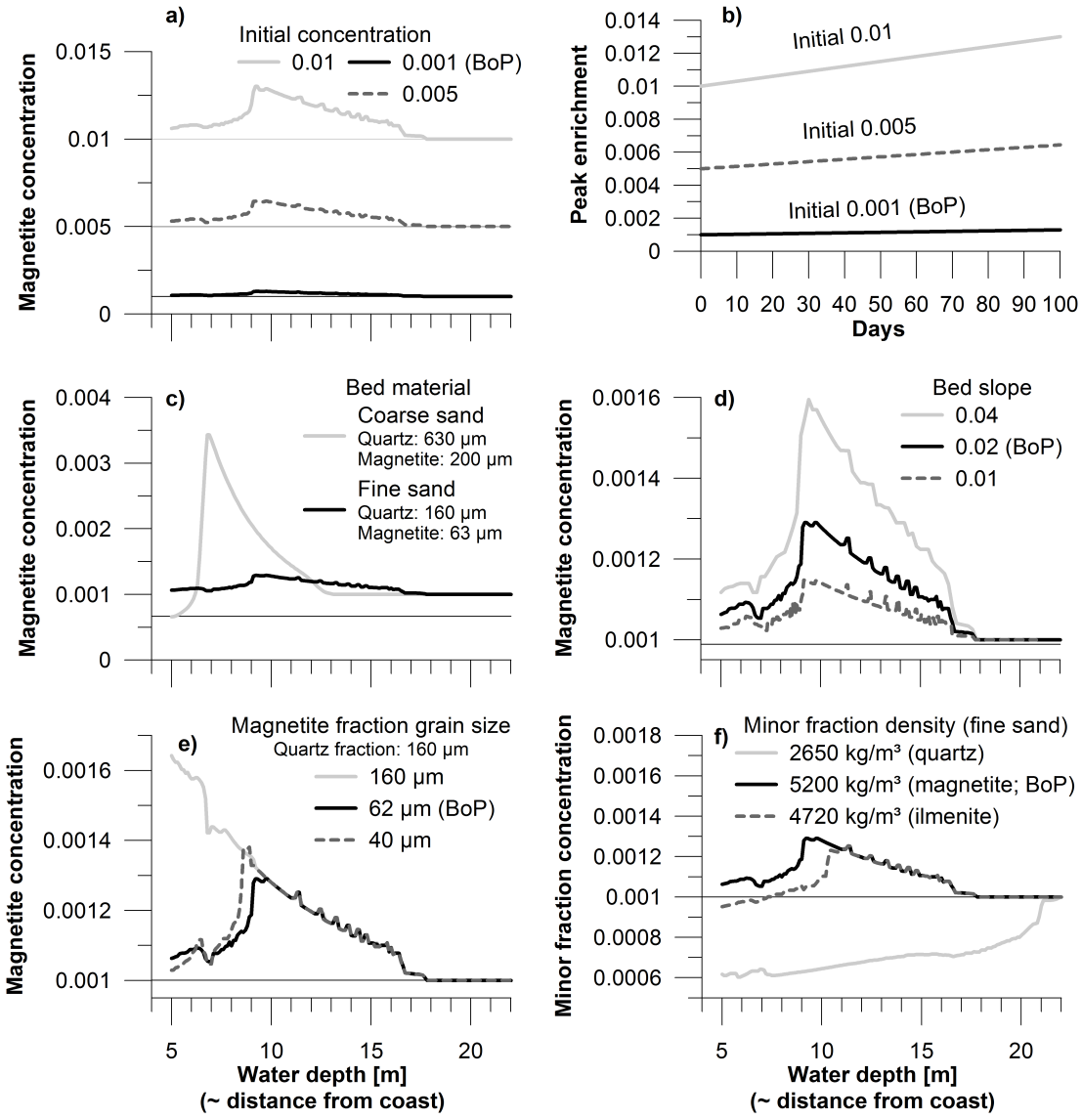

Figure 4.8: Model response after 100 days of constant forcing to variations in the geological conditions. Reference conditions that apply to the bay of Plenty are denoted as (BoP). a) Outcome for different initial (homogeneously distributed) magnetite concentrations, b) development of the peak enrichment over 100 days for different initial magnetite concentrations, c) results for a coarse sand bed, d) results for differing bed slopes, e) results for different magnetite grain sizes, f) result for different mineral densities of the minor fraction; densities correspond to quartz, magnetite and ilmenite.

transport (Steidtmann, 1982; Komar & Wang, 1984; ReidFrostick, 1985), but should still be considered as an alternative.
In both cases, sorting should take place during settling. In still water, this would produce the kind of graded bed that was observed in the cores (Kulgemeyer et al., 2016 b) with the highest concentration of magnetite at the top. In a coastal environment affected by wave and current action a lateral sorting could take place where particles with smaller settling velocity are deposited in less energetic environments, e.g. further offshore. This could theoretically produce a coast-parallel magnetite enrichment, but as the above calculations have shown, the environment of the coast-parallel enrichment structure favors the entrainment of particles, not the deposition. While this may still be considered as a subsidiary process that could support the main sorting process by periodically providing a pre-sorted bed in times of very low wave activity, it is unlikely that this mechanism is primarily responsible for the formation of the structures observed in the BoP.

4.6 Discussion

The results of the numerical model are in general agreement with the observed distribution of magnetite in the study area. Differences concern mostly details, for example the coastward concentration decreases steeper in the model than in the field data. This could be caused by the strictly bimodal nature of the model, whereas the natural sediment contains a variety of magnetic and non-magnetic minerals in different grain sizes (Kulgemeyer et al., 2016 a,b). Also, the frequently changing hydrodynamic conditions of the study area will have an influence on the exact distribution of minerals.
The model response to changes in grain size and density lead to interesting observations. As the connection between the critical shear stress of the minor fraction and its grain size in a fine or coarse sand matrix is modelled after the classical Shields (1936) curve (with modification by the hiding factor), it is always non-linear. It appears that the ratio of quartz to magnetite grain size in the Bay of Plenty sediments is balanced towards a minimum in the overall critical shear

stress (see Fig. 4.9 a) The relation to density is much simpler and follows a linear trend (Fig. 4.9 b). If this is coincidence, predetermined by the source rock or the result of sorting would need to be investigated in a comparative study. If this is in fact an effect of sorting, a likely explanation would be that less mobile phases of the sediment derived from source rock remained further up the transport path and did not enter the sink on the shoreface. If this is a systematic process, it highlights how the sorting of the heavy mineral fraction makes it a more sensitive indicator for transport path and provenance of a sediment than the grain size distribution of the bulk material.

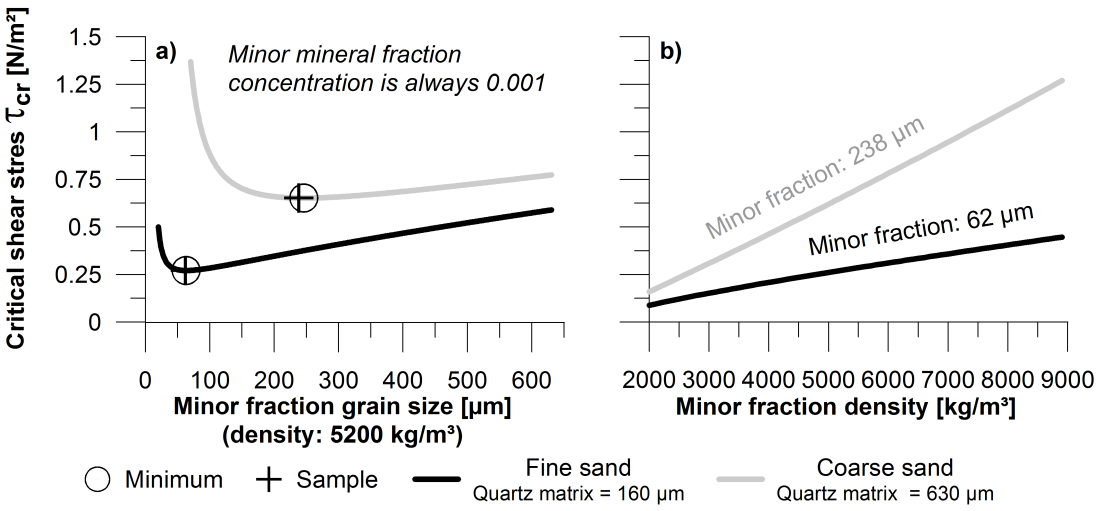

Figure 4.9: a) Variation in critical shear stress τ_{cr} of magnetite (concentration 0.001) in a fine sand (d_{50} = 160 µm) or coarse sand (d_{50} = 630 µm) matrix. Minima are at 63 µm in fine sand and 246 µm. b) Variation of τ_{cr} in the same matrices for minerals with a grain size of 62 µm (BoP fine sand) and 238 µm (BoP coarse sand).

The validity of the model of course hinges on the equations. The behavior of a vast number of irregularly shaped particles in a flowing medium is notoriously difficult to describe. Equations are usually empirically determined in laboratory experiments, and come with their own boundary conditions such as the geometry of the wave and flume tanks used. Often, these equations are only valid for a certain water depth range, or observations made in the gravel to medium sand range are generalized towards finer grain sizes (van Rijn, 2007). Most experiments are performed on quartz, actual empirical data for denser minerals is rare. The curve Shields (1936) is widely used in science and engineering

for many decades in which countless contributions, validations and refinements have been made, yet science is still in the process of approaching a solid theoretical foundation (Miedema, 2010). Like in many models, the chosen governing equations are the ones that best correspond to the field data, and validation comes from the good agreement of model results and observation.

For small concentrations, and on short time scales, the linear trend of the model should be realistic. However, this trend will ultimately result in a 100 % magnetite layer, which is unlikely to be the case in nature – some individual quartz grains will always remain buried in this matrix. An asymptotic approach to saturation would be more realistic. A number of processes are not included in the model, that are nevertheless of sedimentological relevance. This concerns the burial of grains, stabilization of the seafloor by consolidation, and a return flow of sediments from the beach back into the modelled water depth range. The latter process is of importance to balance out erosion. As material that is transported out of the coastward boundary of the model can not return back into the system, it is by default tending towards erosion. This limits its use over long time scales and under extreme conditions. This was especially noteworthy in an attempt to test the response to extreme weather conditions. Here, the erosion was so strong that the slope profile lost a height of 1.25 m of sediment at the coastward boundary within 15 s of run time. The study area in the Bay of Plenty used as a reference is generally described as a storm-dominated environment (Carther & Heath, 1975). The bathymetrical profile should be in a long-term equilibrium with these conditions, and while the formation of the coast-parallel enrichments is evidently linked to average waves and currents, they must be able to withstand stormy periods.

As such, the numerical model is well able to demonstrate the formation process of coast-parallel heavy mineral enrichments based on selective entrainment and differential transport, but does not include their preservation. However, if typical grain sizes of the targeted minerals and the hydrodynamic conditions of an area are known, this approach can guide a survey towards the expected water depth of the enrichment, e.g. to sample high concentrations of iron oxides

or sulphides for climate reconstructions and dating purposes (Razik et al., 2013; Just et al., 2014). An interesting application of the model would be the reverse case: assuming the cross-shore distribution of minerals along with their grain sizes have been determined by sampling or EM profiling, this approach could help to estimate the long-term hydrodynamic conditions affecting the seafloor or in reconstructing palaeo-hydrodynamics. This would need to be tested in example cases.

4.7 Conclusions

The model of Coco et al. (2007 a), modified for use on a slope on grains with different densities, is able to predict the formation of coast-parallel heavy mineral enrichments below 5 m water depth with results close to the patterns observed in the Bay of Plenty. This supports the conceptual formation model of Kulgemeyer et al. (2016 b). The formation is mainly driven by selective entrainment of particles. Above the entrainment depth of magnetite, differential transport can act as a secondary sorting mechanism that has an influence on the degree of enrichment. The models responds to changing hydrodynamic conditions by shifting the enrichment structure closer to or further away from the shore. Generally, enrichments forming in shallower water depth enrich faster than in deep water due to the greater flow velocity of currents. Enrichment is likewise more effective on more inclined slopes due to the greater horizontal change in wave friction and bottom current velocity, and hence sediment transport rate. The balance of bed shear stress to critical shear stress of sediment fractions determine the position of the structure by selective entrainment, and while a slight enrichment is achieved purely by longshore transport, it is the onshore current components that controls the degree of enrichment.

Changing the grain size of the heavy mineral fraction increases the critical bed shear stress either directly through the particle size or the hiding effect. In the BoP sediment, data indicates a balance towards the minimum critical shear stress of the heavy mineral fraction within the respective quartz matrix both in

fine and coarse sand. The cause of this phenomenon is yet unknown.
The model could be further improved by including an estimate for the volume of sediment that periodically enters the system from outside, thus balancing the tendency towards erosion present in the current version. To make predictions about the long-term preservation of formed structures in extreme conditions, the effect of grain burial should likewise be considered. However, it performs overall well as an exploratory tool and produces promising outcomes that should be tested on more field cases in the future.

4.8 Acknowledgments

We deeply thank Giovanni Coco and Evan Goldstein for their helpful comments and suggestions on the model. The deployment of *NERIDIS* was financed by the *RENA* Long Term Environmental Recovery Monitoring Program. This study is a project of the collaborative graduate school INTERCOAST of the universities of Bremen and Waikato, with financing provided by the German Research Foundation (Deutsche Forschungsgesellschaft, DFG).

Bibliography

Badesab, F., von Dobeneck T., Bryan, K.R., Müller, H., Briggs, R.M., Frederichs, T., Kwoll, E. (2012): Formation of magnetite-enriched zones in and offshore of a mesotidal estuarine lagoon: An environmental magnetic study of Tauranga Harbour and Bay of Plenty, New Zealand – Geochemistry, Geophysics, Geosystems, Vol. 13, Q06012, doi:10.1029/2012GC004125.

Bailard, J.A. (1981): An energetics total load sediment transport model for a plane sloping beach – Journal of Geophysical Research, Vol. 86, pp. 10938-10954.

Bartzke, G., Bryan, K.R., Pilditch, C.A., Huhn, K. (2013): On the stabilizing influence of silt on sand beds – Journal of Sedimentary Research, Vol. 83, pp. 691–703, doi:10.2110/jsr.2013.57.

Bartzke, G., Huhn, K. (2015): A conceptual model of pore-space blockage in mixed sediments using a new numerical approach, with implications for sediment bed stabilization – Geo-Marine Letters, doi:10.1007/s00367-015-0399-1.

Blott, S.J., Pye, K. (2001): GRADISTAT: a grain size distribution and statistics package for the analysis of unconsolidated sediments – Earth Surface Processes and Landforms, Vol. 26, pp. 1237-1248.

Bradshaw, B.E., Healy, T.R., Dell, P.M., Bolstad, W.M. (1991): Inner shelf dynamics on a storm-dominated coast, East Coromandel, New Zealand – Journal of Coastal Research, Vol. 7, No. 1, pp. 11-30.

Bradshaw, B.E., Healy, T.R., Campbell, S.N., Dell, P.M., de Lange, W.P. (1994): Holocene sediment lithofacies and dispersal systems on a storm-dominated, back-arc shelf margin: the east Coromandel coast, New Zealand – Marine Geology, Vol. 119, pp. 75-98.

Briggs, R.M., Houghton, B.F., McWilliams, M., Wilson, C.J.N. (2005): $^{40}\mathrm{Ar}/^{39}\mathrm{Ar}$ ages of silicic volcanic rocks in the Tauranga-Kaimai area, New Zealand: dating the transition between volcanism in the Coromandel Arc and the Taupo Volcanic Zone – New Zealand Journal of Geology and Geophysics, Vol. 48, pp. 459-469.

Bryan, K.R., Robinson, A., Briggs, R.M. (2007): Spatial and temporal variability of titanomagnetite placer deposits on a predominantly black sand beach – Marine Geology, Vol. 236, pp. 45-59.

Burton, J.P., Fralick, P. (2003): Depositional Placer Accumulations in Coarse-Grained Alluvial Braided River Systems – Economic Geology, Vol. 98, pp. 985-1001.

Carter, L., Heath, R.A. (1975): Role of mean circulation, tides and waves in the transport of bottom sediment on the New Zealand continental shelf – New Zealand Journal of Marine and Freshwater Research, Vol. 9, pp. 423-448.

Coco, G., Murray, A.B., Green, M.O. (2007 a): Sorted bed forms as self-organized patterns: 1. Model development – Journal of Geophysical Research, Vol. 112, F03015, doi:10.1029/2006JF000665.

Coco, G., Murray, A.B., Green, M.O., Thieler, E.R., Hume, T.M. (2007 b) : Sorted bed forms as self-organized patterns: 1. Complex forcing scenarios – Journal of Geophysical Research, Vol. 112, F03016, doi:10.1029/2006JF000666.

Corbett, I., Burrell, B. (2001): The earliest Pleistocene(?) Orange River fan-delta: an example of succesful exploration delivery aided by applied Quaternary research in diamond placer sedimentology and plaeontology – Quaternary International, Vol. 82, pp. 63-73.

Deltares Systems (2014): Delft3d-FLOW Simulation of multi-dimensional hydrodynamic flows and transport phenomena, including sediments: User Manual – Deltares Systems, Delft, 684 pp.

Egiazaroff, I.V. (1965): Calculation of nonuniform sediment concentrations – Journal of the Hydraulics Division, Vol. 91, No. 4, pp. 225-247.

Elsner, H. (1992): Granulometry and mineralogy of some northeastern Florida placers: a consequence of heavy mineral concentration in nearshore bars – Sedimentary Geology, Vol. 76, pp. 233-255.

Duk-Rodkin, A., Barendregtb, R.W., Whitea, J.M., Singhrey, V.H. (2001): Geologic evolution of the Yukon River: implications for placer gold – Quaternary International, Vol. 82, pp. 5-31.

Fredsøe, J., Deigaard, R. (1992): Mechanics of Coastal Sediment Transport – Worlds Scientific, Singapore.

Frihy, O.E. (1994): Discrimination of accreted and eroded coasts using heavy mineral compositions of the Nile Delta beach sands, Egypt – Sedimentology, Vol. 41, pp. 905-912.

Frihy, O.E., Komar, P.D. (1993): Long-term shoreline changes and the concentration of heavy minerals in beach sands of the Nile Delta, Egypt – Marine Geology, Vol. 115, pp. 253-262.

Frihy, O.E., Lotfy, M.F., Komar, P.D. (1995): Spatial variations in heavy minerals and patterns of sediment sorting along the Nile Delta, Egypt – Sedimentary Geology, Vol. 97, pp. 33-41.

Gallaway, E., Trenhaile, A.S., Cioppa, M.T., Hatfield, R.G. (2012): Magnetic mineral transport and sorting in the swash-zone: northern Lake Erie, Canada – Sedimentology, Vol. 59, pp. 1718-1734.

Goldstein, E.B., Coco, G., Murray, A.B., Green, M.O. (2014): Data-driven components in a model of inner-shelf sorted bedforms: a new hybrid model – Earth Surface Dynamics, Vol. 2, pp. 67–82, doi:10.5194/esurf-2-67-2014.

Gorman, R.M., Bryan, K.R., Laing, A.K. (2003): Wave hindcast for the New Zealand region: Nearshore validation and coastal wave climate – New Zealand Journal of Marine and Freshwater Research, Vol. 37, No.3, pp. 567-588, doi: 10.1080/00288330.2003.9517190.

Hamilton, N.T.M., Collins, L.B. (2001): Placer Formation in a Holocene Barrier System, Southwestern Australia – Journal of Coastal Research, Vol. 14, No. 1, pp. 240-255.

Hughes, M.G., Keene, J.B., Joseph, R.G. (2000): Hydraulic sorting of heavy-mineral grains by swash on a medium-sand beach – Journal of Sedimentary Research, Vol. 70, No. 5, pp. 994-1004.

Jones, H.A., Davies, P.J. (1979): Preliminary studies of offshore placer deposits, eastern Australia – Marine Geology, Vol. 30, pp. 243-268.

Just, J., Schefuß, E., Kuhlmann, H., Stuut, J.-B.W., Pätzold, J. (2014): Climate induced sub-basin source-area shifts of Zambezi River sediments over the past 17 ka – Palaeogeography, Palaeoclimatology, Palaeoecology, Vol. 410, pp. 190–199.

Kleinhans, M.G., van Rijn, L.C. (2002): Stochastic prediction of sediment transport in sand-gravel bed rivers – Journal of Hydraulic Engineering, Vol. 128, No. 4, pp. 412-425.

Komar, P.D., Wang, C. (1984): Processes of selective grain transport and the formation of placers on beaches – Journal of Geology, Vol. 92, pp. 637-655.

Krippner, A., Meinhold, G., Morton, A.C., Schönig, J., von Eynatten, H. (2016): Heavy minerals and garnet geochemistry of stream sediments and bedrocks from the Almklovdalen area, Western Gneiss Region, SW Norway: Implications for provenance analysis – Sedimentary Geology, Vol. 336, pp. 96–105.

Kulgemeyer, T., von Dobeneck, T., Bryan, K.R., Müller, H., de Lange, W., Battershill, C. (2016 a): Lithofacies distribution and sediment dynamics in the western Bay of Plenty (New Zealand) from combined photographic, acoustic and sedimentological methods – Marine Geology, Vol. 376, pp. 158-174, doi:10.1016/j.margeo.2016.03.005.

Kulgemeyer, T., Müller, H. von Dobeneck, T., Bryan, K.R., de Lange, W., Battershill, C. (2016 b): Magnetic mineral and sediment porosity distribution on a storm-dominated shelf investigated by benthic electromagnetic profiling (Bay of Plenty, New Zealand) – submitted to Marine Geology.

Li, G., Yan, W., Zhong, L., Xia, Z., Wang, S. (2015): Provenance of heavy mineral deposits on the northwestern shelf of the South China Sea, evidence from single-mineral chemistry – Marine Geology, Vol. 263, pp. 112-124.

Li, M.Z., Amos, C.L. (1995): SEDTRANS91: A sediment transport model for continental shelves – Computer & Geosciences, Vol. 21, No. 4, pp. 533-554.

Li, M.Z., Amos, C.L. (2001): SEDTRANS96: the upgraded and better calibrated sediment-transport model for continental shelves – Computer & Geosciences, Vol. 27, pp. 619-645.

Li, M.Z., Komar, P.D. (1992 b): Selective entrainment and transport of mixed size and density sands: Flume experiments simulating the formation of black-sand placers – Journal of Sedimentary Petrology, Vol. 62, No. 4, pp. 584-590.

May, J.P. (1973): Selective transport of heavy minerals by shoaling waves – Sedimentology, Vol. 20, pp. 203-211.

McDougall, J.C. (1961): Ironsand deposits offshore from the west coast, North Island, New Zealand – New Zealand Journal of Geology and Geophysics, Vol. 3, pp. 283-300.

Merritt, W.S., Letcher, R.A., Jakeman, A.J. (2003): A review of erosion and sediment transport models – Environmental Modelling & Software, Vol. 18, pp. 761–799.

Miedema, S.A. (2010): Constructing the Shields curve, a new theoretical approach and its applications – WODCON XIX, Beijing.

Müller, H., von Dobeneck, T., Hilgenfeldt, C., SanFilipo, B., Rey, D., Rubio, B. (2012): Mapping the magnetic susceptibility and electric conductivity of marine surficial sediments by benthic EM profiling – Geophysics, Vol. 77, No. 1, pp. 1-14.

Murray, A.B. (2002): Seeking explanation affects numerical modeling strategies – EOS, Transactions, American Geophysical Union, Vol. 83, pp. 418-419.

Murray, A.B. (2003): Contrasting the goals, strategies, and predictions associated with simplified numerical models and detailed simulations – in: Iverson, R.M., Wilcock, P.R. [eds.](2003): Predictions in Geomorphology, American Geophysical Union, Geophysical Monograph, No. 135, pp. 151-165.

Murray, A.B., Thieler, E.R. (2004): A new hypothesis and exploratory model for the formation of large-scale inner-shelf sediment sorting and ”rippled scour depressions” – Continental Shelf Research, Vol. 24, pp. 295-315.

Neumaier, U., Ferrarin, C., Amos, C.L., Umgiesser, G., Li, M.Z. (2008): SEDTRANS05: An improved sediment-transport model for continental shelves and coastal waters with a new algorithm for cohesive sediments – Computers & Geosciences, Vol. 34, pp. 1223–1242.

Nielsen, P. (1979): Some basic concepts of wave sediment transport – Series paper, Vol. 20, Institute of Hydrodynamics and Hydraulic Engineering, technical University of Denmark, Lyngby.

Orpin, A., Bostock, H., Nodder, S., Barnes, P., Lamarche, G. (2009): Resource evaluation, exploration and current prospecting interests of west coast ironsands, North Island, New Zealand – In: Coasts and Ports 2009: In a Dynamic Environment. Wellington, N.Z.: Engineers Australia 2009, pp. 98-104.

Pan, B., Pang, H., Gao, H., Garzanti, E., Zou, Y., Liu, X., Li, F., Jia, Y. (2016): Heavy-mineral analysis and provenance of Yellow River sediments around the China Loess Plateau – Journal of Asian Earth Sciences, Vol. 127, pp. 1–11.

Peters, C., Dekkers, M.J. (2003): Selected room temperature magnetic parameters as a function of mineralogy, concentration and grain size – Physics and Chemistry of the Earth, Vol. 28, pp. 659-667.

Prakash, T.N. (2000): Sediment distribution and placer mineral enrichment in the inenr shelf of Quilon, SW coast of India – Indian Journal of Marine Sciences, Vol. 29, pp. 120-127.

Razik, S., Chiessi, C.M., Romero, O. von Dobeneck, T. (2013): Interaction of the South American Monsoon System and the Southern Westerly Wind Belt during the last 14 kyr – Palaeogeography, Palaeoclimatology, Palaeoecology, Vol. 374, pp. 28–40.

Razik, S., Dekkers, M.J., von Dobeneck, T. (2014): How environmental magnetism can enhance the interpretational value of grain-size analysis: A time-slice study on sediment export to the NW African margin in Heinrich Stadial 1 and Mid Holocene – Palaeogeography, Palaeoclimatology, Palaeoecology, Vol. 406, pp. 33–48.

Razik, S., Govin, A., Chiessi, C.M., von Dobeneck, T. (2015): Depositional provinces, dispersal, and origin of terrigenous sediments along the SE South American continental margin – Marine Geology, Vol. 363, pp. 261–272.

Reid, I., Frostick, L.E. (1985): Role of settling, entrainment and dispersive equivalence and of interstice trapping in placer formation – Journal of the Geological Society, Vol. 142, pp. 739-746, doi: 10.1144/gsjgs.142.5.0739.

Rubey, W. W. (1933): The size distribution of heavy minerals within a water-laid sandstone – Journal of Sedimentary Petrology, Vol. 3, pp. 3-29.

Sallenger, A.H. (1979): Inverse grading and hydraulic equivalence in grain flow deposits – Journal of Sedimentary Petrology, Vol. 49, pp. 553-562.

Shields, A. (1936): Anwendung der der Ähnlichkeitsmechanik und der Turbulenzforschung auf die Geschiebebewegung – Mitteilungen der Preußischen Versuchsanstalt für Wasserbau und Schiffbau, Vol. 26, Berlin, 26 pp.

Slingerland, R. (1977): The effects of entrainment on the hydraulic equivalence relationships of light and heavy minerals in sands – Journal of Sedimentary Petrology, Vol. 47, No. 2, pp. 753-770.

Slingerland, R., Smith, N.D. (1986): Occurence and formation of water-laid placers – Annual Review of Earth and Planetary Sciences, Vol 14, pp. 113-47.

Soulsby, R.L. (1995): Bed shear-stresses due to combined waves and currents – in: Stive, M.J.F., de Vried, H.J., Fredsøe, J., Hamm, L., Soulsby, R.L., Teisson, C., Winterwerp, J.C. (eds.): Advances in Coastal Morphodynamics, pp. 4-20 to 4-23. Delft Hydraulics, Netherlands.

Soulsby, R.L. (1997): Dynamics of marine sand – Thomas Telford Publishing, London, 272 pp.

Soulsby, R.L., Clarke,S. (2005): Bed Shear-stresses Under Combined Waves and Currents on Smooth and Rough Beds – Report TR137, HR Wallingford.

Soulsby, R.L., Smallman, J.V. (1986): A direct method of calculating bottom orbital velocity under waves – Report SR 76, HR Wallingford.

Soulsby, R.L., Whitehouse, R.J.S.W. (1997): Threshold of sediment motion in coastal environments – Proceedings of Pacific Coasts and Ports '97 Conference Christchurch, Vol.1, pp. 149-54. University of Canterbury, New Zealand.

Soulsby, R.L., Hamm, :, Klopman, G., Myrhaug, D., Simons, R.R., Thomas, G.P. (1993): Wave-current interaction within and outside the bottom boundary layer – Coastal Engineering, Vol. 21, pp. 41-69.

Steidtmann, J.R. (1982): Size-density sorting of sand-size spheres during deposition from bedload transport and implications concerning hydraulic equivalence – Sedimentology, Vol. 29, pp. 877-883.

Styles, R., Glenn, S.M. (2002): Modeling bottom roughness in the presence of wave-generated ripples – Journal of Geophysical research, Vol. 107, No. C8, 3110, doi:10.1029/2001JC000864.

Tomkins, M.R., Nielsen, P., Hughes, M. (2003): Selective entrainment of sediment graded by size and density under waves – Journal of Sedimentary Research, Vol. 73, No. 6, pp. 906-911.

van Rijn, L.C. (1993): Principles of Sediment Transport in Rivers, Estuaries and Coastal Seas – Aqua, Amsterdam.

van Rijn, L.C. (2007): Unified View of Sediment Transport by Currents and Waves. III: Graded Beds – Journal of Hydraulic Engineering, Vol. 133, No. 7, pp. 761-775.

Won, I.J., Keiswetter, D.A., Hanson, D.R., Novikova, E., Hall, T.M. (1997): GEM-3: A monostatic broadband electromagnetic induction sensor – Journal of Environmental and Engineering Geophysics, Vol. 2, No. 1, pp. 53-64.

Wilson, K.C. (1989): Friction of Wave-Induced Sheet Flow – Coastal Engineering, Vol. 12, pp. 371-379.

Zhang, S., Cioppa, M., Zhang, S. (2010): Spatial Variations in Particle Size and Magnetite Concentration on Cedar Beach: Implications for Grain-Sorting Processes, Western Lake Erie, Canada – Acta Geologica Sinica (English Edition), Vol. 84, No. 6, pp. 1520-1532.

Chapter 5

Synthesis

The principal aims of this thesis were to develop a method for the assessment of heavy mineral enrichments from integrated electromagnetic, sedimentological, photographic and acoustic datasets, and to derive conclusions about the formation mechanism of the observed structures. This has been achieved in a three-step approach, were each step is the subject of one of the studies presented herein.

The first step was to establish the sedimentological framework in chapter 2. Close-up photography of the seafloor allowed a preliminary classification of the sediment closely oriented on classical sedimentological parameters, especially grain size. This was used as guidance for a sampling campaign. Sedimentological analysis of grain size distribution and mineral composition allowed the definition of lithofacies, which were mapped out between profiles, wherever possible according to their characteristic acoustic backscatter. Sediment distribution, turbidity and the type and orientation a bedforms along with comparison to literature allowed to determine the main pathways of net sediment transport. The high spatial density along profiles achieved by continuous seafloor photography resolved changes in lithofacies over a scale of ca. 20 meters along an 8 km profile. This technique could be improved in the future by implementing an automatic classification scheme to reduce processing time.

On this background, the distribution of magnetic minerals was investigated in chapter 3. The innovative electromagnetic sensor on board the benthic profiler *NERIDIS III* provided insight into magnetic susceptibility and electric

conductivity patterns in the uppermost section of the seafloor, where active transport and sorting processes take place. The EM parameters are related to the sedimentological parameters of magnetic mineral concentration and sediment porosity. This method reveals where sorting processes have taken place within the boundary of the established lithofacies and provides insight into the next level of detail of seafloor sediments. A comparable result would have been very difficult to achieve using classical sedimentological methods.

The magnetic mineral fraction was characterized as consisting of titanomagnetite in various compositions hematite and ilmenite. It was found that sorting mostly takes place in a water depth between 5-15 m, on the crest of smaller scale dune or megaripple structures, and away from ebb tidal deltas were tidal currents and fresh or circulating sediment are regularly interrupting the sorting process.

Enrichments have been found as coast-parallel structures within fine sand deposited during the late Holocene, and as more widespread structures in older, and coarser, facies. The results further showed that modern enrichments in fine sand are connected with a relatively low porosity. Selective entrainment has been pointed out as the main driving force behind the formation of these structures. Enrichments in highly porous coarse sands have been interpreted as a relic of the Holocene transgression. Due to the rising sea level, the changing bed shear stress was targeting a wider range of grain sizes. Some of these were previously protected within the pore space of the surrounding matrix, but could be entrained once this matrix was sufficiently depleted of larger particles.

The formation mechanism was investigated in chapter 4 with an exploratory numerical model. It confirmed the critical role of selective entrainment and expanded the concept by including differential transport. While the former determines the position of an enrichment, the latter is largely responsible for the degree of enrichment. The response to changing hydrodynamics conditions was tested, as well as the development of enrichments with different geological constraints. It was found that while both longshore and cross-shore currents can influence the position of the enrichment due to their bed shear stress, the differential transport is most effectively enriching sediment in cross-shore direction.

According to the model, the enrichment process follows a linear trend, which seems to be reasonable for small concentrations. This trend also increases linearly to the concentration of heavy minerals in the initial sediment. The bedslope is greatly influencing the differential transport by horizontally concentrating changes in shear stresses and current velocity on a smaller area. This means that sediment can be more effectively enriched on a steeper slope. As an exploratory model, the model is reduced to key processes given by the aims of the research. While it demonstrate the basic process of formation, it is not suitable to make claims about the preservation of enrichments, especially under extreme conditions.

The outcomes of this work can be used for purposes in science, coastal management and industry. The distribution of heavy minerals is a key component to investigate sediment transport and provenance, and the relatively easy *in situ* accessibility of magnetic minerals by means of electromagnetic measurements make them an ideal proxy. Increased concentrations are connected to erosive environments (Frihy, 1994), meaning that deposits of freshly supplied sediment will likely not be stable over long time frames. However, the grain size ratio of the remaining lag may provide armoring to the seafloor and be more stable than it was before (Bartzke et al., 2013). Enrichments of magnetic minerals reveal where sediment transport takes place and where the maximum depth of entrainment for the bulk material of a given facies is located under the regional hydrodynamic conditions. Hydraulic sorting must be considered when investigating the provenance of sediments, if the concentration of heavy minerals is used as an indicator of a certain source rock (Garzanti & Ando, 2007).

Future perspectives for research are to test the model and hypothesis on the formation of magnetic mineral enrichments by the comparison of these results to other environments and other minerals. Repeated surveys in the same area would also provide very useful insight into the stability or mobility of the observed structures. Apart from this, open questions are:

- Reliable wave and current data is often collected over several years and can be biased by climatic fluctuation (eg. El Niño); how can the distribution

of magnetic minerals be used to derive long-term hydrodynamic conditions in areas where no such data exists?

- The exploratory model used here is not suited to explain the long-term stability of enrichments under extreme conditions, how can effects like burial and additional sediment supply by beach erosion be incorporated to overcome these shortcomings?
- Highly enriched placers can reach concentrations of 90 % or more, which makes metallic placers conductive bodies; what constraints does this put on surficial EM measurements and porosity estimates?
- Magnetite grains are the main carrier of natural remanent magnetization; is there a measurable influence on the stability of magnetite placers due to intergranular magnetic attraction and what degree of enrichment is required to make this a measurable effect?

Bibliography

Bartzke, G., Bryan, K.R., Pilditch, C.A., Huhn, K. (2013): On the stabilizing influence of silt on sand beds – Journal of Sedimentary Research, Vol. 83, pp. 691–703, doi:10.2110/jsr.2013.57.

Frihy, O.E. (1994): Discrimination of accreted and eroded coasts using heavy mineral compositions of the Nile Delta beach sands, Egypt – Sedimentology, Vol. 41, pp. 905-912.

Garzanti, E., Ando, S. (2007): Heavy mineral concentration in modern sands: implications for provenance interpretation – in: Mange, M.A., Wright, D.T. [eds.](2007): Heavy Minerals in Use, Developments in Sedimentology, Vol. 58, pp. 517-545.

Danksagung

Zunächst einmal gilt mein Dank meinen Betreuern, Tilo von Dobeneck und Karin Bryan, die mir stets durch ihre Fachkenntnis, aber auch Freundlichkeit und Geduld mit Rat und Tat zur Seite standen. Ebenso danke ich den restlichen Co-Autoren meiner Paper: Hendrik Müller, Willem de Lange und Chris Battershill für ihre wertvolle Hilfe durch Diskussion, Organisation. An der Universität Bremen danke ich den anderen Mitgliedern der AG Marine Geophysik, Thomas Frederichs, Christian Hilgenfeldt, Liane Brück, Martina Braun und Heike Piero, und an der University of Waikato Dirk Immenga, Annette Rodgers, Janine Ryburn, Chris Morcom und Renat Radosinsky für ihre Unterstützung in Labor- und Feldarbeit

Weiterhin danke ich der Deutschen Forschungsgemeinschaft, und dem durch diese finanzierten INTERCOAST-Programm, welches diese einzigartige und schöne Gelegenheit ermöglicht hat.

Persönlich danke ich Christina Gawrych, Merle Bollen, Brice Blossier, Alex Port und allen anderen Freunden bei INTERCOAST und in Neuseeland. Durch euch ist diese Zeit überhaupt erst so schön geworden, an diesem und am anderen Ende der Welt.

Ganz besonders danke ich natürlich meiner Familie, meinen Eltern Susanne und Bernfried und meinem Bruder Christoph. Und weil ich unmöglich einzeln aufzuzählen kann wofür, mache ich es mir leicht: Danke, für alles.